FLOATECH

D5.1. Report on the LCOE improvement of AWC controlled floating wind farms

DATE OF DELIVERY - 31/10/2023

AUTHORS - D. P. COIRO, G. TROISE, G. LAZZERINI, A. GRIECO, F. PAPI, A. BIANCHINI, R. BEHRENS DE LUNA

SEAPOWER SCRL, UNIVERSITY OF FLORENCE, TECHNISCHE UNIVERSITÄT BERLIN, SAIPEM S.A., IDEOL S.A.

This project has received funding from the European Union's Horizon 2020 research and innovation programme under grant agreement No 101007142

FLOATECH
THE FUTURE OF FLOATING WIND TURBINES

Document track details

Project acronym	FLOATECH
Project title	Optimization of floating wind turbines using innovative control techniques and fully coupled open-source engineering tool
Starting date	01.01.2021
Duration	36 months
Programme	H2020-EU.3.3.2. - Low-cost, low-carbon energy supply
Call identifier	H2020-LC-SC3-2020-RES-RIA
Grant Agreement No	101007142

Deliverable Information	
Deliverable number	5.1
Work package number	5
Deliverable title	Report on the LCOE improvement of AWC controlled floating wind farms
Lead beneficiary	SEAPOWER
Authors	D. P. Coiro, G. Troise, G. Lazzerini, A. Grieco, F. Papi, A. Bianchini, R. Behrens de Luna
Reviewers	Prof. Giovanni Ferrara (University of Florence) Peter Naaijen (NextOcean)
Due date	31/10/2023
Actual submission date	26/10/2023
Type of deliverable	Report
Dissemination level	Public

Version management

Document history and validation			
Version	**Name**	**Date**	**Comment**
Rev 1	D. Coiro, G. Troise, A. Grieco, F. Papi, A. Bianchini, R. Behrens De Luna	06/10/2023	First version
Rev 2	Revision by UNIFI and NextOcean	25/10/2023	

Background: about the FLOATECH project

The FLOATECH project is a Research and Innovation Action funded by the European Union's H2020 programme aiming to increase the technical maturity and the cost competitiveness of floating offshore wind (FOW) energy. This is particularly important because, due to the limitations of available installation sites onshore, offshore wind is becoming crucial to ensure the further growth of the wind energy sector.

The project is implemented by a European consortium of 5 public research institutions with relevant skills in the field of offshore floating wind energy and 3 industrial partners, two of which have been involved in the most recent developments of floating wind systems.

The approach of FLOATECH can be broken down into three actions:

- The development, implementation and validation of a user-friendly and efficient design engineering tool (named QBlade-Ocean) performing simulations of floating offshore wind turbines with an unprecedented combination of aerodynamic and hydrodynamic fidelity. The advanced modelling theories will lead to a reduction of the uncertainties in the design process and an increase of turbine efficiency.
- The development of two innovative control techniques: the Active Wave-based feed-forward Control, combining wave prediction and anticipation of induced platform motion to reduce oscillations and loads, and the Active Wake Mixing, aimed at minimizing wake effects in floating wind farms, leading to a net increase in the annual energy production of the farm.
- The economic analysis of these concepts to demonstrate qualitatively and quantitatively the impact of the developed technologies on the Levelized Cost of Energy (LCOE) of FOW technology.

In addition to the technological and economic impacts, the project is expected to have several impacts at societal, environmental and political levels, such as: public acceptance, due to no noise and visibility issues of FOWT; very low impact on biodiversity and wildlife habitat because no piles are needed be to installed into the seabed; the use of less material and space thanks to an environmentally friendly design; the promotion of the installation of FOW in transitional water depths (30-50 m), as the costs for FOW at those locations will become more competitive compared to the fixed bottom foundations.

Table of contents

List of acronyms and abbreviations

Acronym / Abbreviation	Meaning / Full text
FOW	Floating Offshore Wind
FOWT	Floating Offshore Wind Turbine
LCOE	Levelized Cost of Energy
CRF	Capital Recovery Factor
AEP	Annual Energy Production
WP	Work package
AWC	Active Wave Control
AWM	Active Wake Mixing
FF	Feed-forward
DEL	Damage Equivalent Load
GDP	Gross Domestic Product
PPI	Producer Price Index (TPPI indicates the total PPI, comprising domestic and international trading price index)

List of symbols

Acronym / Abbreviation	Meaning / Full text
CAPEX	Capital Expenditures
OPEX	Operational Expenditures
DECEX	Decommissioning costs
$M_{xy_{TB}}$	Combined bending moment at the tower base

1 EXECUTIVE SUMMARY

This document is related to the results of Work Package (WP) 5 of the FLOATECH project. The main goal of WP 5 is the estimation of the impact of the newly developed technologies on FOWT economic performance. Specifically, WP5 will investigate the effects on the overall component costs due to the introduction of two new control strategies: Active Wave Control (AWC), related to the feed forward control methodology developed in WP 3 of FLOATECH project, and Active Wake Mixing (AWM), related to the wake mixing control strategy developed in WP 4. Two different tasks are devoted to the new control models, Task 5.1, dedicated to the study of AWC, and Task 5.2 dedicated to AWM. In order to explore the economic effects of the implementation of the new controls, a cost model parametrized on the main geometrical and performance data of the FOWT, is simultaneously under development in Task 5.3. This report is specifically related to the economic assessment of the AWC control implementation. This study exploits the results of simulations performed using QBlade, in order to estimate the loads on the main FOWT components. The methodology used to estimate the possible improvements due to the newly introduced control technology is based on a hybrid approach: on the one hand, some cost contributions will be estimated using expressions based on statistical regression, typically derived from literature, while, on the other hand, the costs of the FOWT components mainly affected by the control variation will be estimated using a simplified preliminary design calculations, in order to evaluate possible changes in design parameters due to the predicted load variations.

In LCOE estimation, possible changes in the annual energy production are also accounted for. Results are presented in terms of variation of the LCOE between a reference case and a modified design including the AWC control technology, developed at the Ecole Central Nantes with an innovative control system designed by TUDelft.

The analysis showed, in fact, very small variations in loadings and performance induced by the introduction of the AWC control strategy. Consequently, no increase in LCOE has been observed due to this type of control for the specific configuration considered in this study. On the other hand, a reduction in output power oscillations has been observed, particularly for severe sea states, with potential benefit for the enhancement of output power quality. These results illustrate the potential of the considered control technique when applied to different types of FOWT, possibly more sensitive to the reduction of wave induced oscillations.

2 INTRODUCTION

The FLOATECH project is mainly focused on the development of new technologies for the analysis and performance improvement of floating offshore wind turbines.
In fact, while onshore wind turbine technology has reached a high level of maturity, offshore applications are affected by some technical issues. However, the large amount of wind energy resource potentially available in offshore locations makes the exploitation of such sites very attractive for the development of floating wind farms, also based on EU and national polices, prospecting global targets for the total installed power in the next future. The current 30 GW offshore power installed in Europe, by the end of 2022 according to [1], is expected to significantly increase in the next 5 years, although, the predicted installation rate is currently still lower than the expected theoretical trend needed to meet the target installed power, due to the conjunctural economic conditions with high inflation rate and material prices.
The largest part of the currently installed offshore wind plant comprises installations with bottom fixed foundations. Anyway, in order to broaden the wind energy exploitable areas, the diffusion of floating offshore installations can help to overcome the depth limitations of bottom fixed solutions, whose costs rapidly increase with the depth of the installation site [2]. On the other hand, Floating Offshore Wind Turbines (FOWT) are still the subject of a large research effort aimed at mitigating several complex technical issues, which result in the higher costs typically observed for this technology with respect to their bottom fixed and onshore counterparts. The *FLOATECH* project has the main objective of developing a simulation tool (QBlade-Ocean) aimed at accurately and efficiently reproduce the behaviour of wind floating wind turbines under a wide range of environmental conditions. At the same time, two innovative control technologies were investigated during the project. The AWC control technique, which is the subject of this study, uses a feed-forward strategy, based on the measurement of the incoming wave field through a radar sensor, to improve the desired response of a FOWT by acting on its pitch control system, as described in FLOATECH deliverable D3.1 [3].

The introduced control technique acts on blade pitch influencing several aspects of the FOWT overall response. In particular, it can be used for two different objectives:

- mitigate loads on specific turbine components;
- improve output power quality.

The purpose of this study is to provide an estimate of the effect of the AWC control technique on costs and energy production summarized in the levelized cost of energy (LCOE).

3 GENERAL DEFINTIONS AND ASSUMPTIONS

Sections 3 and 4 describe the approach adopted for the estimation of the levelized cost of energy (LCOE) of a floating wind turbine and its application to the case of AWC control technique. The cost and energy production models developed in this study have been concurrently developed for two innovative control strategies (AWM and AWC), developed in the FLOATECH project. Part of the related deliverables (D5.1 and D5.2) share the same approach and a similar content, with some modifications, mainly due to the

differences in the considered FOWT model and in the results of the simulations used for the LCOE assessment.

The level of accuracy of the estimations here indicated is considered adequate for a preliminary evaluation of costs and energy production, as expected in the initial design stages, where an exploration of different solutions, compared also through their economic effectiveness, can be useful for the designer. However, the presented procedure uses a simulation-based approach for load and power estimation, thus requiring a certain level of detail in the definition of the configuration in order to setup at least a simplified simulation model.

The effect of the variation of control strategy on LCOE will be addressed in this study. Specifically, a comparison between a configuration implementing the AWC control technique and a configuration using a traditional control system without the feed-forward component will be considered. This change may affect two different technoeconomic aspects:

- on the one side, the control system behaviour may influence the loadings acting on the different FOWT components; a variation of the loading levels may, in turn, affect the sizing and thereby the costs of the components; it is also assumed that this size variation can be estimated using a simplified preliminary design approach;

- on the other side, the power curve may also be influenced by the variation of the control strategy, both in terms of average output power and in terms of power fluctuations (related to the output power quality); the choice of the control strategy may directly affect the response of the rotor, in terms of rotor speed response, thereby altering the power generation behaviour; moreover, a variation of the control may also affect rotor thrust, through blade pitch variation, thus possibly affecting the overall FOWT motion response; the floater motion, in turn, may affect the relative wind speed at the rotor, indirectly influencing power performance.

A suitable metric has to be defined to establish the economic effectiveness of the chosen design configuration. In the process of economic assessment of an energy related project, one of the most significant parameters is represented by the Levelized Cost of Energy (LCOE), defined by the following expression (as described, for example, in [4]):

$$LCOE = \frac{CAPEX + \sum_{n=1}^{t} \frac{OPEX}{(1+i)^n} + \frac{DECEX}{(1+i)^{t+1}}}{\sum_{n=1}^{t} \frac{AEP}{(1+i)^n}} \quad (1)$$

where $CAPEX$, measured in €, indicates the capital expenditures, $OPEX$ represents the annual operating costs, measured in €/year, $DECEX$, in €, is referred to the decommissioning costs, AEP is the annual energy production, measured in MWh/year and the factor i is a *discount rate* assumed to estimate the present value of future costs and energy production at the start time of the project. The estimate of the discount rate will be based on available literature data.

The LCOE concept is intended to capture the economic effectiveness of an energy related project using a single compound metric. This parameter involves both the costs sustained during the project (at the numerator in eq. (1)) and the possible revenues in terms of energetic production (at the denominator). The LCOE value can be assumed to provide an estimate of the average unit cost of energy production and is generally expressed in units of currency divided by an energy unit (for example €/MWh). The considered costs comprise the initial capital costs, the operating costs sustained to support the continuous operation of the plant and the costs sustained at the end of the project to remove the plant and possibly mitigate the residual environmental impact. An important problem to be faced in this type of economic analysis, applied to long term projects, is related to the need for considering costs and revenues occurred in different period of time. To assess this problem, a discounting procedure is applied to the costs and incomes for each time period: the discounting process estimates the current value of a future economic cash flow by reducing it based on a given discount rate (indicted as i in eq. (1)). Thus, the value of the cost of energy represented by the LCOE is reduced (levelized) to a given reference time, generally at the start of the project.

It is worth to note that the literature on the technoeconomic evaluation of energy production processes has introduced other metrics in this context (a survey of some alternatively proposed parameters is, for example, reported in [5] and [6]). However, in this study the LCOE metric has been considered able to represent, in a relatively simple approach, the effects of the newly introduced technologies both on the configuration design and on energy production performance.

An alternative way to express the LCOE is reported in equation (2).

$$LCOE = \frac{CAPEX \times CRF + \ OPEX + DECEX \times \dfrac{i}{(1+i)^t - 1}}{AEP} \tag{2}$$

which introduces the *Capital Recovery Factor (CRF)* estimated through the following relation:

$$CRF = \frac{i(1+i)^t}{(1+i)^t - 1} \tag{3}$$

where t is the service life of the project. This expression is related to the previous one, based on the expression for the partial sum of a geometric series of ratio $1/(1+i)$ [1]. The total time of the project, t,

[1] The partial sum, s_n, of a geometric series, $\sum_1^t ap^n$, with ratio $p \neq 1$, is expressed as $s_t = ap\,(1-p^t)/(1-p)$; in this case the ratio of the series is related to the discount rate i by the expression $p = 1/(1+i)$, thus the partial sum is equal to

$$s_t = a(1/(1+i))\,(1-1/(1+i)^t)/(1-1/(1+i))$$

with t the current time in the succession of annuities. s_t indicates the present value of future costs sustained at time t, converted to an equivalent value at the start of the project, using the given discounting factor. This result can be applied to the expression for LCOE, considering constant values for *OPEX* and *AEP*. The *DECEX* cost, sustained only once at the end of the project, is directly converted to present value with a scaling factor equal to $s_{DECEX} = 1/(1+i)^{t+1}$, assuming, simplistically, that one year after the end of the project is needed for the decommissioning process.
Using these results, the LCOE expression can be reformulated as

is considered equal to 20 years. The expression presented in eq. (1), which is more general, may be used when a variable cash flow over the project duration has to be considered, explicitly including the summation of the levelized costs and revenues in each year of the project. The simpler expression in eq. (2) can be derived from (1) when constant values for the costs and revenues are considered, as here assumed; in such simplified expression, used throughout this study, a constant factor (indicated as CRF) accounts for the discounting procedure.

The value of the so called *Weighted Averaged Capital Cost* (WACC) will be used in order to estimate the discount rate in the LCOE, as suggested in a study by the Fraunhofer Institute [7], which reports a set of typical values for several renewable energy sources. The WACC metric indicates the expected rate of return on the assets used to finance the project, generally comprising a term related to the part of costs financed through debt and a term related to the expected return on equity (the capital invested by the shareholders). This parameter, strongly dependent on the considered market and on the economic situation, in this study will be estimated based on data from energy related market study.

WACC, thus, comprises a share related to the interest rate and a share related to the return on equity and it is variable with the market conditions. For the offshore wind sector, a value of about 6.5% is indicated in the cited source for the nominal WACC value by the year 2021 on the European market, where the nominal WACC value is affected also by the current inflation rate, w, (in the cited study it was assumed equal to $w = 1.2\%$) and may show a significant dependence on the conjunctural economic situation. The real WACC value can be estimated, according to Fisher's equation [8], using the expression $1 + WACC_{nominal} = (1 + WACC_{real})(1 + w)$, which according to Fraunhofer study yields $WACC_{real} = 5.24\%$, based on 2021 data. Assuming the same real WACC value and considering an increased value for the current inflation rate of about $w = 6\%$, the assumed value for $WACC_{nominal} = 11.5\%$; the calculations reported in this study will be based on such value. It has to be noted that the actual value of these financial parameters is difficult to be reliably estimated and can be subject to continuous

$$LCOE = \frac{CAPEX + OPEX \frac{1}{1+i}\frac{1-1/(1+i)^t}{1-1/(1+i)} + \frac{DECEX}{(1+i)^t}}{AEP \frac{1}{1+i}\frac{1-1/(1+i)^t}{1-1/(1+i)}}$$

Considering the following relation,

$$\frac{1}{1+i}\frac{1-1/(1+i)^t}{1-1/(1+i)} = \frac{1-1/(1+i)^t}{(1+i)-1} = \left(\frac{(1+i)^t-1}{i(1+i)^t}\right)$$

the LCOE expression can be rewritten as

$$LCOE = \frac{CAPEX + OPEX\left(\frac{(1+i)^t-1}{i(1+i)^t}\right) + \frac{DECEX}{(1+i)^t}}{AEP\left(\frac{(1+i)^t-1}{i(1+i)^t}\right)}$$

Introducing the Capital Recovery Factor,

$$CRF = 1/\left(\frac{(1+i)^t-1}{i(1+i)^t}\right)$$

the final expression for LCOE can be found

$$LCOE = \frac{CAPEX \times CRF + OPEX + \frac{DECEX}{(1+i)^t}\left(\frac{i\,(1+i)^t}{(1+i)^t-1}\right)}{AEP}$$

fluctuations related to the evolution of the market. Anyway, an assumption deemed reasonable has been made for the current study, with the main aim to estimate the possible LCOE variations due to the introduction of the considered new control technology, rather than to provide an estimation of the LCOE absolute values. Anyway, the chosen value is a parameter of the LCOE evaluation model and can be adapted to different economic scenarios.

4 FLOATING TURBINE CONFIGURATION AND CONTROL

For the present study a specific choice of the analysed configuration has been made. Specifically, the Softwind configuration has been considered, a design solution developed at Ecole Central de Nantes (ECN) [9] and subjected to an intensive experimental test campaign; this model has also been already used for the analyses performed in FLOATECH WP2.

It has to be noted that the LCOE estimation process and its results are significantly affected by the choice of the specific model used in the analysis, in a twofold way: from a general point of view, different configurations are clearly characterized by different component and operating costs, with different dependence on configuration specific parameters; moreover, in the specific approach used in this study, which aims to account for the effect of control related load variations, the behaviour of the assumed FOWT model, in the considered operating conditions, has a noticeable impact on the evaluation of the expected costs. As discussed in more details later in section 5, in fact, a set of simulations, deemed significant for a preliminary design study, will be considered to estimate the loadings and performance of the considered FOWT. In this perspective, thus, the results here reported for the expected LCOE levels and variations are bounded by the choice of the floater and turbine models; the defined procedure can be applied, with the needed adjustments, to different FOWT configurations, possibly yielding different estimations for the economic performance of the examined control strategy.

The following assumptions on system modelling have been considered:

- rotor and nacelle from DTU 10MW RWT have been considered;
- the tower from OOStar project has been considered, consistently with the assumptions of WP2;
- the Softwind platform studied at ECN has been considered (with a modification of the mooring line system described in 5.5.2).

The geometry of the overall system is illustrated in Figure 1. The platform has a spar buoy configuration with a mooring system composed by a set of three mooring lines connected to the platform by a system of delta connected bridles.

The rotor geometry is descripted in more details in [10]. Two control systems will be considered in the analysis: the baseline control will be the original control already used in WP2 simulations, while the modified control will implement the AWC control technique. This control technique, described in [11], uses blade pitch control to improve the overall motion response of the floating system to the disturbances generated by the incoming waves. Wave field is measured using a remote sensing radar device. Measurements are fed to the control system for two alternative purposes: controlling the power output or mitigate loads.

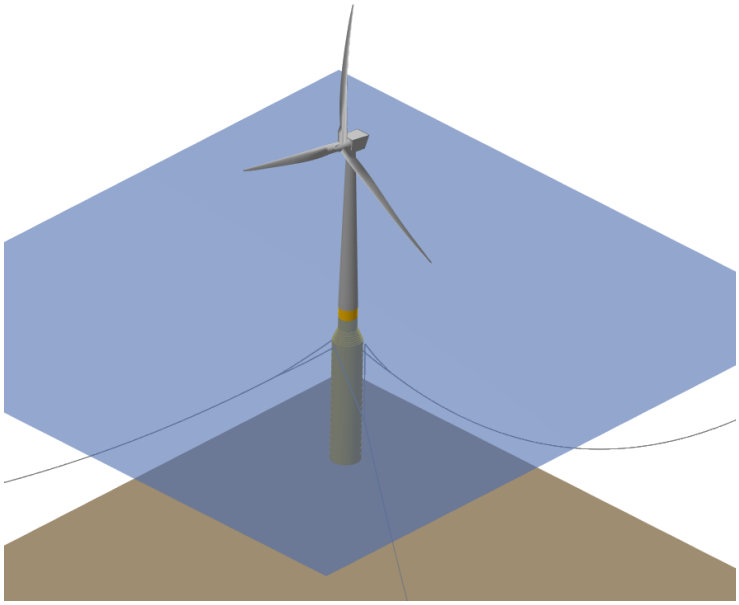

Figure 1. Softwind model.

5 METHODOLOGY

5.1 GENERAL APPROACH

In order to estimate the LCOE level for a FOWT, a cost model is needed for both capital and operational costs. This part of the work is essentially shared with the complementary study related to the other control strategy investigated in WP5 (Active Wake Mixing), reported in D5.2. Some details of the analysis are anyway specific to each particular study and will be indicated in this work together with the overall model structure. A more detailed description of the cost model will be eventually shown in D5.3 report.

The first part of the work is related to the definition of a procedure to estimate the cost contribution to LCOE as a function of the main configuration parameters, defining a cost model. Regarding the estimation of capital costs, a typical approach is based on a bottom-up procedure, which decompose the total capital expenditures in several contributions associated to the main components of a FOWT, as described for example in [2], [12], [13]. Typically, the models reported in literature are related to the overall size and dimensions of the considered components (such as the rotor diameter, tower height or other geometric feature of interest) or to some performance parameter (such as the turbine rated power). This approach is particularly useful in preliminary cost estimations and scaling studies, but, in the specific case considered in the present work, it has some difficulties in taking into account the possible effects of a change in the control strategy, which directly affects the overall FOWT response and loadings but is only indirectly related to the geometrical parameters considered by the aforementioned cost models. The methodology adopted to evaluate the LCOE variation induced by the AWC control strategy therefore needs to pursue a slightly different approach to take into account the possible effects of a change in the control strategy. Specifically, for some components of the FOWT, which are considered more significantly affected by the choice of the control technique, the following scheme is applied:

1) a baseline configuration is defined and a subset of the design parameters, considered more significant for component sizing, is chosen (such as, for example, the local thickness of structural elements or other geometrical features influencing the component load bearing capacity);
2) a simplified design procedure is set up in order to relate the chosen design parameters to a set of main loads acting on the considered components; more specifically, prior to the evaluation of the loads with the FOWT simulation model (developed in QBlade, in this study), a structural model will be defined for the determination of the required component size for a given set of loads (for example the tower top loads, or the blade bending moments); using this structural model, a relation between loads and structural weight is estimated for each component; successively (as detailed in the next steps), the FOWT simulations are carried out (with QBlade or other similar software) and the effective loads are estimated for the different considered configurations (with and without the control); once the loads are known, the load-weight relation, determined with the structural model, will be used to estimate the component weights and the related costs;
3) a simulation-based approach is used to estimate
    a. the main loading parameters for the baseline case;
    b. the same set of loadings for the configuration with the control technique implemented;
4) the simplified design procedure from point 2) is used to estimate the variation in design parameters between the baseline configuration and the configuration with the control technique needed to preserve the same level of structural safety (preserving the safety margins with respect to fatigue and maximum loads);
5) the variation in costs is estimated, based on the estimated change of the design parameters, mainly considering the required variation on the component mass.

The components for which this procedure is applied are indicated in the following list:

- the rotor blade;
- the tower;
- the platform;
- the mooring lines.

The other costs are estimated from traditional cost models from literature, mainly based on [12] [14] [15]. Some details on the evaluation of the simplified design parameter choice for the considered components is reported in the following sections.

It is important to note that the choice of design parameters here presented is far from being a detailed and complete design procedure and has only the purpose to give an initial estimate of the possible trends in cost variation induced by the considered control technique. A detailed design, which is outside the scope of the present cost estimation analysis on the one hand would require to consider a larger set of operating and environmental conditions to fully comply with standard requirements, on the other hand it would probably need an iterative approach (changing the design parameters may alter the FOWT response, thereby changing, in turn, also component loadings). The simplified design procedure is shared between the cases studied in the deliverables D5.2 and D5.3; it is reported here as a reference for the other deliverables.

5.2 SELECTION OF TOWER DESIGN PARAMETERS

The procedure used for the preliminary structural analyses of the tower has been implemented using a Matlab code, which defines a simplified redesign procedure aimed to search for a new set of geometric characteristics of the tower, preserving the overall structural safety under the varied loadings associated to the new configuration implementing the AWC control technique.
First of all, the procedure represents the tower as a truncated conical beam, whose geometry is defined by:

- tower base diameter;
- tower top diameter;
- tower shell thickness, variable along tower height.

The geometrical data used for the baseline tower configuration are derived from the OOStar project data, as also assumed in the analyses for the FLOATECH WP2.
Furthermore, the structural model takes as input the initial set of loads, comprising the following data:

- tower top forces and moments;
- DEL in different sections of the tower;
- wind speed at the top of the tower;

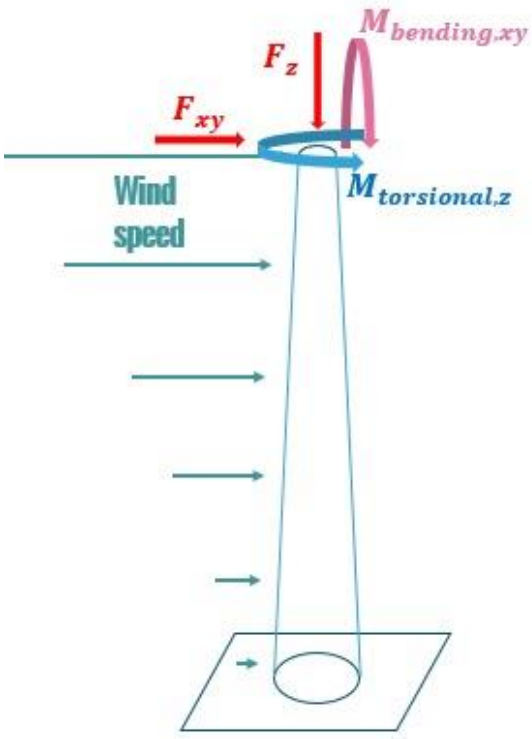

Figure 2. Schematic view of the tower geometry and loading conditions.

In the estimation of the stress distribution along the tower height, section bending moments and shear actions are estimated also accounting for the effects of the wind speed distribution profile with the elevation from sea surface. Such contribution is estimated considering a power law (with exponent $\alpha = 0.14$) and assuming a section drag coefficient equal to $C_{D_t} = 1.0$.

In order to check the structural safety requirements, the following criteria are taken into account:

- maximum stress not exceeding the material yielding stress;
- maximum compressive normal stress below the buckling limit of the tower shell structure;
- fatigue failure index, based on the cumulative damage theory, below the unit limit value.

Initially, the procedure calculates the mass and the weight of the tower and estimates the margin of safety for each of the abovementioned failure criteria for the baseline case loadings, comprising the above-mentioned tower top loads, fatigue loads and wind loads. Subsequently, a new set of loadings data are given as input to the procedure as well. The algorithm, then, iteratively searches for a new geometry, changing local thicknesses and diameters, aiming to a new configuration that meets the following conditions under the action of the modified set of loads:

- The maximum stress acting on the new tower is less than or equal to the maximum stress acting on the original tower.
- The maximum damage index of the new tower is less than or equal to the maximum damage index acting on the original tower.
- Minimum difference between compressive normal stress and buckling limit of the new tower is greater than or equal to Minimum difference between compressive normal stress and buckling limit of the original tower.
- The outer diameter of the tower base is less than or equal to the diameter of the platform base.
- The mass of the tower must be as low as possible.

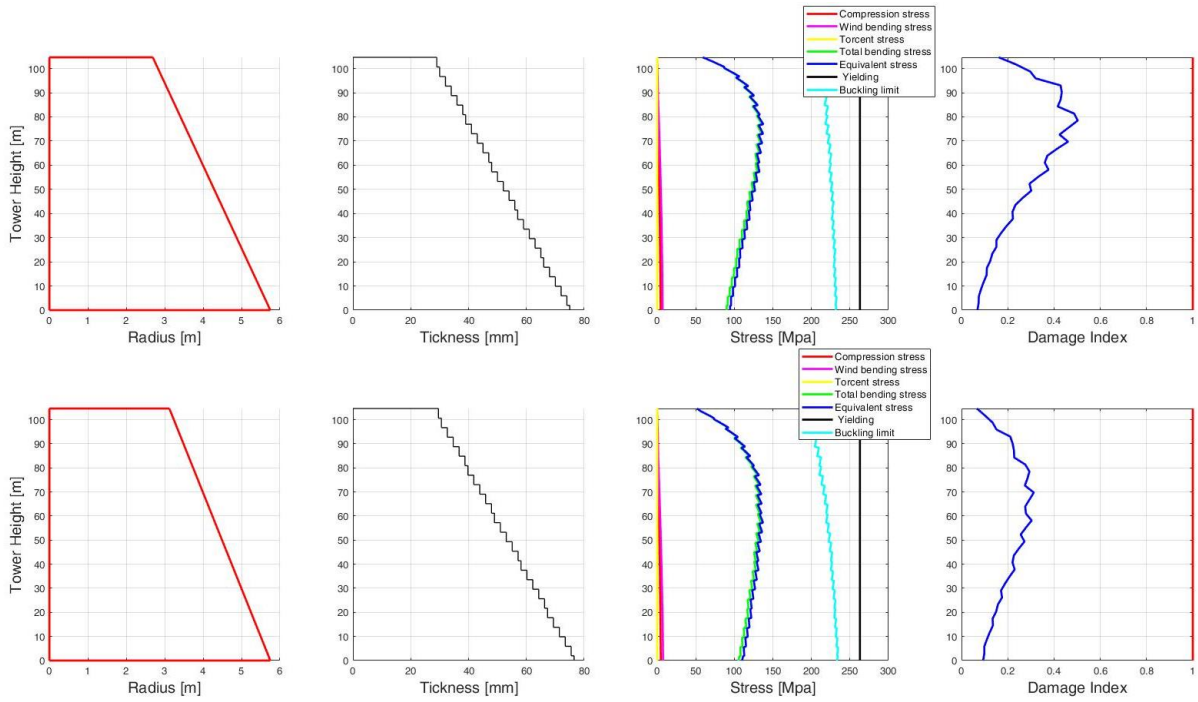

Figure 3.Typical set of results of the algorithm for the simplified tower structural sizing. (Baseline section stress distribution is reported in the upper plots, while the same target stress distribution for the modified case is reported in the lower plots).

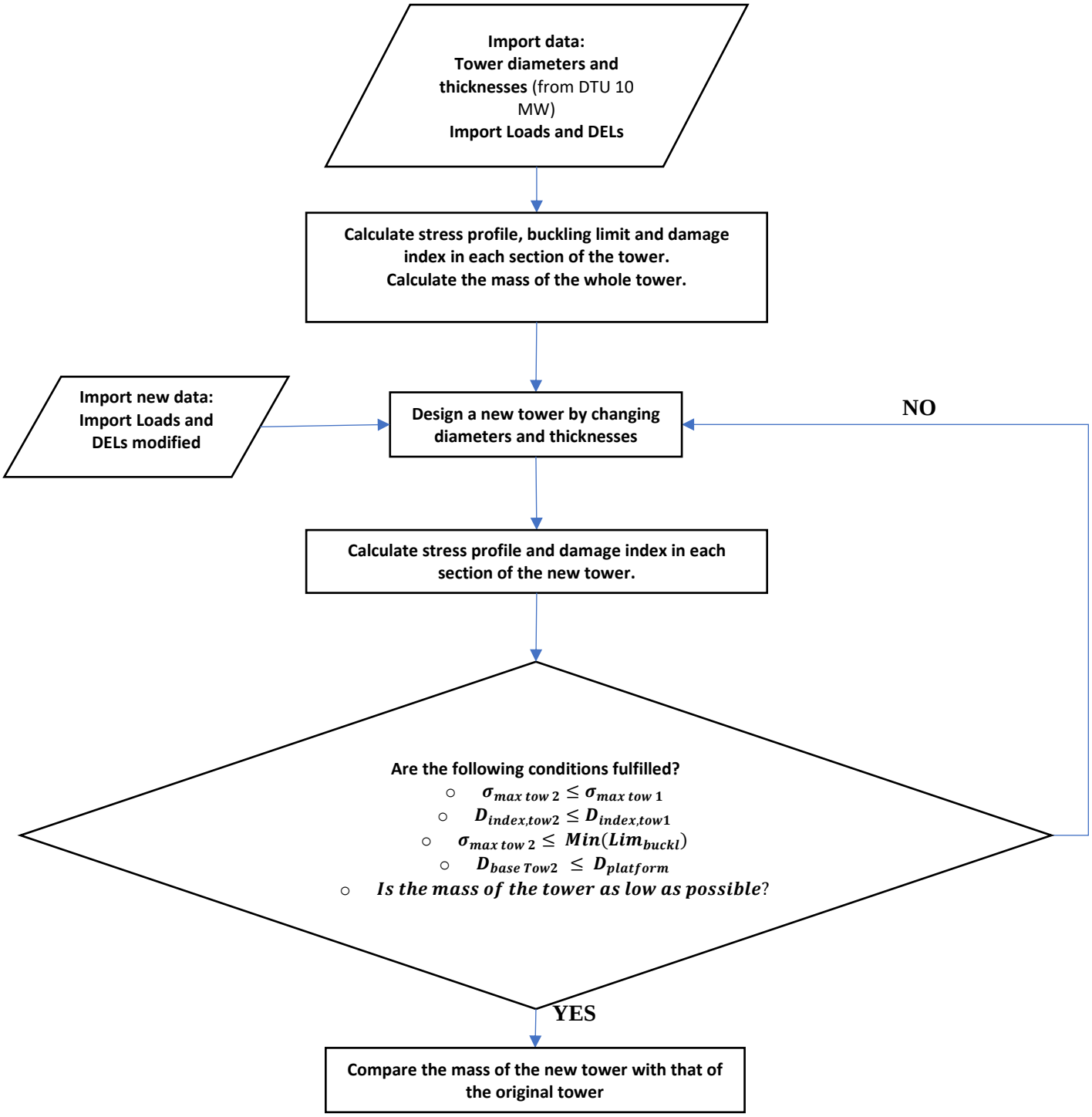

Figure 4. Description of the algorithm to model a tower as a function of applied loads and DELs.

In Figure 3 the results obtained assuming an increase in loads of 20% and of 10%. In the first row are the dimensions, stresses and damage indexes of the original tower, in the second those of the tower generated by the algorithm.

The whole procedure can be summarized in the diagram shown in Figure 4, where the symbols in Table 1 have been used.

Table 1. Symbol definition (for tower design algorithm).

$\sigma_{max\ tow\ 1}$ / $\sigma_{max\ tow\ 2}$	Maximum stress in the baseline tower / modified tower
$D_{index,\ tow1}$ / $D_{index,\ tow2}$	Maximum damage index in baseline and modified tower
$Min(Lim_{buckl})$	Minimum section buckling limit of the modified tower
$D_{base\ Tow2}$ / $D_{platform}$	Tower base diameter, platform diameter (assumed as a limit size for the tower base)

Using the above illustrated procedure, a relation between the total weight of the tower and the maximum and damage equivalent loads can be estimated. Such relation is reported in the following figure for the considered Softwind case.

To simplify further analyses, the effects of the separate variations of maximum loads and DELs are shown in Figure 5 and Figure 6. Two separate parametric studies have been carried out: in a first analysis the DELs have been varied while leaving constant the maximum loads, then the variation of maximum loads have been considered for constant DELs. In order to avoid unfeasible solutions, the following constraints have been taken into account for each separate load effect analysis:

- $\sigma_{max\ tow2} \leq \sigma_{yielding}$ **(for DEL variation)**
- $D_{index,\ tow2} \leq 1$ **(for maximum load variation)**

where $\sigma_{yielding}$ is the yielding stress of the assumed material (in this study a value of 355 MPa, typical of structural steel, has been assumed).

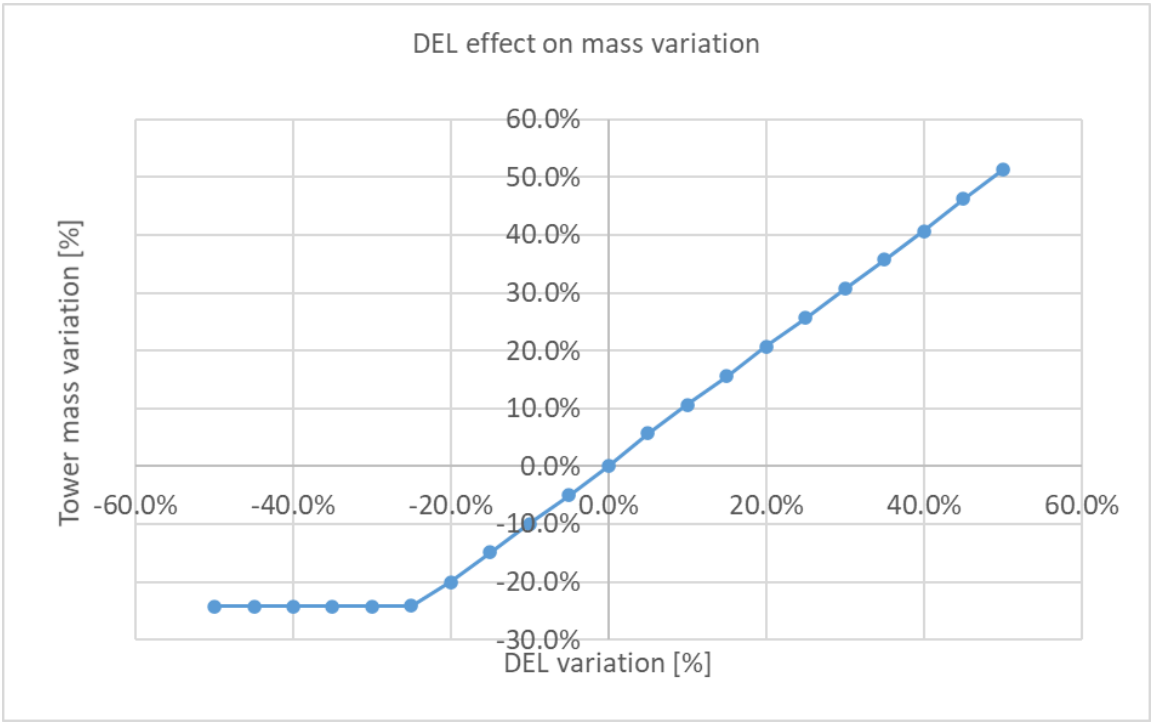

Figure 5. Tower mass variation (percent) as a function of the DEL.

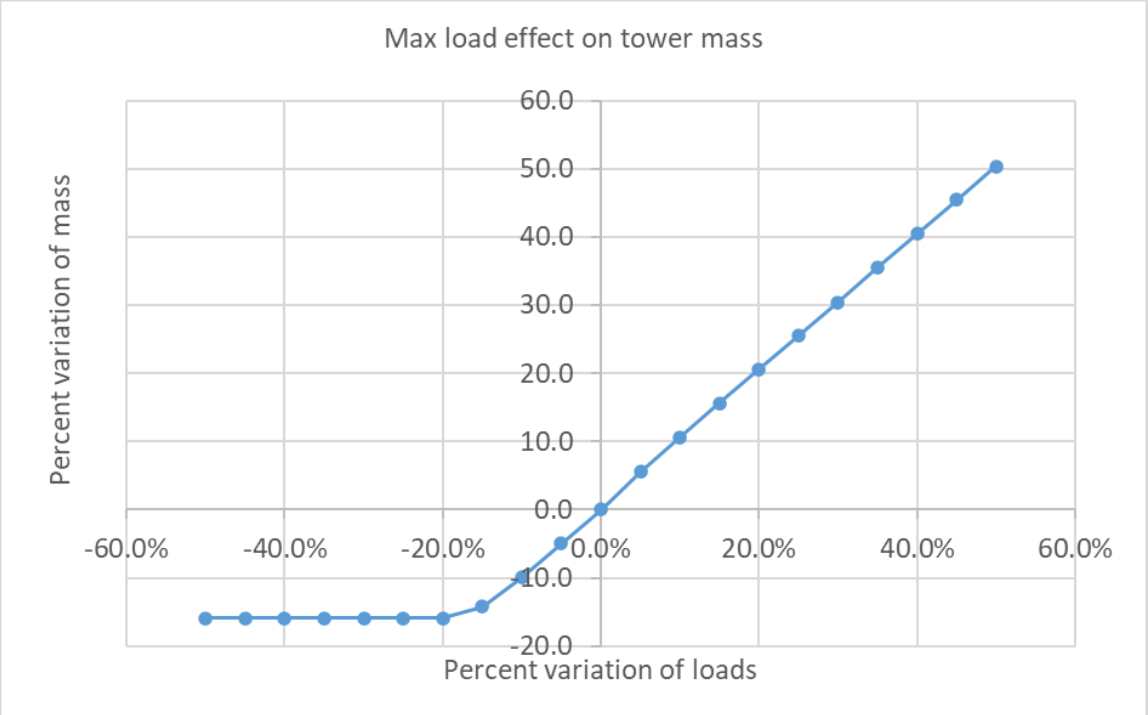

Figure 6. Tower mass variation (percent) as a function of the percent variation of the max tower base bending moment.

An approximately linear trend and an elbow can be observed in both diagrams. The elbow on the negative side of load variation is due to the fact that the mass of the tower cannot decrease further without the maximum stress caused by the original maximum loads (Figure 5) or the damage index caused by the original DELs (Figure 6) exceeding the allowable values.

Anyway, the effect of both DEL and maximum load variations on component mass will be accounted for, in the overall cost model, using an interpolation procedure applied to the estimated trends, starting from the baseline case. In this way, the tower mass in the new configuration can be estimated, allowing for the assessment of load variation effects on the tower capital costs, considered proportional to the component mass.

5.3 SELECTION OF BLADE DESIGN PARAMETERS

For the estimation of blade mass variation, a procedure similar to the one implemented for the tower has been defined. A MATLAB code has been written with the purpose of estimating the mass of the blade after a variation of the applied loads, represented by the blade root bending moment. In the approach used for this study, for the bending load calculations along the entire blade, a triangular load distribution acting on the blade has been assumed, which yields the same bending moment at the root.

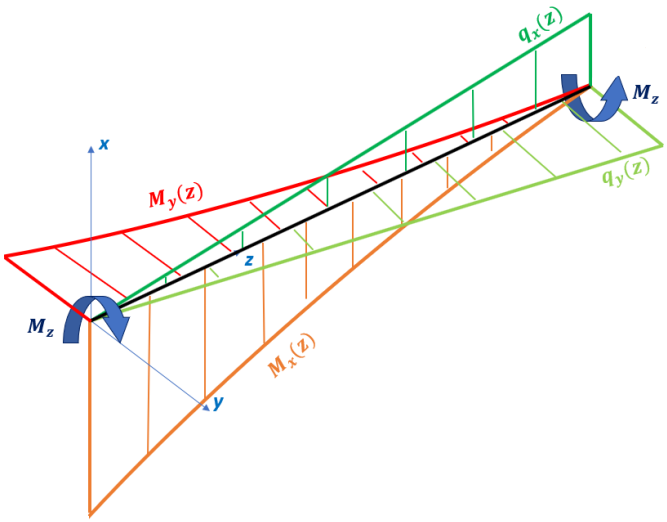

Figure 7. Qualitative distribution of loads and moments acting on the blade.

For each blade section, the external geometry is considered fixed, in order to avoid variation in the aerodynamic behaviour; the only parameter varied throughout the procedure is represented by the blade shell thickness. Starting from a given input geometry, schematically shown in Figure 8, defined by

- chord distribution;
- twist angle;
- section airfoil geometry;
- initial thickness;

an estimate of the stress distribution along the blade is assessed.

The procedure also assumes a simplified equivalent shape of the sections. In order to simplify the analysis, a rectangular section with sectional inertial characteristics equal to the ones of the real blade is considered.

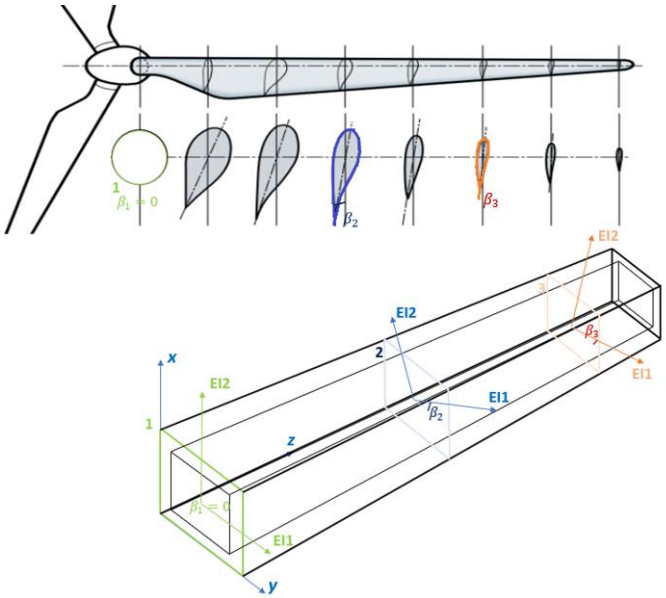

Figure 8. Blade section distribution and simplified equivalent rectangular beam representation.

Assuming given material characteristics, typical of glass fibre of common use in blade construction, the maximum stress and fatigue design criteria have been considered also for the blade. Once the new set of blade root loads are known (both DEL and maximum loads), the algorithm searches for a modified thickness distribution which preserve the same safety margins as the original configuration. With the new thickness distribution, the modified blade material volume and mass are estimated.

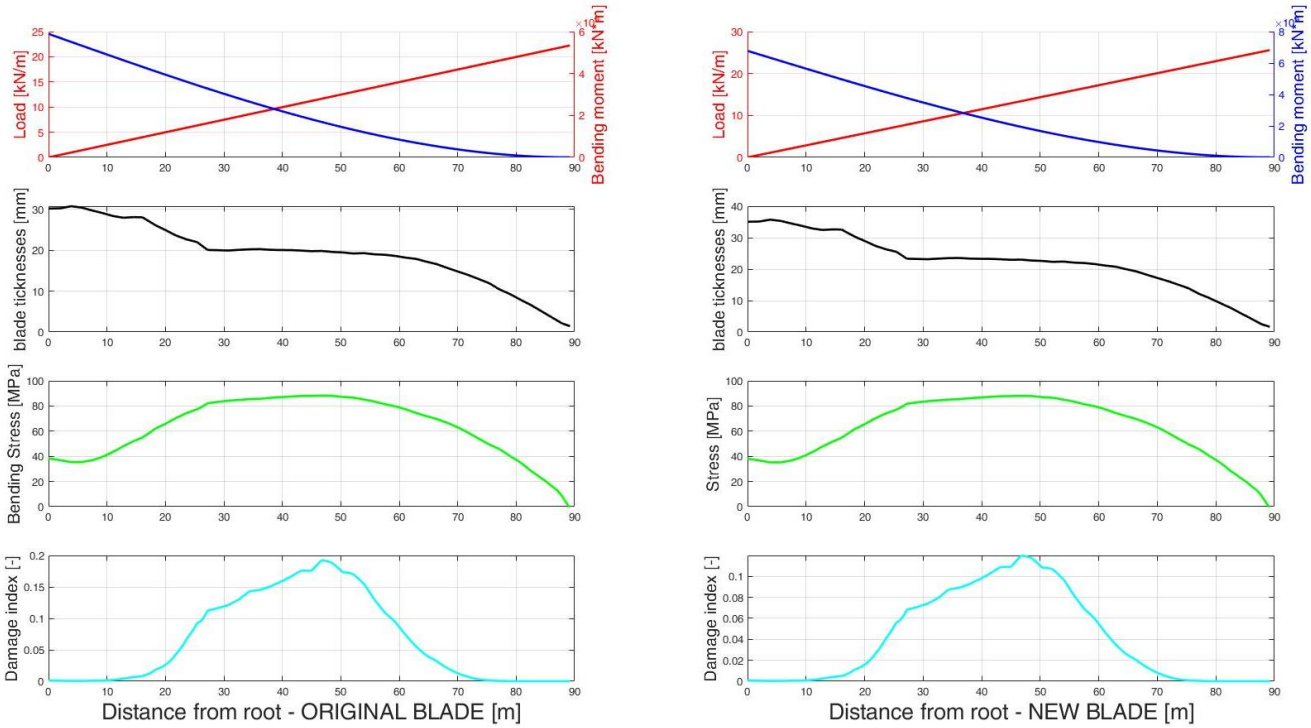

Figure 9. Results of the algorithm for the simplified blade structural modelling. Baseline stress distribution on the left, target distribution for modified case on the right.

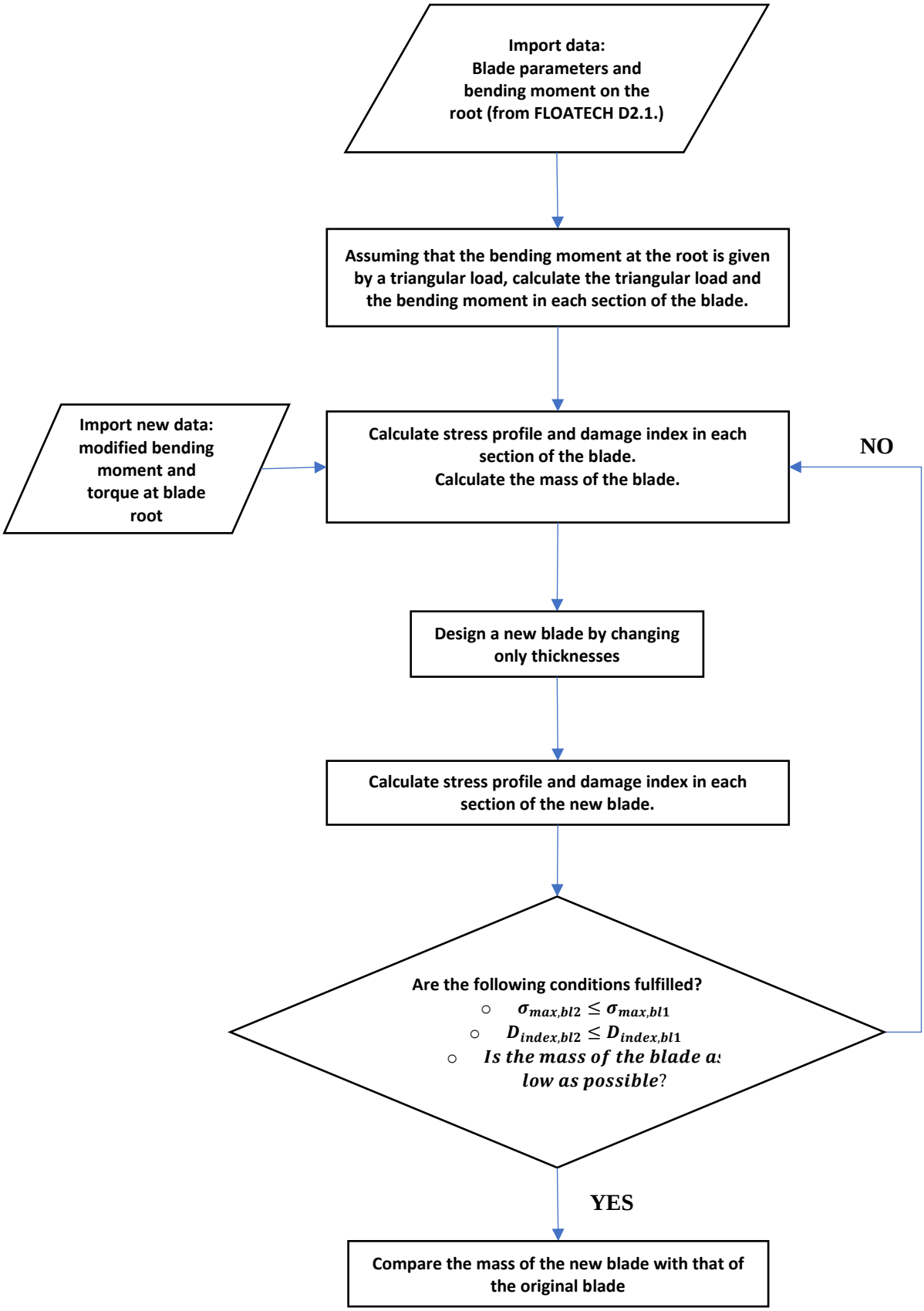

Figure 10. Description of the algorithm for the simplified structural model of the blade as a function of applied loads and DELs.

In the above flow chart, the symbols indicate in Table 2 have been used.

Table 2. Symbol definition (for blade design algorithm).

$\sigma_{max,bl1}$ / $\sigma_{max,bl2}$	Maximum stress in the baseline blade / modified blade
$D_{index,\ tow1}$ / $D_{index,\ tow2}$	Maximum damage index in baseline and modified blade

As for the tower, also in the case of the blade, in order to simplify further analyses, the effects of the separate variations of maximum loads and DELs have been investigated. The results of the analyses for the blade mass trends are shown Figure 11 and Figure 12. A similar approach has been used as in the case of the tower, considering the following feasibility conditions

- $\sigma_{max,bl2} \leq \sigma_{max}$ (for DELs variation)
- $D_{index,bl2} \leq 1$ (for maximum loads variation)

where σ_{max} is the considered stress limit for the blade (assumed equal to 300 MPa, for a fiber glass material).

Similar trends can be observed for the mass variations associated to fatigue and maximum loads. In the assumed simplified procedure, only the blade thickness is changed based on the section stress level. An almost linear trend in the relationship between load and mass can be observed for both the fatigue and maximum load variations.

Both diagrams show an elbow on the load reduction side, due to the fact that the mass of the blade cannot decrease further without violating the constraint on the maximum stress (Figure 11) or the constraint on damage index (Figure 12).

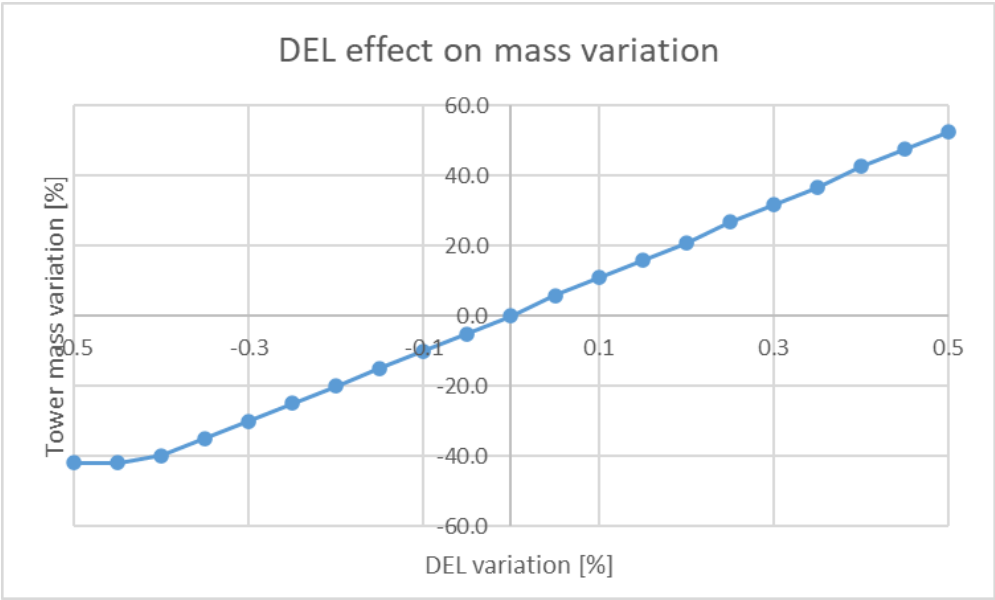

Figure 11. Effect on blade mass of the variation in blade root bending moment DEL.

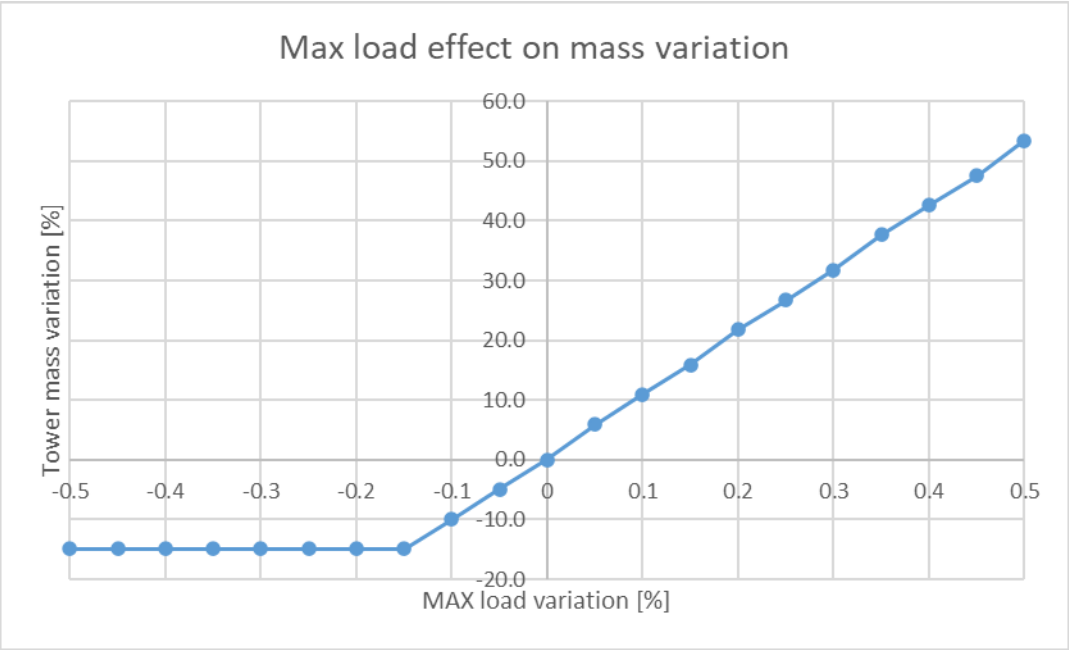

Figure 12. Effect on blade mass of the variation in blade root bending moment maximum load.

5.4 SELECTION OF PLATFORM DESIGN PARAMETERS

The model considered for the analysis is based on the Softwind spar buoy platform. The external dimensions of the platform are considered fixed, being related to the hydrostatic and hydrodynamic behaviour of the buoy used for the estimation of the overall FOWT response. The main dimensions are reported in the Figure 13.

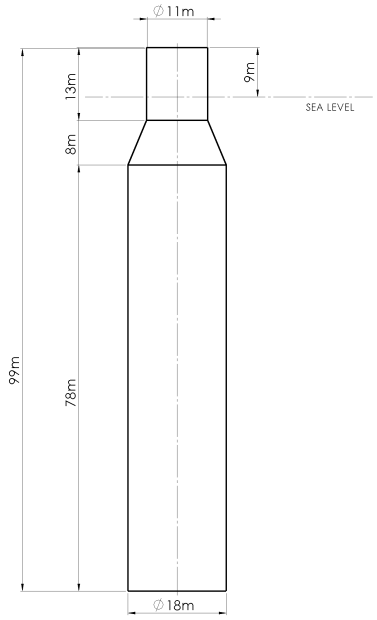

Figure 13. Softwind spar buoy platform external dimensions.

The simplified design parameter choice procedure for the platform includes the following steps:

1) choose the thickness of the main section of the spar buoy as design parameters for the preliminary assessment;
2) consider the following set of loadings on the spar buoy structure:
    - mooring line loads;
    - hydrostatic and hydrodynamic loads;
    - tower base loads;
3) set up a FEM model of the system with the given load set (a simplified, coarse mesh, shell elements model is deemed sufficient for the preliminary analysis considered in this work and allows a larger number of analyses to be performed in the next step);
4) run a set of FEM analysis for a number of combinations of the considered model parameters (loadings and thickness); in order to explore a significant set of combinations, a design of experiment (DOE) approach has been used; specifically, a Latin hypercube technique has been used to the define a set of parameter combinations; subsequently, a FEM analysis is run for each input combination in order to evaluate the maximum equivalent stress in the structure. The results of this analysis are used to get an explorative survey of the main dependencies between the configuration parameters and the maximum equivalent stress in the structure. A simplified approach has been assumed for the estimation of the wave loads; in particular, a regular wave condition has been considered (with wave height H=3 m and period T=8 s, assumed as approximately representative of the average site climate) and the resulting hydrodynamic loads have been applied to a structural model of the platform together with the moments at the tower base and the loads applied at the fairlead by the mooring lines. Wave loads are considered over a wave period and the maximum stress in the cycle, resulting from the combined loads, has been considered. The wave loads accounts for the hydrostatic and hydrodynamic actions (comprising the radiation and diffraction contributions). The tower base and mooring loads are varied in the design exploration process, together with the thickness of the main spar components considered in the study; for each combination of loads a static analysis has been performed for the;
5) determine the “iso-stress” contours in the parameter space: find the curves which join the combination of parameters with the same stress level; once the reference stress level is known for the reference configuration and the load sets are known for the configuration including the new control technique, one can search, within the parameter space, a different thickness combination which ensures the same stress level under a different set of loads;
6) once the new thickness combination has been determined, the variation in weight of the structure can be estimated; the cost of the new configuration is evaluated as a linear function of the material weight used for structure manufacturing, possibly accounting for a complexity factor to consider the amount of work needed for different elements of the platform.

The parameter used in the analysis to represent the stress state in the structure depends on the type of loading conditions to be considered: for the maximum loads the von Mises equivalent stress has been used, while for the fatigue analysis the maximum principal stress has been taken into account. These

parameters are expressed as a function of the principal values of the local stress tensor, generally denoted as σ_1, σ_2, σ_3. The von Mises stress, σ_{eq}, is defined as

$$\sigma_{eq} = \sqrt{(\sigma_1 - \sigma_2)^2 + (\sigma_2 - \sigma_3)^2 + (\sigma_3 - \sigma_1)^2}$$

while the maximum principal stress is simply defined as the value of the larger principal stress in absolute value.

A possible set of thickness parameters of interest for the considered configuration is indicated in Figure 14. In the case under examination, the areas deemed more likely to be influenced by the change in control strategies are located

- near the tower base, for which changes in the control strategy could, in principle, produce effective variations of the thrust and the platform pitch response, thereby, affecting the tower base loads;
- near the fairlead locations, in order to account for possible variation in mooring line tensions.

The range of variation of the applied loads is defined based on the results for the DEL (Damage Equivalent Load) analysis performed in Floatech WP2, considering a range comprised between about one half and the double of the predicted baseline loads.

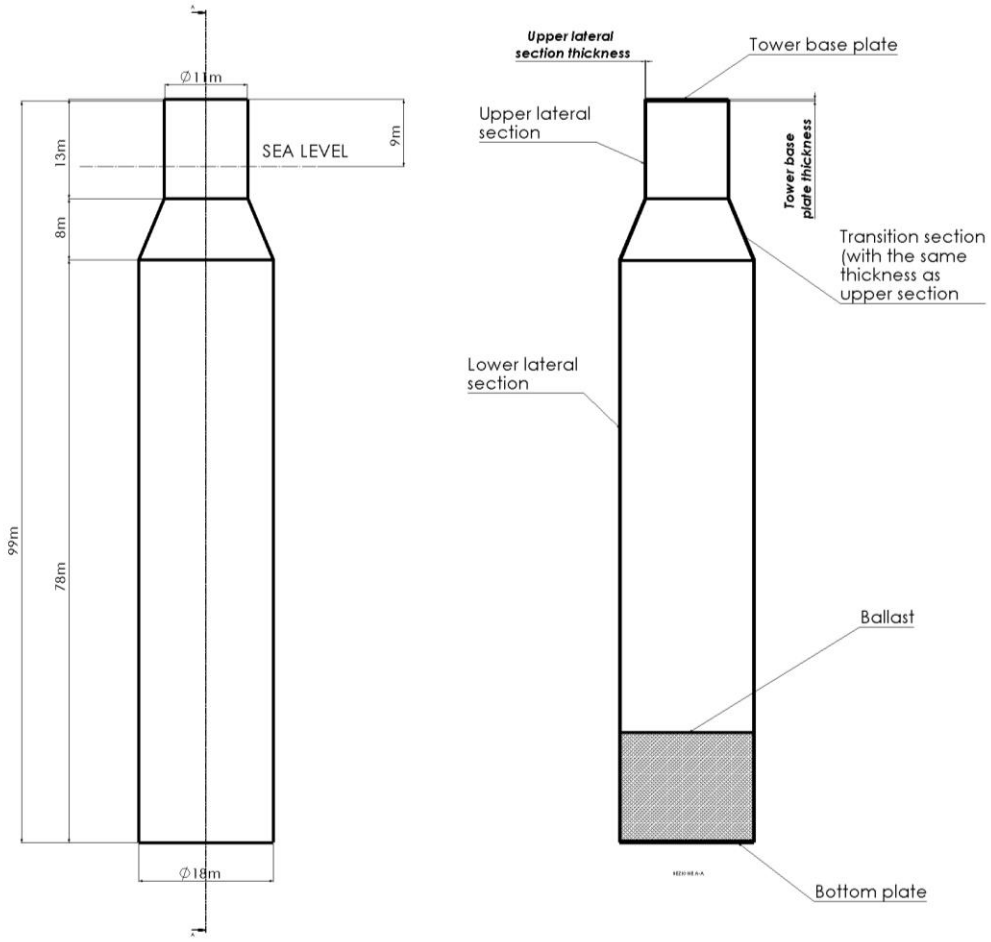

Figure 14. Location of the thickness values assumed as parameter in the model. (The thickness in bold in the figure have been considered in the estimation of mass modification due to load variation).

An initial wide range exploration of the design space has been performed considering all the aforementioned variables. The ranges of variation of the considered parameters are indicated in Table 3.

Table 3. Parameters' variation range.

Parameter	Min	Max
Roll tower base moment (Nm), M_x	20e6	200e6
Pitch tower base moment (Nm), M_y	20e6	200e6
Mooring line forces (kN)	50	200
Base plate thickness (m), t_b	0.15	0.55
Transition section plate thickness (m), t_t	0.15	0.55
Mooring reinforcement plate thickness (m), t_t	0.08	0.12

Together with the external local actions at the tower base, a pressure distribution along the spar buoy is also considered based on a regular wave, considered approximately representative of a normal sea state condition, with amplitude of 3 m and period of 8 s. . The use of a regular wave is based on consideration about the computational cost of long irregular sea state simulations, impractical for the limited amount of resource and too demanding for the purpose of the analyses, which is not oriented to a final design but only to a preliminary cost-oriented study.

Moreover, another approximation is related to the treatment of the mooring lines in the simulation of wave loads: it was not possible to simulate the exact mooring line configuration of the Softwind platform, comprising a delta connection, with the available wave-body interaction software code. Thus, the simulation has been performed using a simplified mooring line system with three catenary lines with the same position of the anchoring points and a length equal to the overall mooring length comprising the bridles. Anyway, this modification is deemed acceptable in the assumed approach for two reasons: on the one hand, as already stated, this treatment only serves for the assessment of the effect of wave loads in a preliminary design and, as such, does not require a fully detailed simulation of the final configuration; on the other hand, the correct simulation of real mooring line loads will, anyway, be taken into account using the simulation results from QBlade-Ocean, which will take into account the effective mooring line configuration.

The results of the DOE analysis are reported in Figure 15 considering as output variable the maximum equivalent Von Mises stress. It can be noticed that the chosen design parameters, which are considered more significantly affected by the control action, have a relatively small impact on the overall output stress variable. The reason for the observed lack of sensitivity may be related to the fact that, for the spar buoy under the assumed loading conditions, the overall maximum stress level can be found in the lower part of the platform and seems to be influenced more by the hydrostatic and hydrodynamic actions than by the tower base loads. Thus, the control load variations are expected to have, in turn, a relative lower impact on platform weights and costs, at least in the limits of the present preliminary analysis.

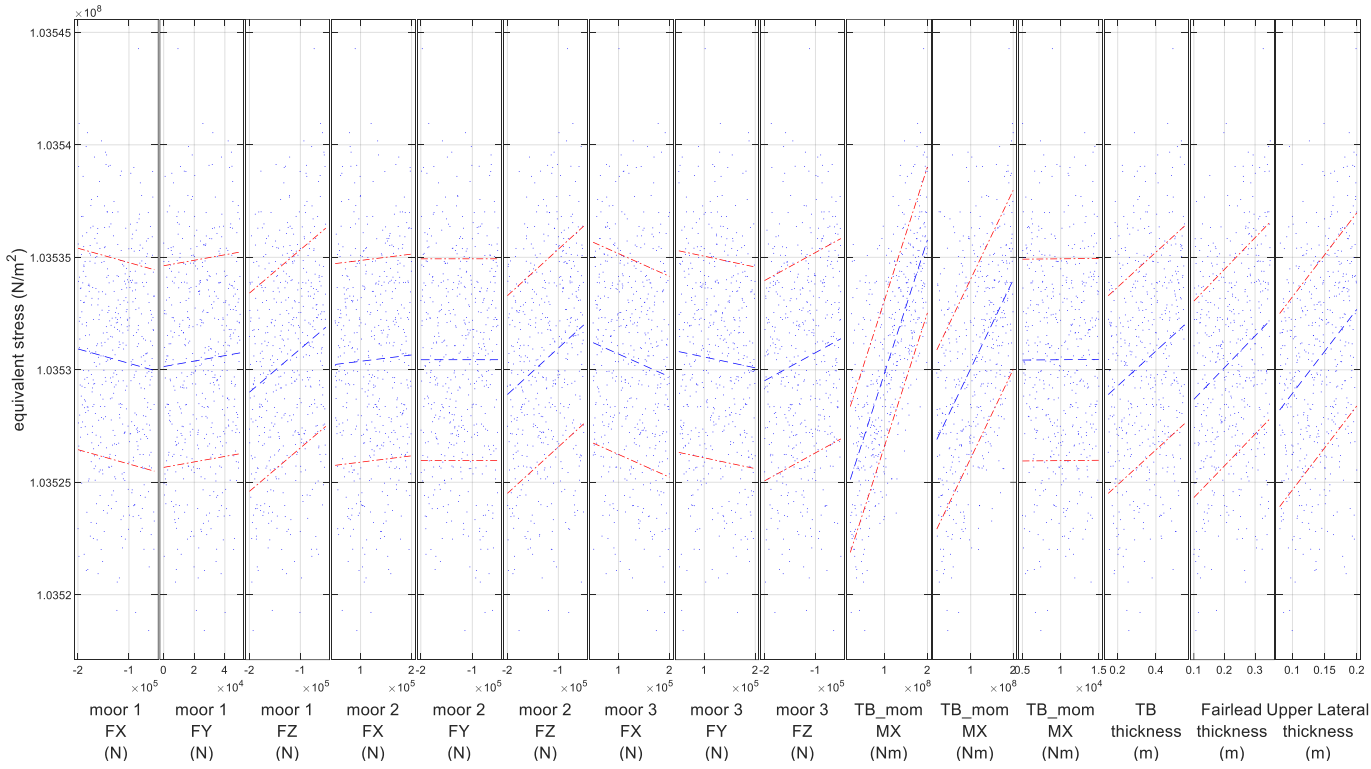

Figure 15. First exploration of the global design space using a DOE technique, considering the maximum equivalent stress as output variable. (Small variations of the maximum stress can be observed on y axis for the explored set of variables).

It has to be noted that this result on the influence of loadings on platform weight is strictly related to the configuration chosen for this study: different platform concepts and different structural interface between tower and platform may exhibit different behaviour.

However, in order to get an estimate of possible local effects on the weight, a more detailed analysis can be performed, observing the relation between the considered loads and the local geometric characteristics of some chosen areas, deemed more interesting. Thus, the results of the above reported FEM study are analysed with respect to the local stress and thickness for a set of subcomponents of the platform.

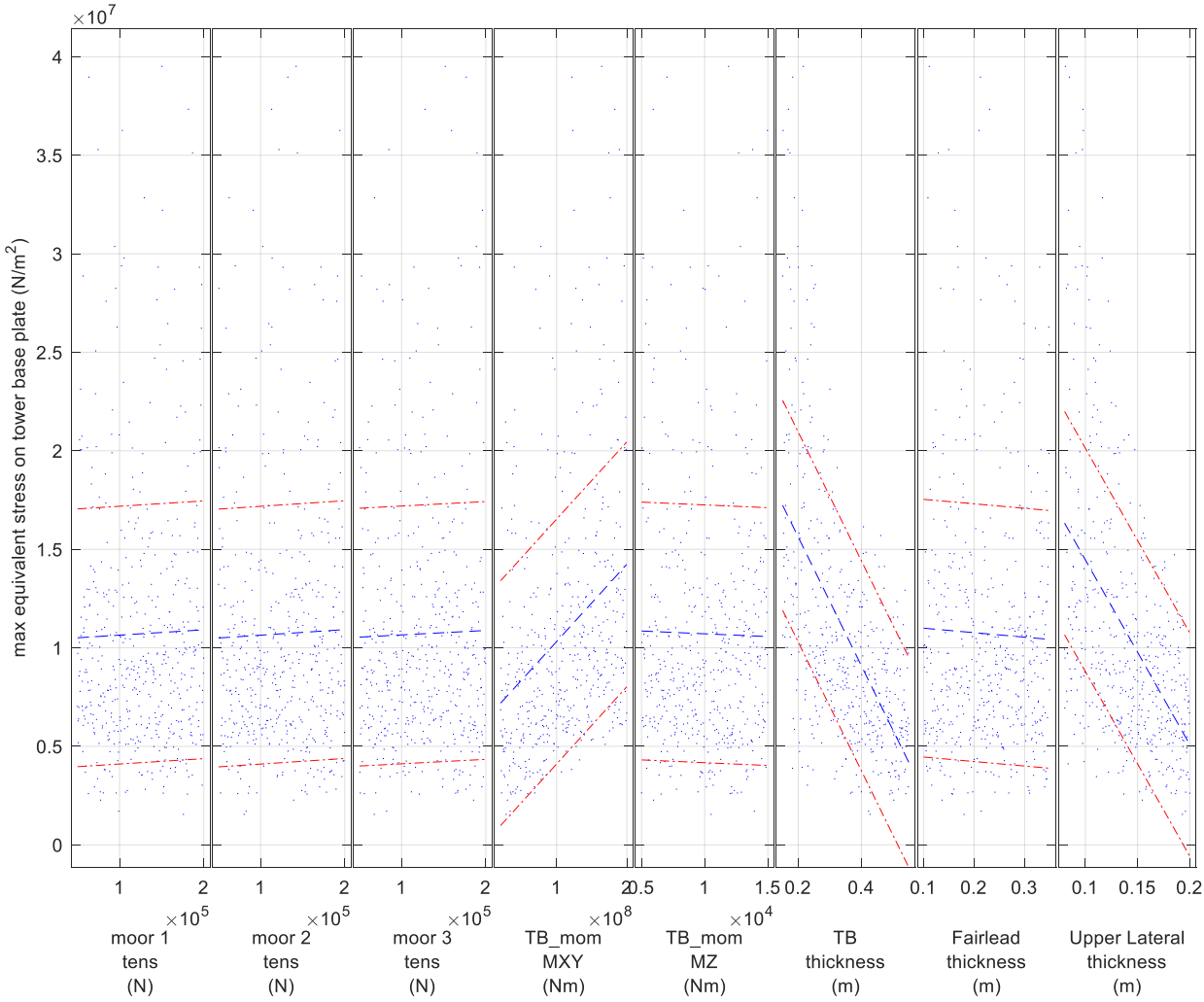

Figure 16. Exploration of the restricted design space related to tower base loads and thickness. A larger significance can be attributed to the relation between tower base bending moment and tower base plate thickness.

In particular, the top of the platform is assumed to be consisting of a plate with given thickness linked to the tower base. The local stress over such plate has been estimated for all the DOE test cases. The more significant loads acting on this structural feature are, as expectable, the tower base moments, here represented by the combined bending moment $M_{xy_{TB}}$ at the tower base. Indeed, considering the relation between tower base plate thickness and tower base bending moment a more significant relation can be inferred, as illustrated in Figure 16. In this figure, the effects on the equivalent von Mises stress are illustrated for the following parameters:

- the mooring loads;
- the tower base bending moment;
- the tower base plate thickness;
- the upper lateral section thickness.

The denominations of the considered areas are illustrated in Figure 14.

A statistical regression approach is applied to the analysis of the correlation between loads and thickness, as illustrated in Figure 17. This figure represents a scatter plot obtained from the design exploration

analysis, relating the Von Mises equivalent stress observed on the tower base plate, the tower base plate thickness and the tower base bending moment.
A regression plane is fitted to the scattered data, allowing to find a simple analytic expression for the relation between bending moment and design thickness, represented by the constant stress contour lines indicated in the figure.

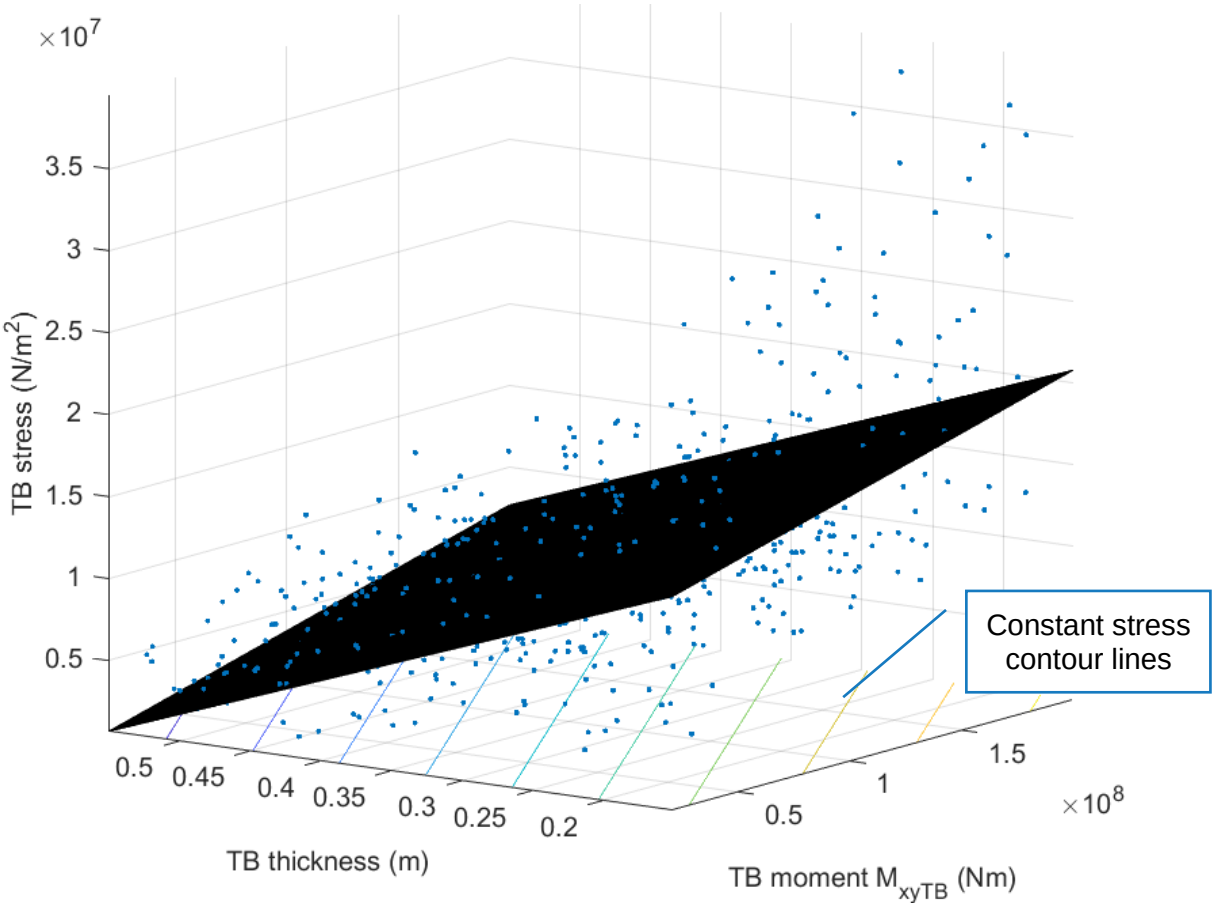

Figure 17. Regression relation between considered loads and the design variable. Example of application to the tower base plate. The considered design variable is the tower base plate thickness, the considered significant load is the combined tower base moment, the output parameter is the stress in the tower base plate.

Although a general trend can be arguably found, a large dispersion of the results can be observed. This approach is, in fact, only useful to roughly estimate the expected configuration variations and, as repeatedly stated, a full design assessment requires further and more detailed redesign studies, outside the scope of this analysis. Moreover, one of the reasons for the observed large scattering is the dependence of the estimated stress values on several variables not explicitly represented in the plot and not explicitly accounted for in the regression model, which, for simplicity, considers only the thickness and the tower base moment. The result of this regression will be used to find constant stress curves

(indicated in Figure 17) and predict an expected variation of the thickness needed to preserve a constant stress level for a given variation of the loading conditions.
The procedure for the determination of the modified thickness is illustrated in Figure 18. The slope of the constant stress line can be used to estimate the required variation in thickness associated to a given load variation.

A similar approach can be applied to other areas of interest with the structure. For the geometry considered in this problem, a graph similar to the one in Figure 18 is reported in Figure 19 for the relation between the tower base bending moment and the thickness of the upper lateral section.

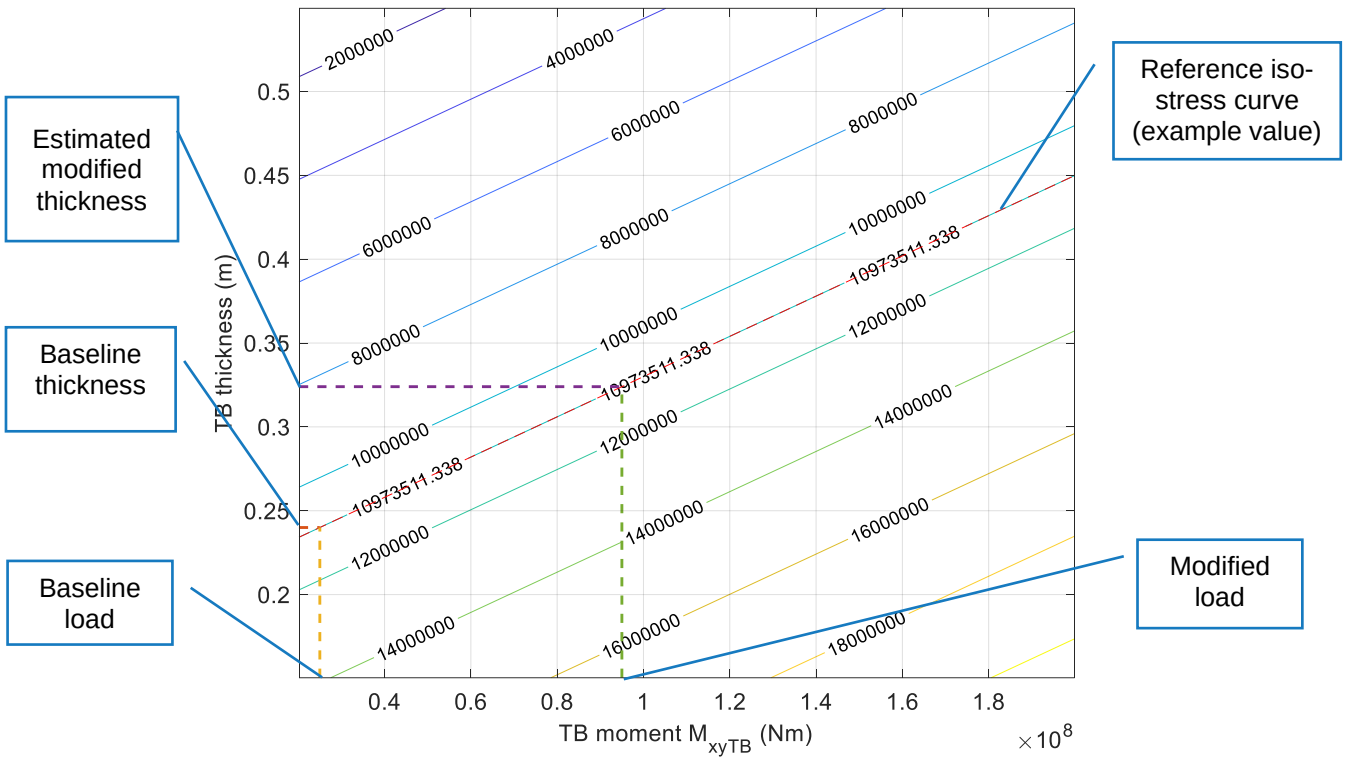

Figure 18. Procedure for the estimation of the modified thickness for the case of the plate at the tower base (top of the platform). (Values shown are only used to exemplify the procedure).

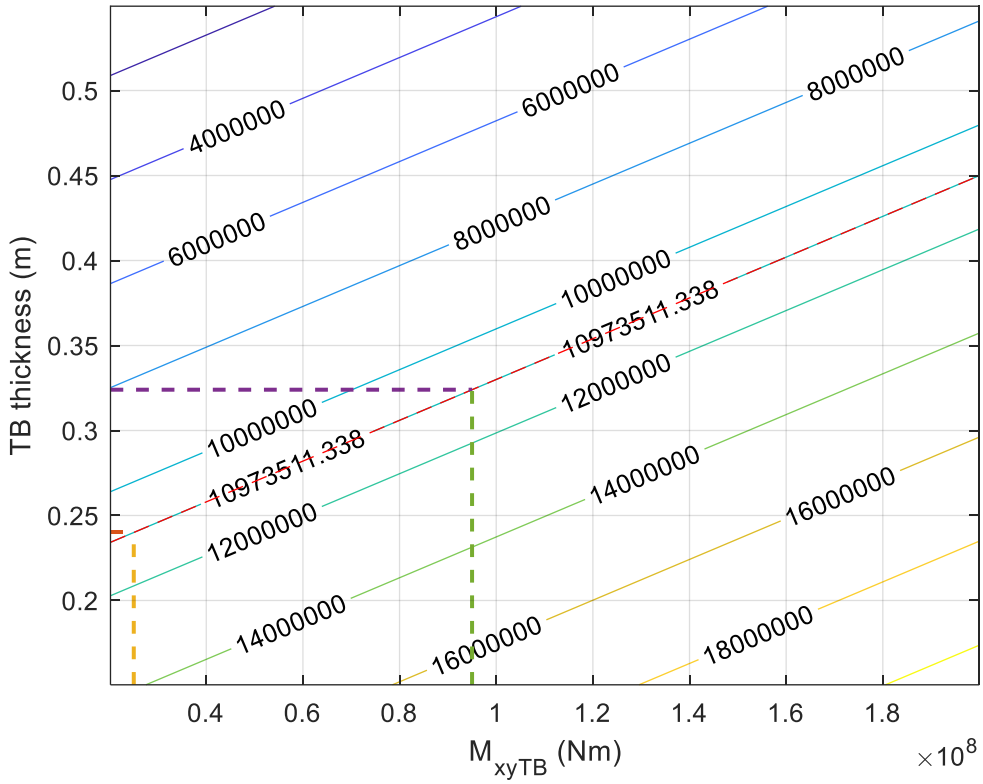

Figure 19. Procedure for the estimation of the modified thickness for the case of the upper lateral section (between transition and top of the platform). (Values shown are only used to exemplify the procedure).

A similar approach could be used also for the thickness of the reinforcement areas around the fairlead attachment points. Anyway, the effect of mooring loads seems to be relatively smaller compared to the effect of tower base load and, on the other hand, the contribution of this zone to the overall mass and costs is considered small.

Furthermore, although the above examples refer to the equivalent Von Mises stress, oriented to maximum load analyses, a similar approach can be assumed for the fatigue analyses, by considering the maximum principal stress instead of the equivalent stress.

The final result of this search is represented by a set of scaling coefficients, which represent the variation of required thickness for a given variation of loads, needed to preserve the same safety level of the assumed initial geometrical configuration. For the present case, the thickness scaling factors for load variation reported in Table 4 have been estimated.

Table 4. Thickness scaling factor.

	Maximum stress (m/Nm)	**Fatigue stress (m/Nm)**
Tower base plate thickness-to-load ratio	2.2574e-07	4.0573e-08
Upper lateral section thickness-to-load ratio	3.7777e-08	4.0085e-08

5.5 EFFECTS OF MOORING LOADING

5.5.1 Mooring cost estimation

In order to account for the effect of mooring loads variation, a mooring chain system has been considered in this study and the variation of the chain section has been analysed with a procedure similar to the size adjustment procedure used for the platform configuration. The mooring chain characteristics are mainly defined by its nominal diameter d_c (the diameter of the steel bar from which the links of the chain are formed), which is related to the main mechanical properties of the chain line. Some standards (such as [16]) give expressions for the relation of the Maximum Breaking Load (MBL) of the chain to the nominal section diameter. The considered standard defines different chain classes, in the present work an R3 class chain has been considered, for which the following relation between MBL and nominal diameter can be assumed

$$MBL = 0.0223\, d_c^2\, (44 - 0.08 d_c)$$

According to [17] the cost of the chain and of the anchor can be related to MBL value, thus the present analysis will be oriented to give an estimate of the variation in MBL related to the mooring load variations. The set of diameters considered in the study is reported in the following figure together with estimated MBL values [18].

dc (mm)	MBL (kN)	dc (mm)	MBL (kN)	dc (mm)	MBL (kN)
34	1064.1	**82**	5613.9	**137**	13828.8
36	1188.4	**84**	5866.0	**142**	14676.8
38	1319.0	**87**	6251.9	**147**	15535.8
40	1455.7	**88**	6382.7	**152**	16404.6
42	1598.7	**90**	6647.2	**157**	17281.7
44	1747.6	**92**	6915.7	**162**	18165.9
46	1902.6	**95**	7325.8	**165**	18699.2
48	2063.4	**97**	7603.9	**168**	19234.3
50	2230.0	**100**	8028.0	**171**	19770.9
52	2402.3	**102**	8315.2	**175**	20488.1
54	2580.3	**105**	8752.5	**178**	21027.0
56	2763.7	**106**	8900.0	**180**	21386.6
58	2952.7	**107**	9048.3	**185**	22286.0
60	3147.0	**111**	9649.5	**188**	22825.4
62	3346.6	112	9801.8	191	23364.5
64	3551.3	114	10108.6	194	23902.8
66	3761.2	117	10574.4	197	24440.0
68	3976.1	120	11046.5	200	24976.0
70	4196.0	122	11364.7	205	25865.5
73	4534.8	124	11685.5		
76	4884.3	127	12171.5		
78	5123.0	130	12662.8		
81	5489.6	132	12993.3		

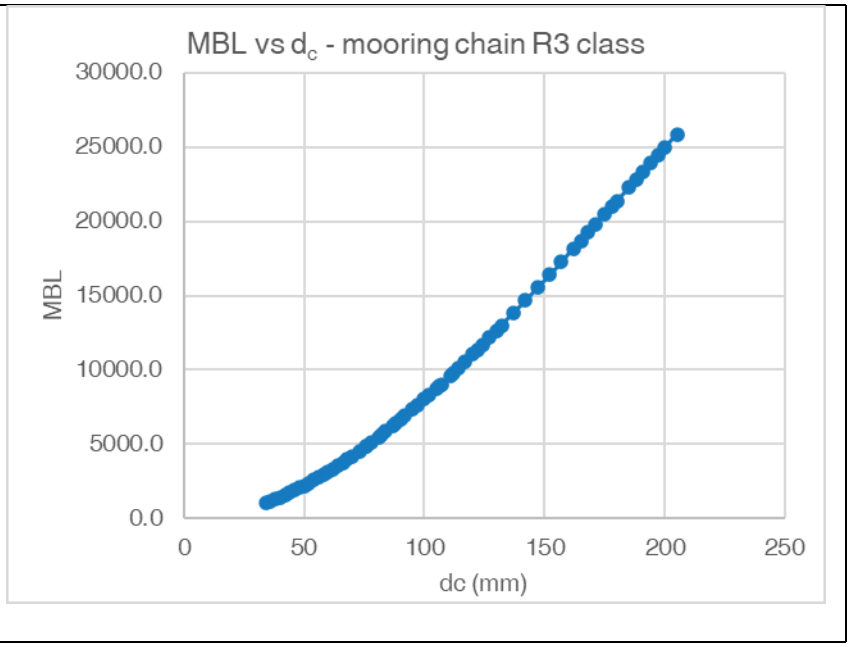

Figure 20. Assumed nominal diameters and Maximum Breaking Load.

The effect of a variation in maximum mooring loads will be accounted for by considering the variation of chain diameter with an MBL value which preserve the same safety factor as the original configuration.

In order to take into account fatigue stresses, a similar approach will be assumed estimating a modified chain diameter which ensure the same safety level against fatigue:

- first the damage index for the initial configuration will be estimated based on the mooring tension baseline DEL value and on the original diameter; the damage index, $\mathcal{D}$, is estimated as the ratio of the number of equivalent cycles, N_{eq}, for the considered DEL to the number of cycles to failure, N_f, for the stress cycle in the chain link, $\mathcal{D} = N_{eq}/N_f$;

- the stress cycle range, $\Delta\sigma$, is estimated considering the stress induced by the DEL applied on the nominal section of the chain link ($A_s = 2 \times \pi d_c^2/4$): $\Delta\sigma = \frac{Tension\ DEL}{A_s}$;

- the required number of cycles to failure, N_f, can be estimated as a function of $\Delta\sigma$ using the relation indicated in the standard [19]: $N_f = a_D \Delta\sigma^{-m}$, with $a_D = 1.2 \times 10^{11}$ and $m = 3$ for a stud chain;

- once the modified DEL load is known, the section of the chain is modified in order to obtain the same stress level or higher in order to preserve the same safety level.

5.5.2 Assumed mooring system characteristics

The characteristics of the baseline mooring system, are reported in Table 5. Both the configuration and length of the mooring system will be considered unchanged, but a possible variation of the chain section size will be taken into account according to the variation of mooring loads due to the effects of control strategy.

Table 5. Mooring configuration for the original Softwind case

	Baseline configuration
Overall arrangement	Three mooring lines with bridles and delta connection point
Mooring line length (m)	732 m (*)
Fairlead height	-13.4 m
Fairlead radial position (*distance from tower axis*)	10.4 m

(*) the total length of a single line here reported is defined summing the length of the mooring line after the delta connection and the length of the two bridles (636 + 48*2= 732 m) between the fairlead and the delta connection point.

6 SIMULATION RESULTS

In the proposed methodology for LCOE analysis, a simulation-based approach has been assumed: results from a simulation model in QBlade, implementing the AWC control strategy, are used to evaluate the loads and the power curve variations in comparison to the results of the baseline model, provided with a traditional pitch control system without the wave feed-forward enhancement.

6.1 PRELIMINARY STUDY OF THE EFFECT OF CONTROL SETTINGS

The AWC control operating parameters have been defined based on the results of a set of initial analyses. As mentioned above, two kind of control objectives can be set: a platform motion reduction strategy, which aims to reduce wave induced oscillations using the action of blade pitch variation, and a target rpm/power strategy, which has the aim to reduce the oscillations in output power thereby improving the quality of the power delivered to the grid.
The results of such investigation are summarized in the following figures in terms of a set of variables affected by the control behaviour:

- blade pitch;
- electric power;
- platform heave, pitch and surge motion;
- tower base bending moment;
- blade root bending moment.

The reported comparison is related to an above rated wind speed of 15 m/s, for normal turbulence conditions (according to IEC standard) and for fixed sea state characteristics with significant height $H_s = 5\ m$ and peak period $T_p = 12\ s$. The choice of the considered test environmental conditions is based on the consideration that during the development of the control such conditions has been frequently used both in simulations and experiments. Moreover, it has been noted, during the study, that larger effects of the control can be observed for the wind-wave codirectional cases; thus, for this comparison case study, the misalignment has been set equal to zero.

The denomination of the control modes is here indicated

- Mode 1: baseline control (feed-forward strategy not activated);
- Mode 2: Feed-forward control active, platform motion reduction mode selected;
- Mode 3: Feed-forward control active, power quality improvement mode selected.

The effect of control mode choice on blade pitch motion is shown in the following figure; a detail of the blade pitch time history, extending over 400 s, is reported in Figure 22. The gain in the compared cases is equal to 0.5.

The pitch variations due to the feed-forward control are superimposed to the baseline control (mode 1), which implements a standard power limitation control strategy.

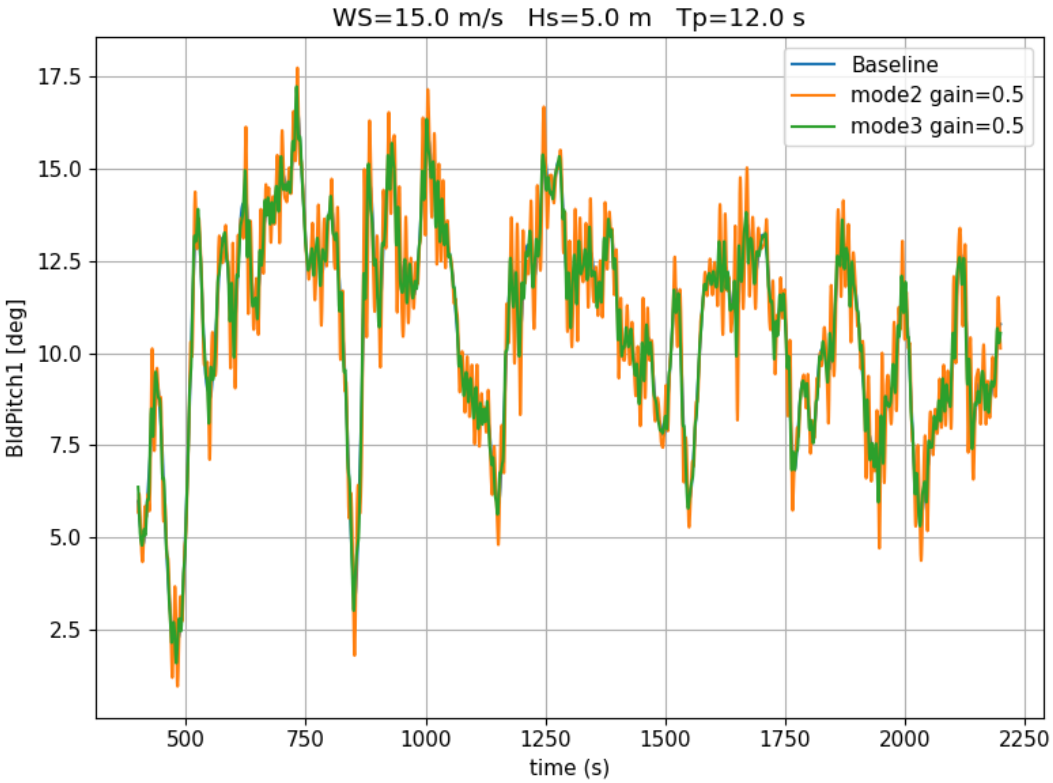

Figure 21. Blade pitch activation for different control modes.

It can be noted that significantly larger blade pitch oscillations are observed in the case of the platform motion reduction strategy.

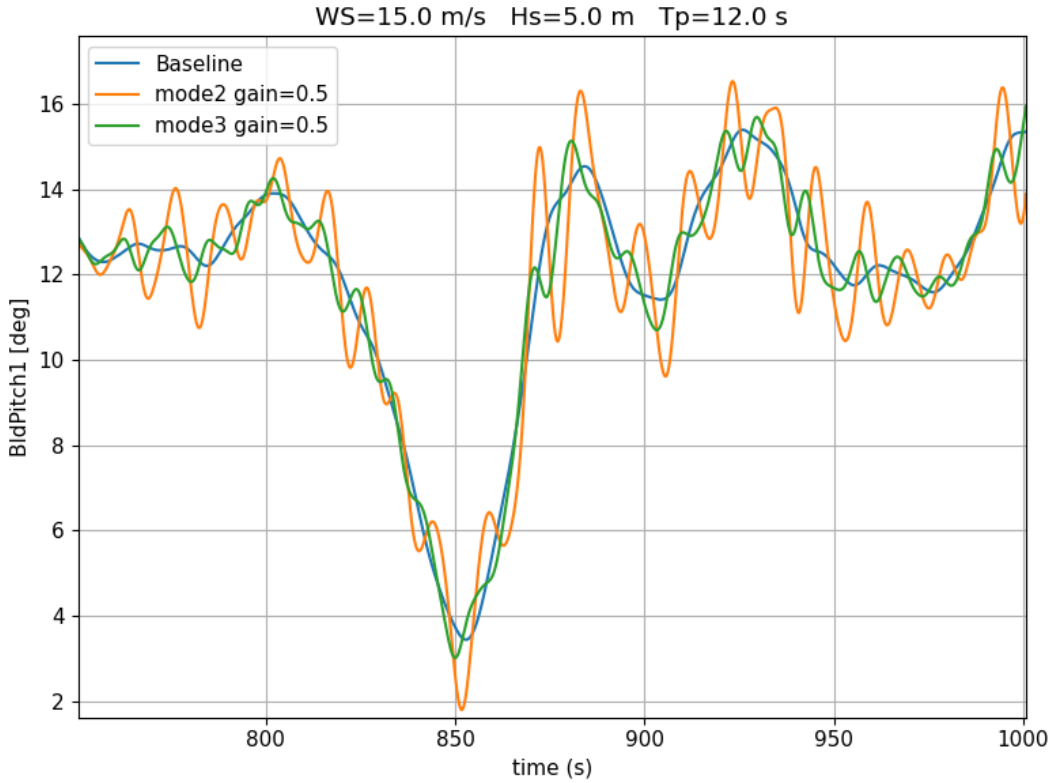

Figure 22. Blade pitch activation for different control modes. Detail.

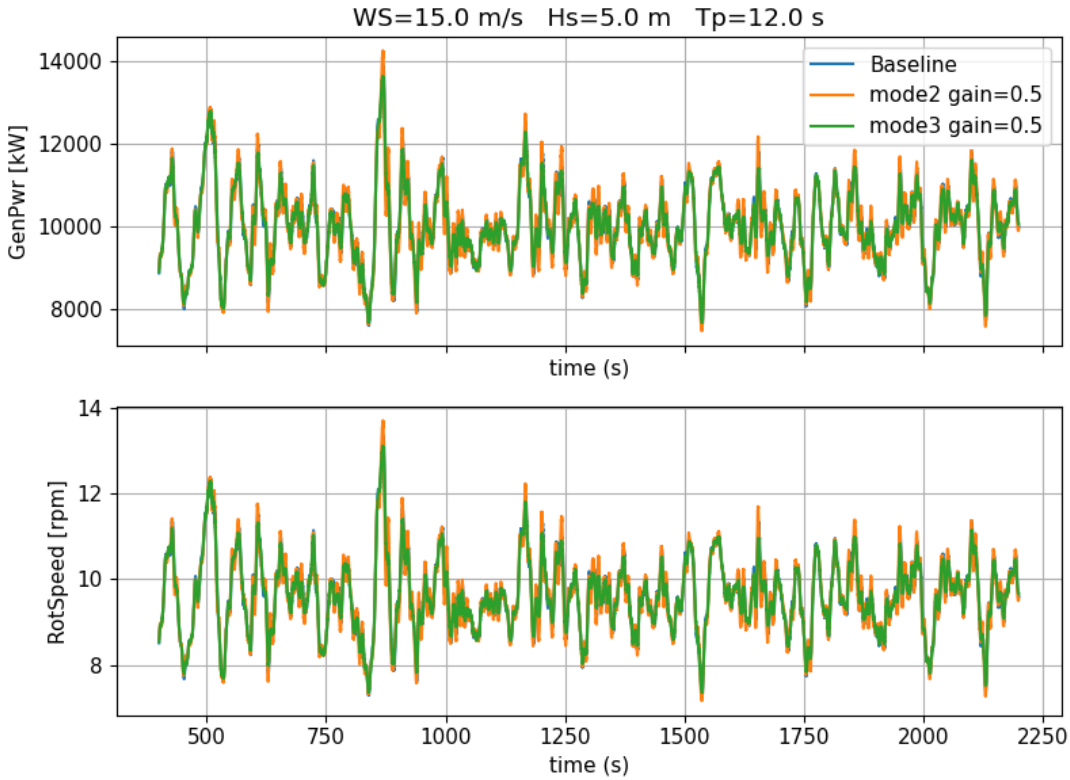

Figure 23. Power output and rotational speed for different control modes.

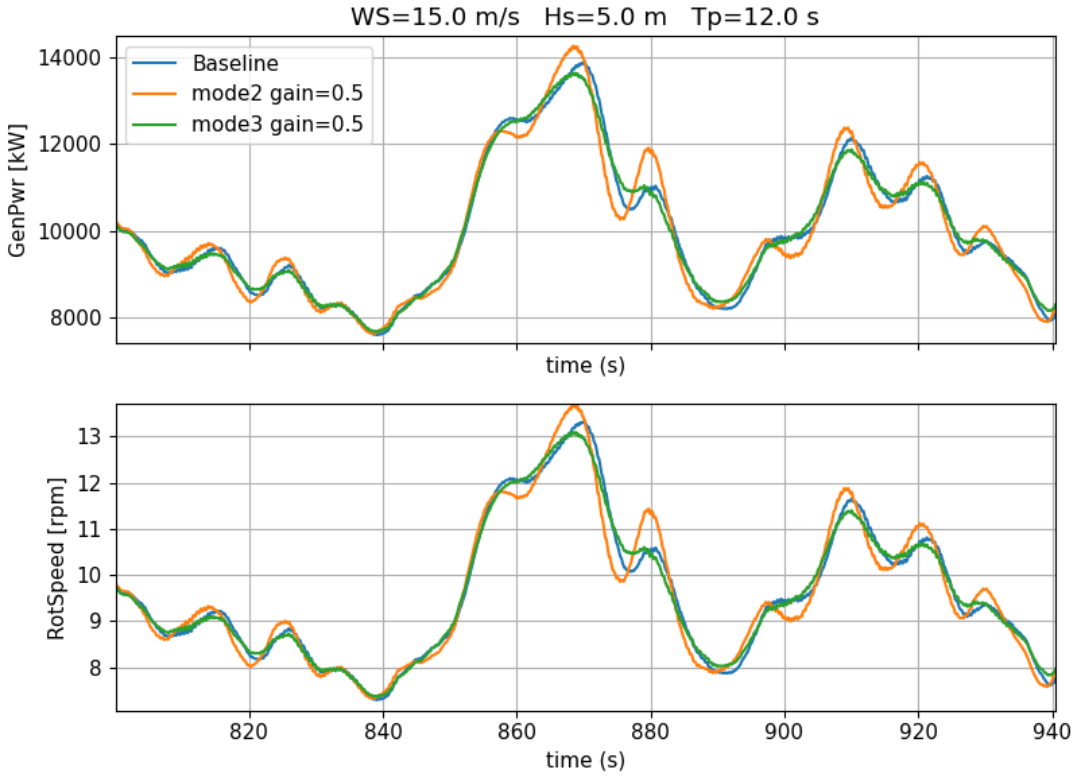

Figure 24. Power output and rotational speed for different control modes. Detail.

When comparing the power output, as shown in Figure 23 and in Figure 24 for a reduced time interval, it can be noted that rotational speed and power are essentially proportional, due to the constant generator torque assumed by the controller in the above rated regime. It can also be noted that, according to the different targets of the two control modes, larger power oscillations are observed in the case of the platform motion reduction mode. On the other hand, as expected, a slightly smoother trend in power and rotational speed can be seen for the power quality mode, confirming that the control strategy has been effectively implemented.

Larger oscillations can be observed for the reduced motion mode also in the case of the tower base bending moment, $TwrBsMyt$, shown in Figure 25 and Figure 26. The differences are anyway relatively small. As discussed in the introduction, this may be partially related to case study selected. In the case of a different floating foundation with respect to the spar used herein (e.g., a semi-sub), this gain could be potentially more significant. Even smaller differences are observed with respect to the tower bending moment for the power quality mode. A similar trend can be seen for the blade root bending moment, shown in Figure 27 and Figure 28. The motion reduction mode produces larger load oscillations, while the power quality mode seems to yield a slight reduction of the root bending moment fluctuations.
Platform motion, on the other hand, seems to be less affected by the control action, even in the motion reduction mode, as shown in Figure 29 and Figure 30 with respect to the platform heave, pitch and surge. The blade pitch variations required to obtain a larger effect on platform oscillations would too large and would likely produce larger load oscillations, as already observed for the blade root and tower base bending moments.

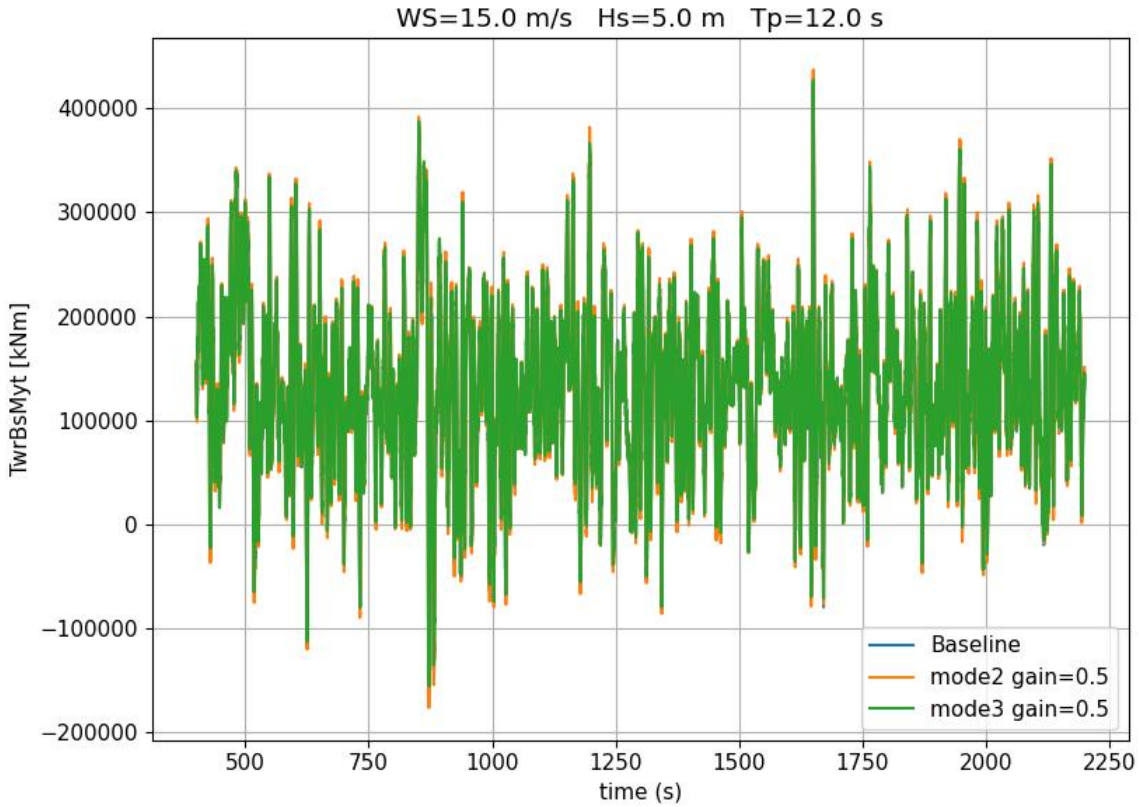

Figure 25. Tower base fore-aft bending moment for different control modes.

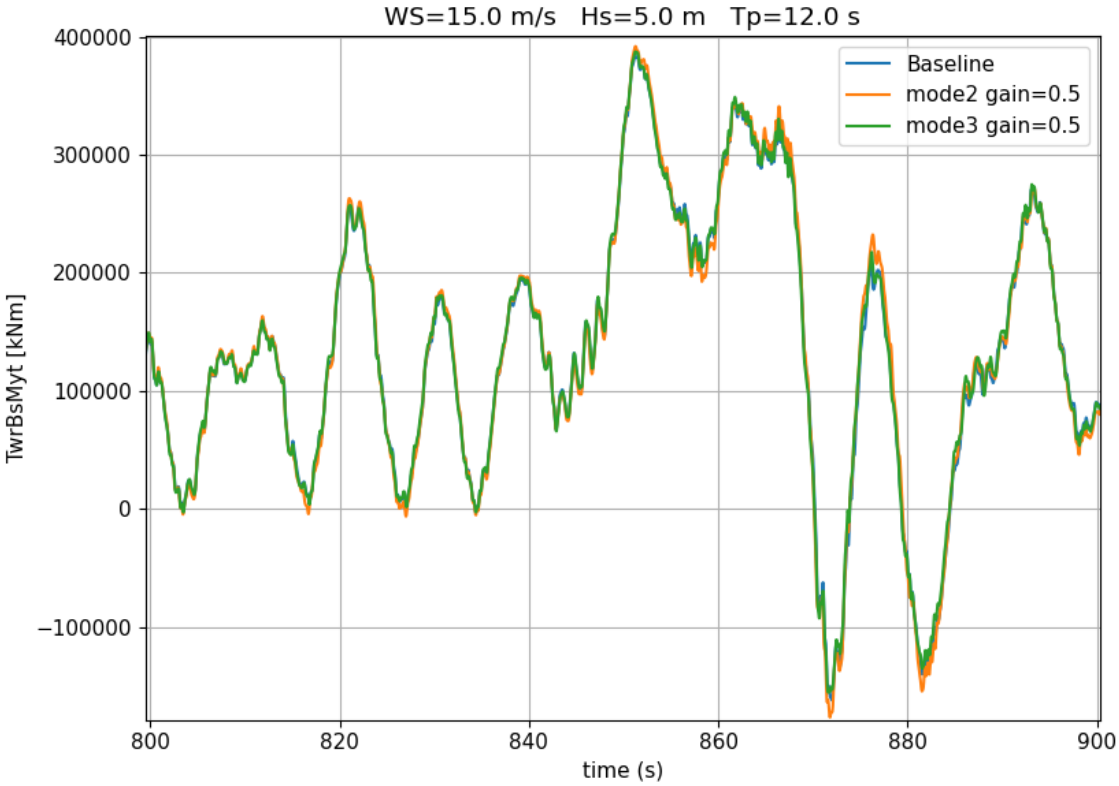

Figure 26. Tower base fore-aft bending moment for different control modes. Detail.

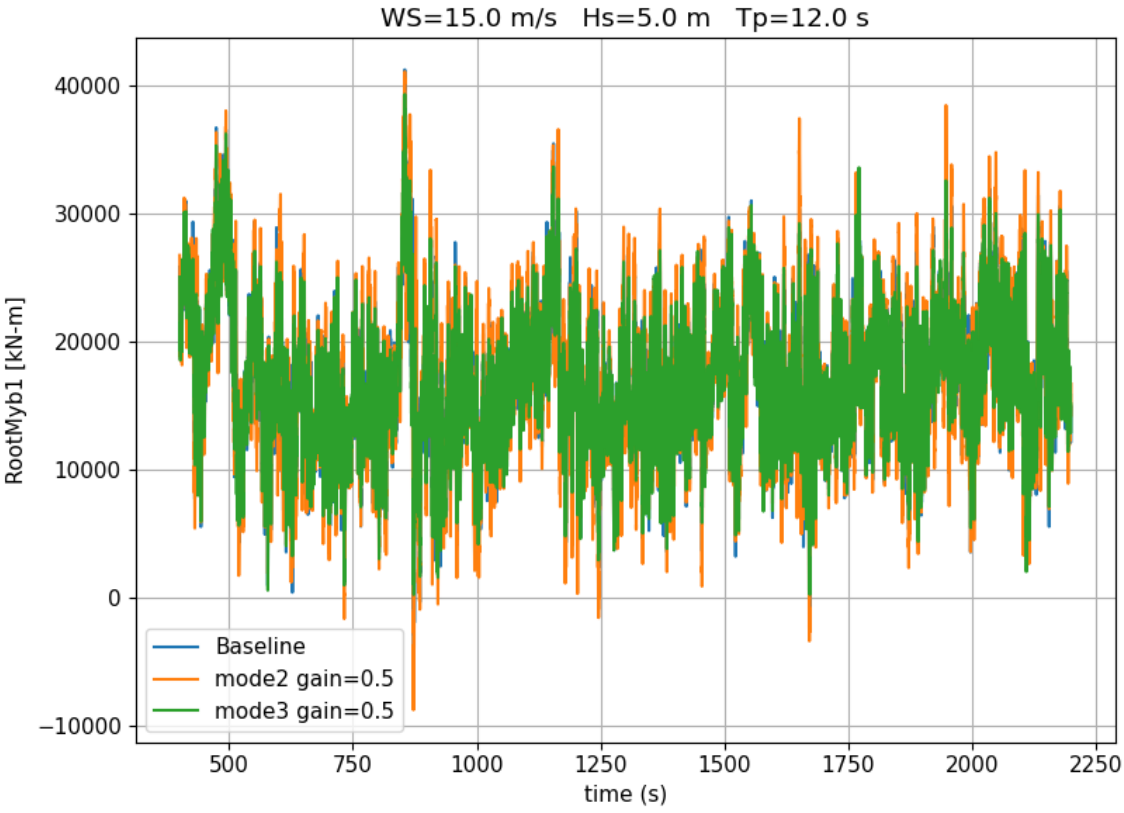

Figure 27. Blade root bending moment for different control modes.

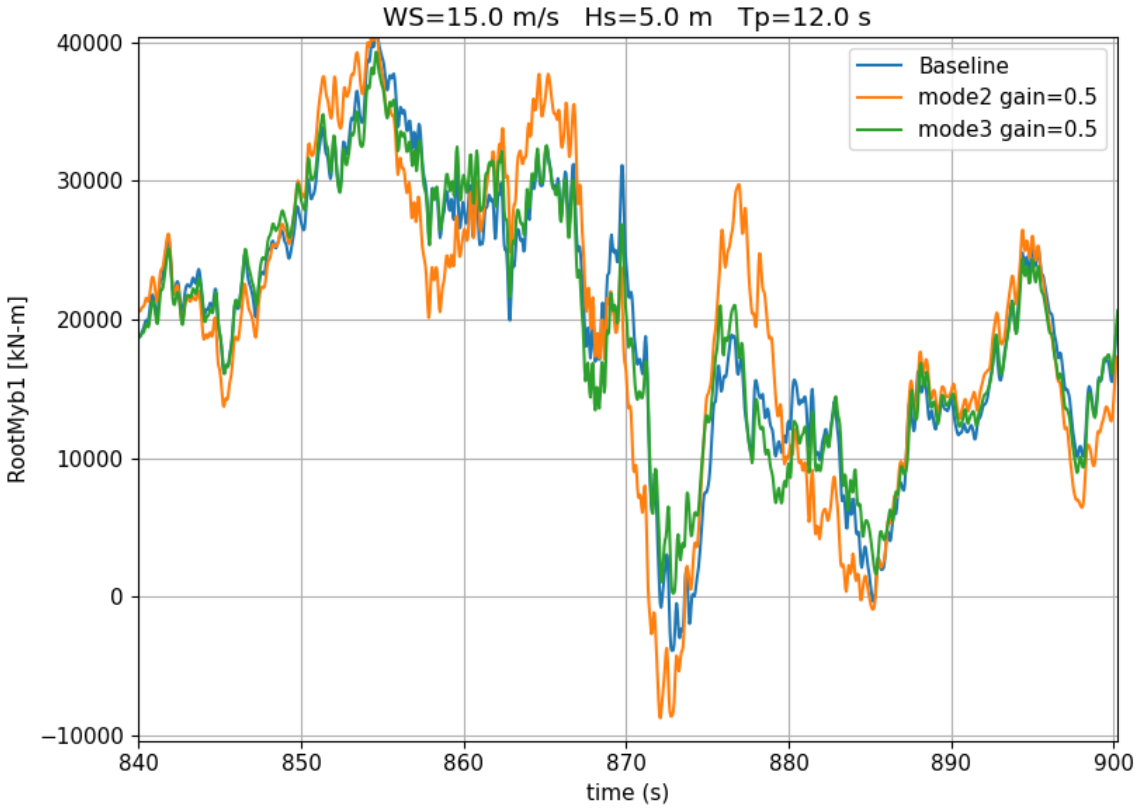

Figure 28. Blade root bending moment for different control modes. Detail.

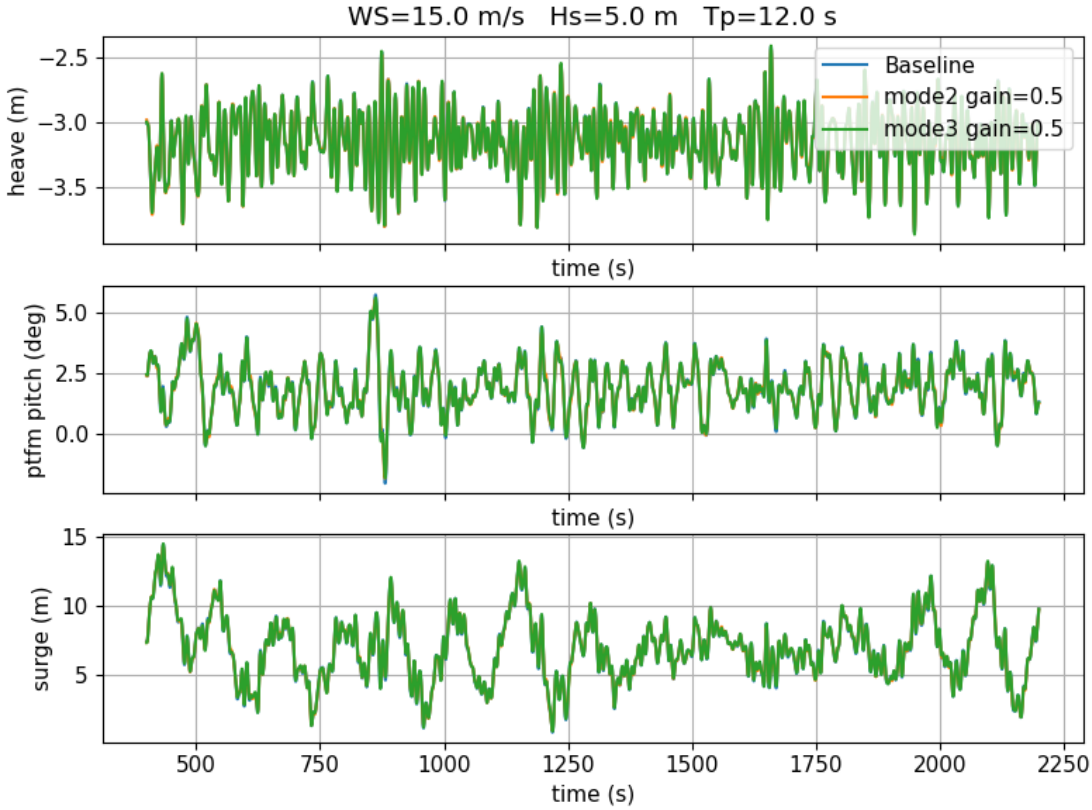

Figure 29. Platform motion for different control modes.

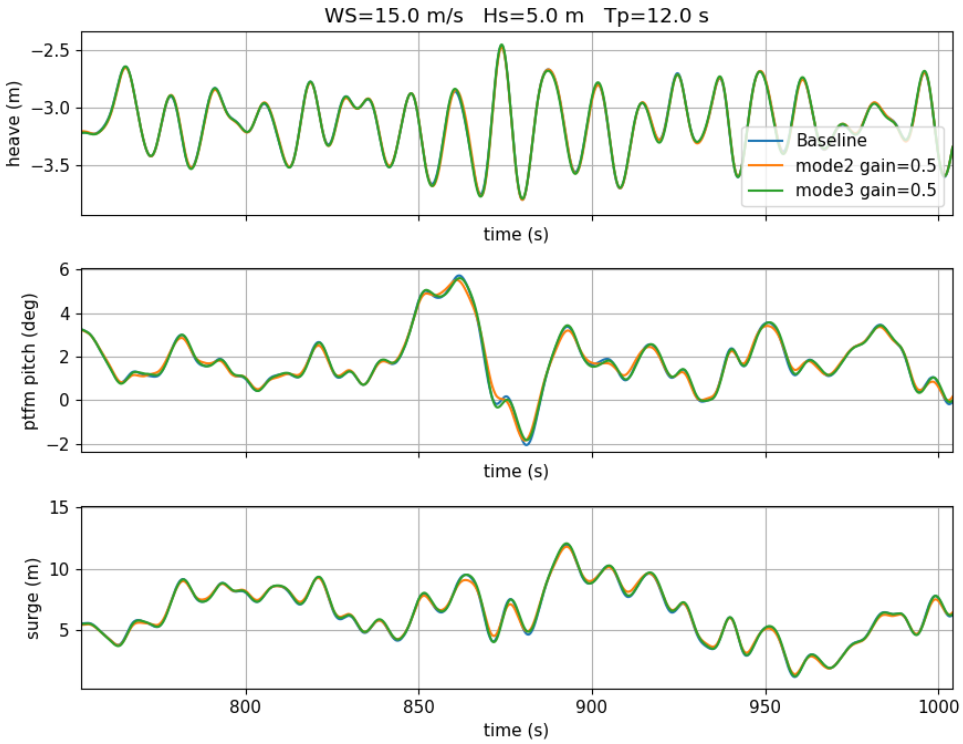

Figure 30. Platform motion for different control modes. Detail.

Beside the qualitative analysis of the trends reported above, in order to give a quantitative estimation of the differences between the different control modes, the standard deviations of the considered signals are reported in the table below.

Table 6. Standard deviation for the test cases comparing different control modes. (The percent variations with respect to the baseline case are shown in parentheses).

Parameter Name	mode1 gain=0.5	mode2 gain=0.5	mode3 gain=0.5
GenPwr [kW]	906.4	935.8 (+3.24%)	881.2 (-+2.79%)
RotSpeed [rpm]	0.870	0.898 (+3.24%)	0.846 (-+2.79%)
BldPitch1 [deg]	2.773	2.898 (+4.48%)	2.792 (+0.68%)
RootMyb1 [kN-m]	5610.4	6358.8 (+13.34%)	5347.3 (-+4.69%)
TwrBsMyt [kN-m]	77128.9	80477.1 (+4.34%)	77521.9 (+0.51%)
PtfmPitch [deg]	1.009	0.981 (-+2.76%)	1.001 (-+0.76%)

The above reported values for the standard deviations seem to confirm the qualitative observations derived by the inspection of the time histories for the three considered control mode settings. In particular, larger variance values can generally be noted for mode 2 (intended to motion reduction) except for a slight reduction of the platform pitch oscillations. On the other hand, a smaller power variance can be observed for mode 3 (power quality) with slighter variations for the other variables (in this particular case, also a slight reduction in the variance of the blade root moment can be observed).

The observed behavior of the control modes suggested to avoid the use of the motion reduction control mode, which seems to be less effective and potentially detrimental with respect to the increase of load oscillations. Again, this conclusion could be strongly related to the selected case study. Future work will be devoted at understanding if these conclusions also hold true for other types of floating foundations. In the rest of the study, the power quality control mode will be, thus, considered. Anyway, from the observation of the above results, generally, only slight load and power variations can be expected between the baseline and controlled scenarios. Moreover, during the development of the project, it has been observed that the major potential benefit of the AWC control is expected in terms of improved power quality, which could not be included in the LCOE estimation model used in this study, since no methodology can be found in literature which allows this type of estimation.

The preliminary study also allowed to check the expected effect of the control gain. The following figures illustrate the effect of changing the gain value from 0.5 to 1.0 for both the possible control mode (motion reduction and power quality). In the case of the motion reduction control mode (mode 2), the effect of gain variation is reported in the following figures over a relatively short time interval to highlight the differences between the observed responses. Clearly, increasing the control gain yields a larger amplitude of the blade pitch oscillations as observed in Figure 31. The platform pitch oscillation effectively shows a reduction in amplitude, as observed in Figure 32. On the other hand, a corresponding increase in the loads acting on the blade root and can be observed in Figure 33 and a slight increase can also be observed on the tower base bending moment (Figure 34).
In Table 7, the standard deviations of the considered signals are reported for the considered conditions with variable control gains. Reported results give a quantitative representation of the trends: an increase in the variance of the considered bending moments can be observed, while a reduction can be seen for the platform pitch motion.

Table 7. Standard deviations of several variables for variable control gain values with the motion reduction mode (indicated as mode2). (The percent variations with respect to the baseline case are shown in parentheses)

Parameter Name	mode1 gain=0.5	mode2 gain=0.5	mode3 gain=0.5
GenPwr_[kW]	906.4	935.8 (+3.24%)	1006.1 (+10.99%)
RotSpeed_[rpm]	0.870	0.898 (+3.24%)	0.966 (+10.99%)
BldPitch1_[deg]	2.773	2.898 (+4.48%)	3.246 (+17.05%)
RootMyb1_[kN-m]	5610.4	6358.8 (+13.34%)	7664.6 (+36.61%)
TwrBsMyt_[kN-m]	77128.9	80477.1 (+4.34%)	83934.7 (+8.82%)
PtfmPitch_[deg]	1.009	0.981 (-+2.76%)	0.964 (-+4.42%)

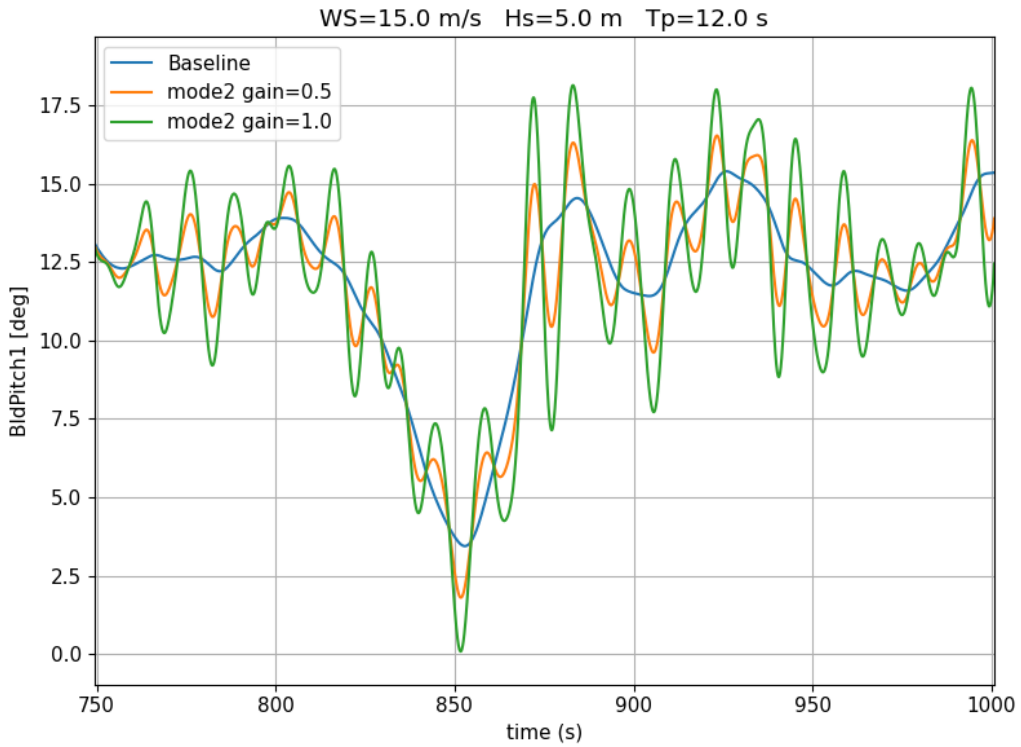

Figure 31. Blade pitch comparison for different gains (mode 2, motion reduction control mode).

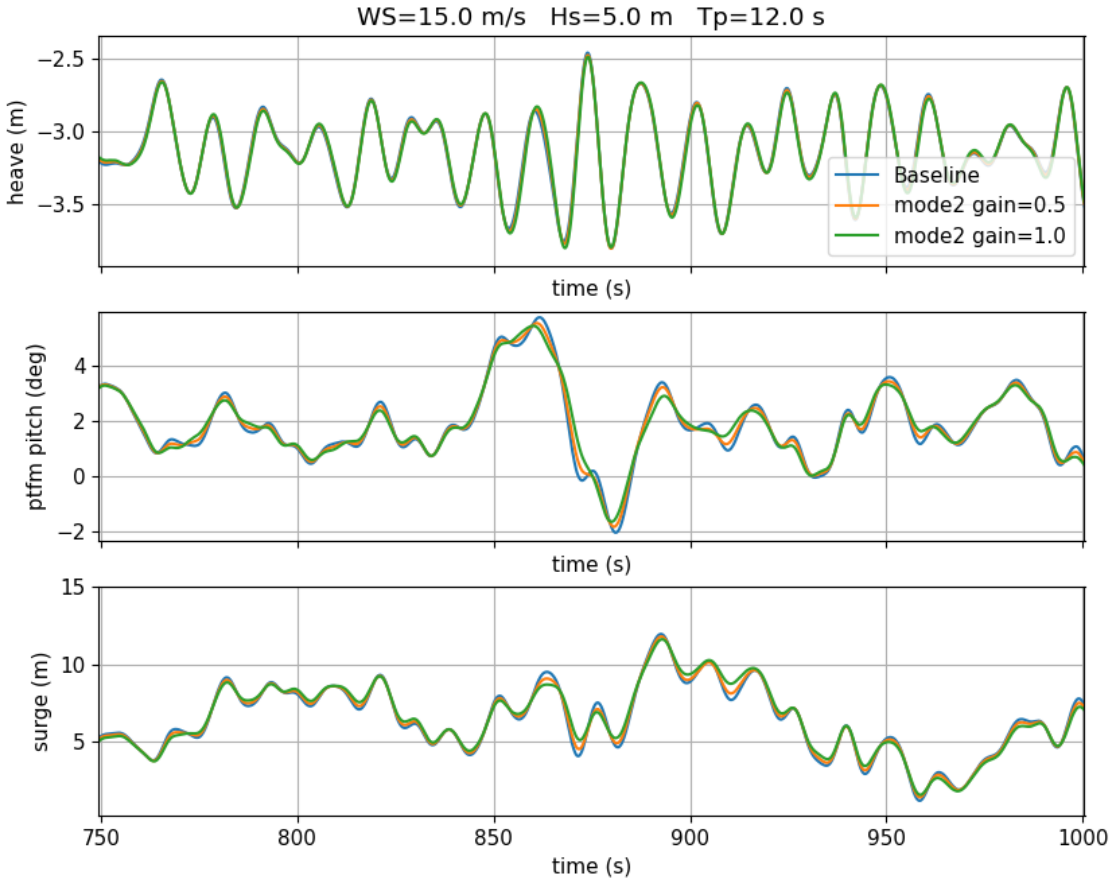

Figure 32. Platform motion comparison for different gains (mode 2, motion reduction control mode).

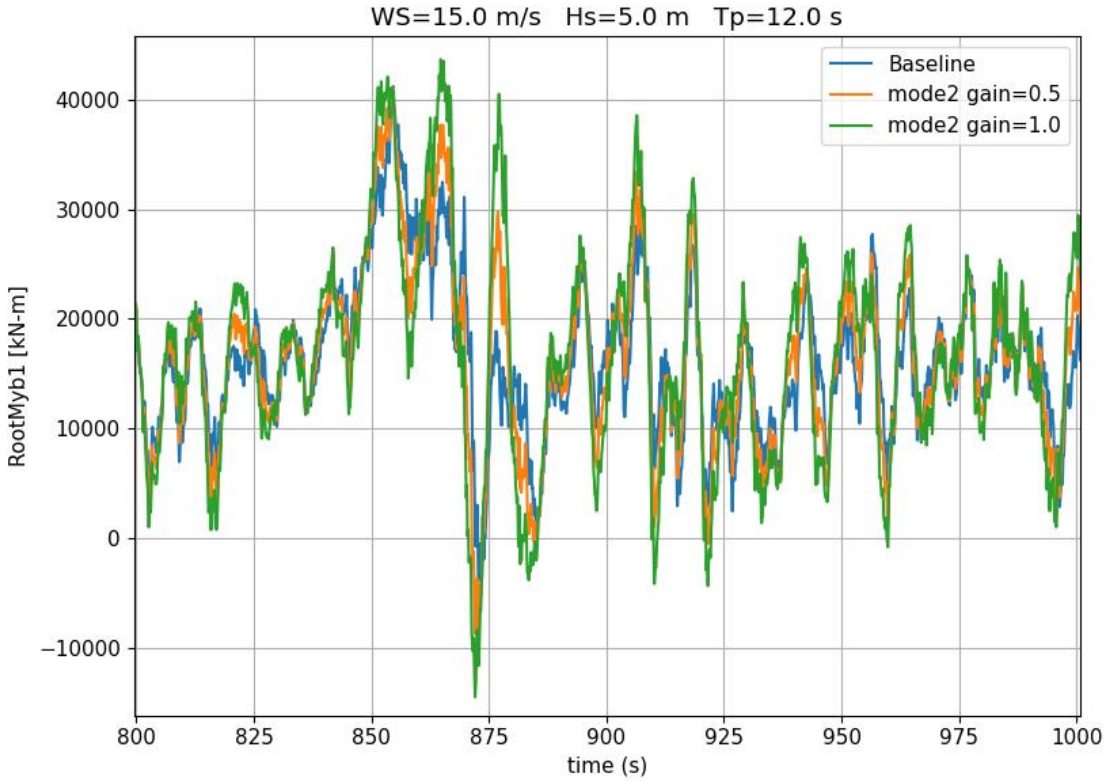

Figure 33. Blade root bending moment comparison for different gains (mode 2, motion reduction control mode).

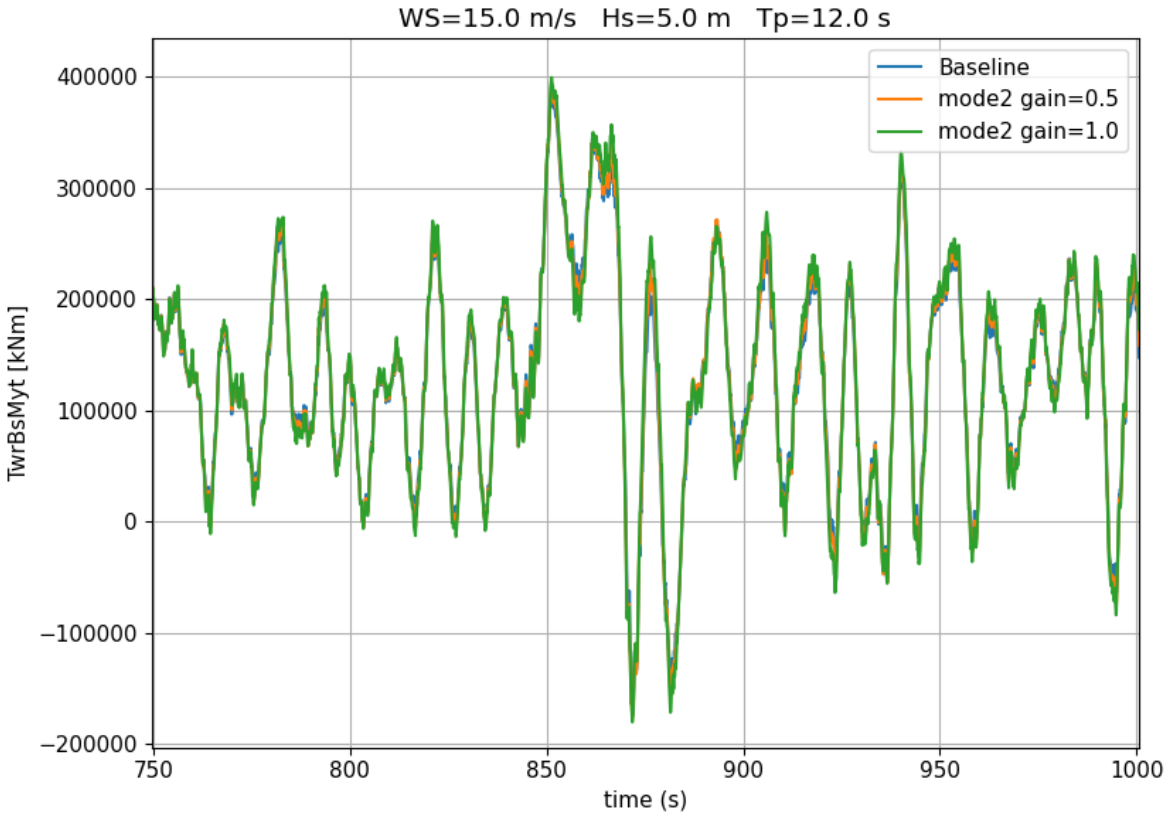

Figure 34. Tower base fore-aft bending moment comparison for different gains (mode 2, motion reduction control mode).

In the case of the power quality control mode (indicated as mode 3), similar observations can be reported for the considered variables. In particular, also in this case the gain increase is clearly visible in an increase of the required pitch oscillations compared to the baseline case. Anyway, in this case, a slight reduction in load oscillations can be observed for the blade root and tower base bending loads (Figure 36 and Figure 37). Small reduction can also be observed for the platform motion. Moreover, a slight reduction in power oscillations can be seen (Figure 36).
The standard deviations for the power quality mode, reported in Table 8, confirm the observed trends.

Table 8. Standard deviations of several variables for variable control gain values with the power quality mode (indicated as mode3). (The percent variations with respect to the baseline case are shown in parentheses).

Parameter Name	mode1 gain=0.5	mode2 gain=0.5	mode3 gain=0.5
GenPwr_[kW]	906.4	935.8 (+3.24%)	1006.1 (+10.99%)
RotSpeed_[rpm]	0.870	0.898 (+3.24%)	0.966 (+10.99%)
BldPitch1_[deg]	2.773	2.898 (+4.48%)	3.246 (+17.05%)
RootMyb1_[kN-m]	5610.4	6358.8 (+13.34%)	7664.6 (+36.61%)
TwrBsMyt_[kN-m]	77128.9	80477.1 (+4.34%)	83934.7 (+8.82%)
PtfmPitch_[deg]	1.009	0.981 (-+2.76%)	0.964 (-+4.42%)

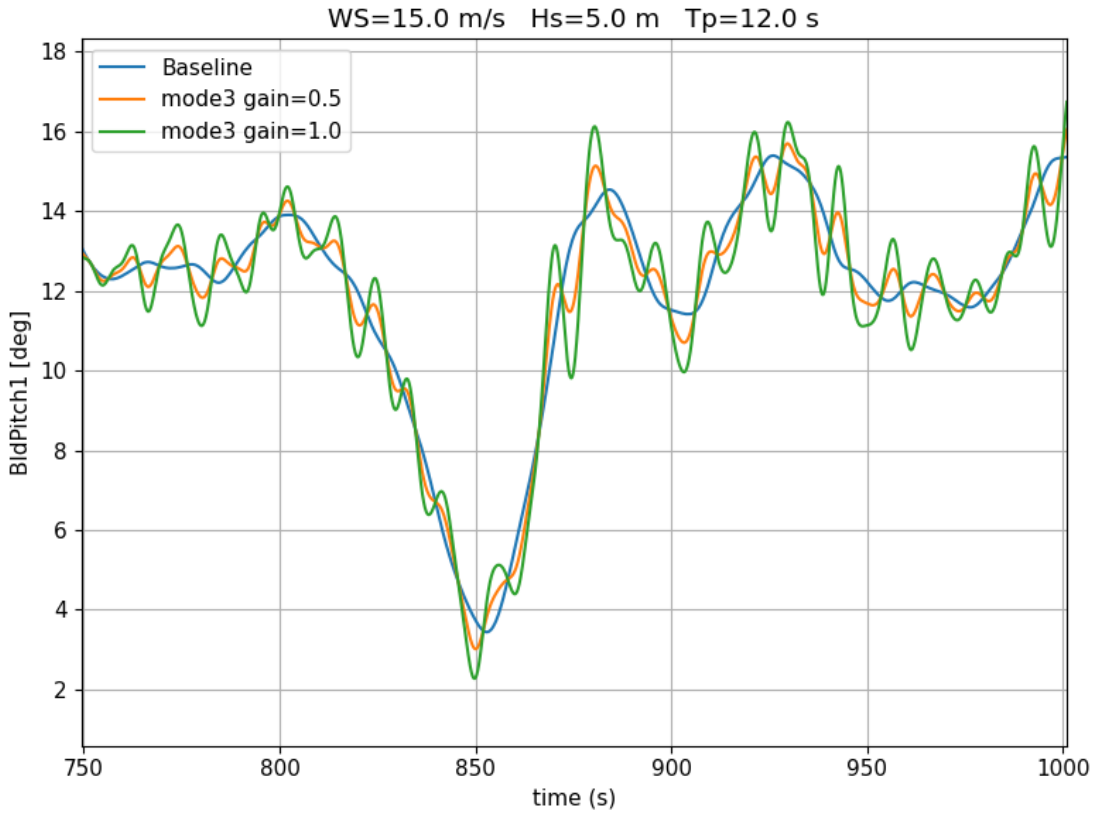

Figure 35. Blade pitch comparison for different gains (mode 3, power quality control mode).

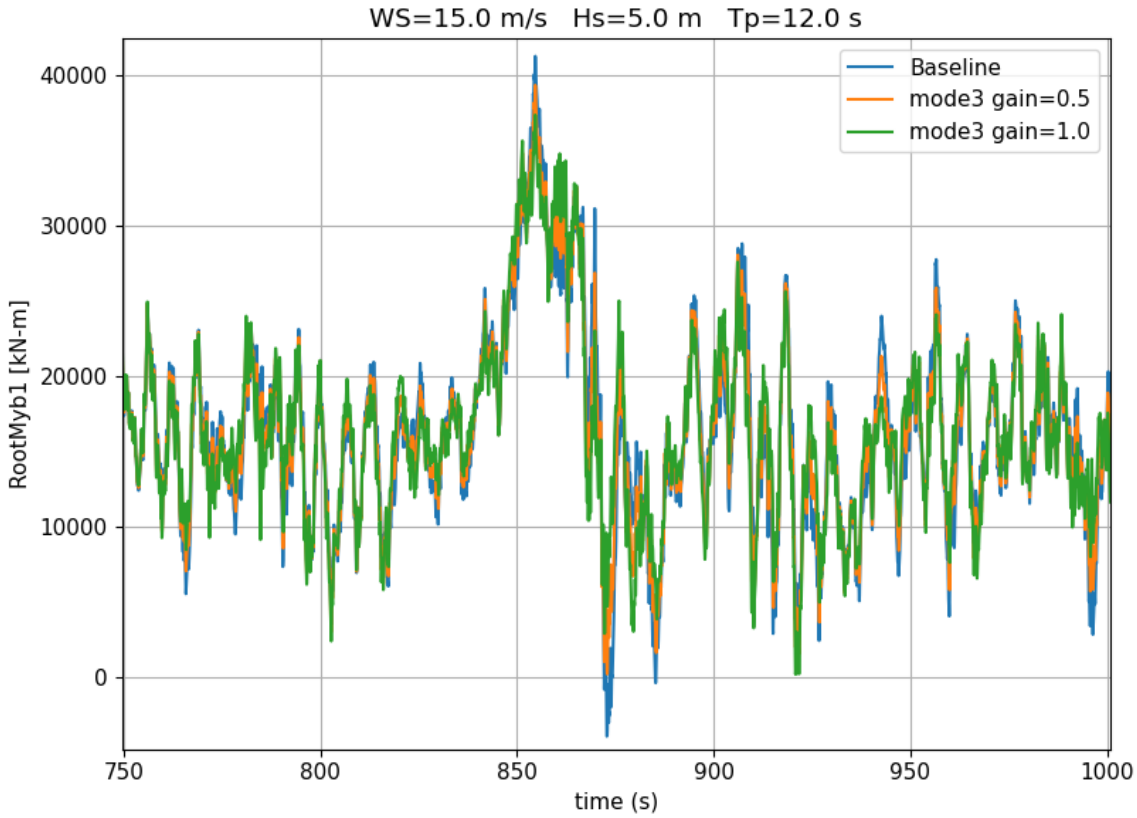

Figure 36. Blade root bending moment comparison for different gains (mode 3, power quality control mode).

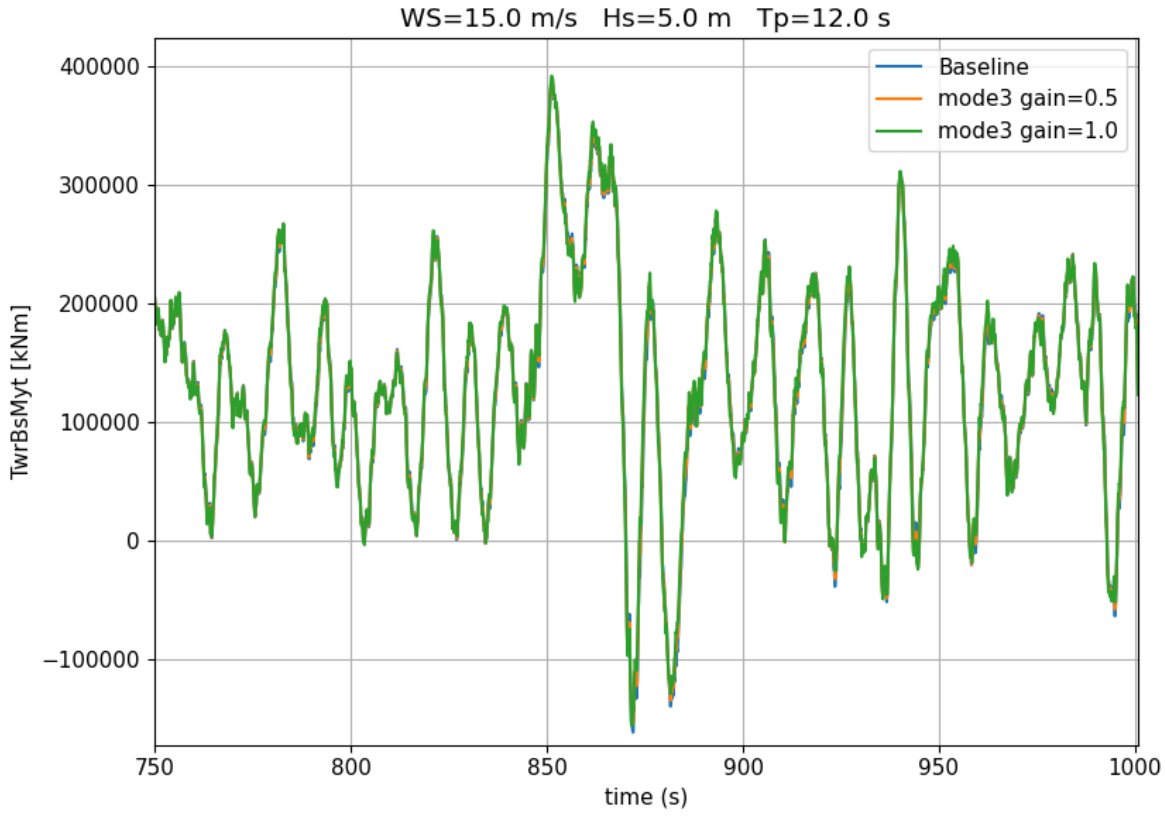

Figure 37. Tower base fore-aft bending moment comparison for different gains (mode 3, power quality control mode).

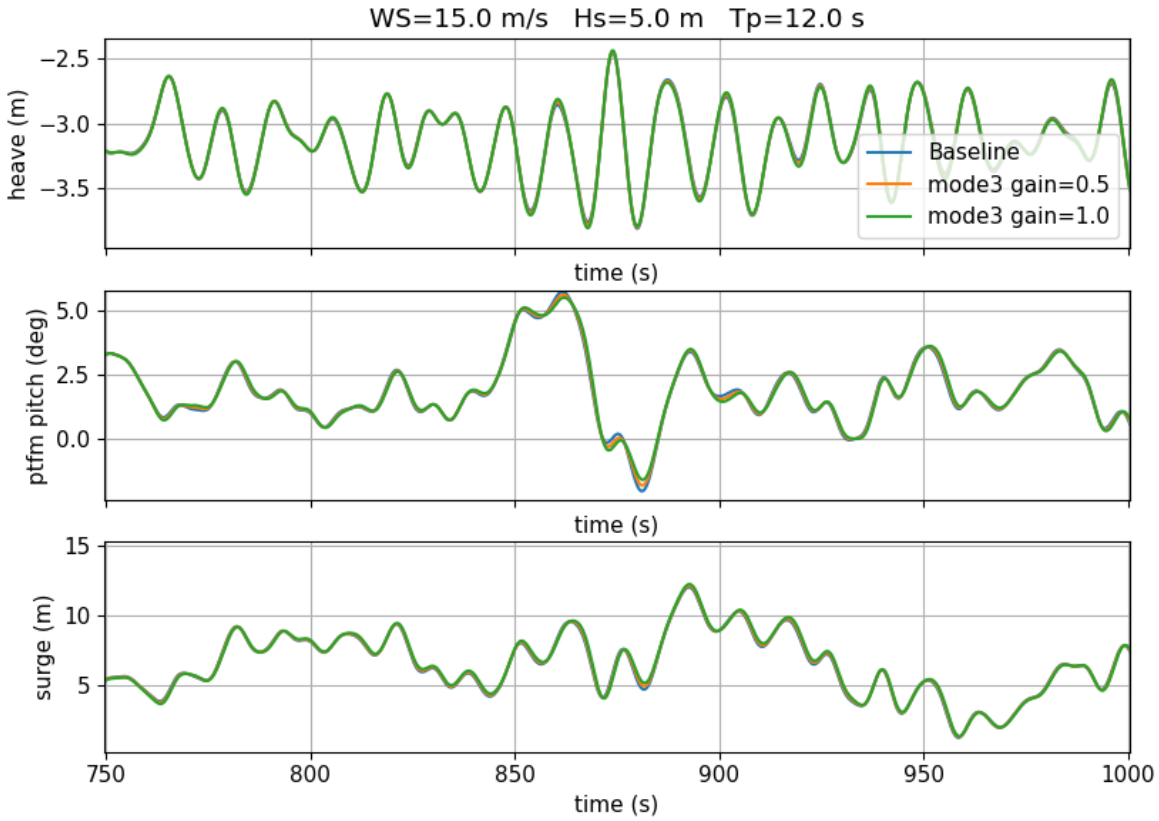

Figure 38. Platform motion comparison for different gains (mode 3, power quality control mode).

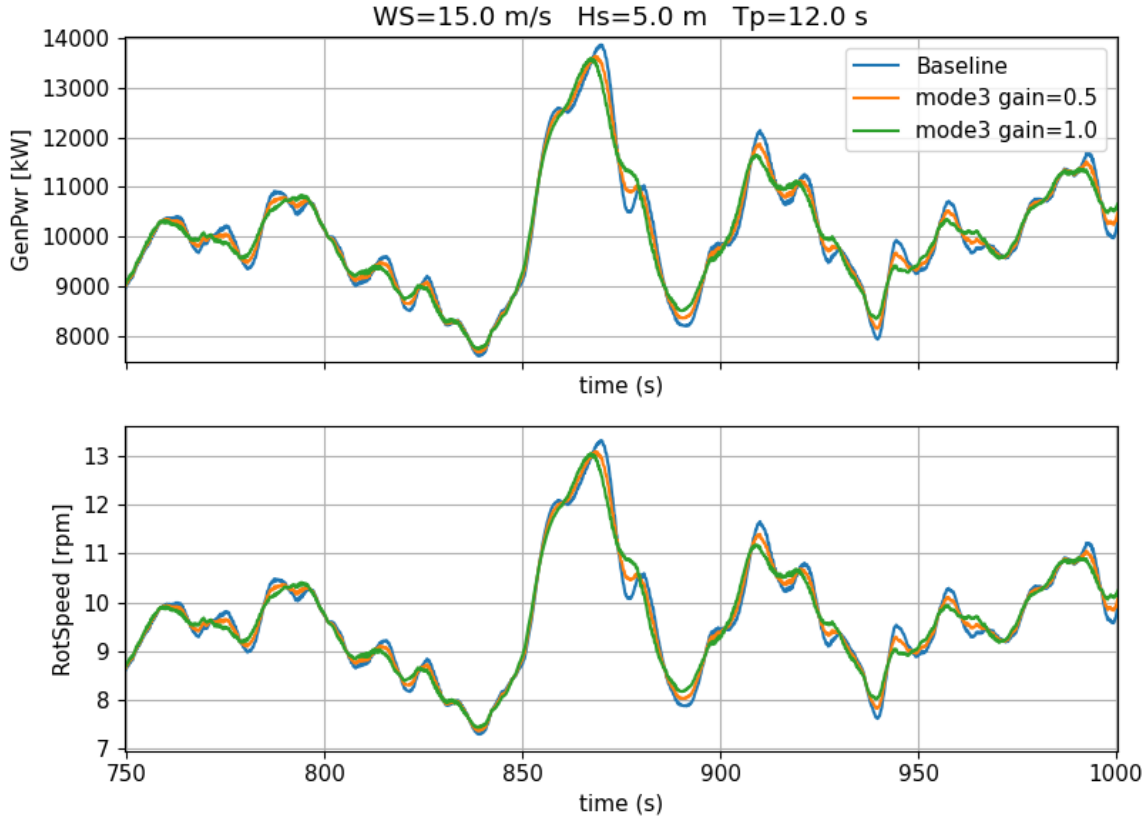

Figure 39. Power output comparison for different gains (mode 3, power quality control mode).

Based on the results presented above, the motion reduction control mode was not considered in the analysis, particularly due to the observed increase in load oscillations. On the other hand, the power quality mode seems to provide more interesting results, at least in the considered test cases, with respect to the reduction of load oscillations. Moreover, this control mode offers a reduction of power oscillation, complying with its main objective, as indicated by the reduction in power variance shown in Table 8, which may in turn yield a possible additional benefit, improving the output power quality, even if this effect is not directly accounted for in the developed LCOE estimation model.

In the following sections, a set of analyses (sect. 6.2) will be first performed for the power quality control mode with gain equal to 0.5, considering a range of operating and environmental conditions, limited to a subset of the design cases generally considered by standard requirements.

Then, a further set of analyses (restricted to DLC 1.3 of the IEC standard) has been considered, taking into account the cases with no wind-wave misalignment, which seemed to be more effective, and with gain equal to 1, in order to highlight the potential improvement of the control technique under investigation.

6.2 QBLADE MODEL AND SIMULATION SET-UP

The Softwind model, already analysed in WP2 in combination with a traditional pitch control, has been investigated in a limited set of design load cases (DLCs) with a control system implementing the wave feed-forward technique described in deliverable D3.1 [11]. As mentioned in the previous section, this technique has the objective to mitigate the perturbations induced by the incoming wave field. The controller comprises a feed-back block, related to wind disturbances, and feed-forward block, which takes into account the wave input time series and is aimed at modifying the pitch variation in order to counteract the effect of waves. The behaviour of the controller can be tuned by setting a gain input parameter. Such value has been set after a series of initial tests, indicated in the previous section, looking for the optimal overall response in terms of load reduction. Once the control gain has been chosen, a simulation dataset has been generated for a number of different design load cases. The simulated set of operating conditions, described in the following table, is a subset of the conditions explored during the task 2.2 of WP2.

Table 9. DLCs considered for the analyses of wave feed-forward control effect.

DLC	Description	Type of analysis
1.2	Power production in normal operating condition: Normal Sea State, normal turbulence model.	Fatigue
1.3	Power production in normal operating condition with extreme turbulence: Normal Sea State, Extreme Turbulence Model.	Extreme loads
1.4	Power production with extreme coherent gust with direction change	Extreme loads
1.6	Power production in severe sea state	Extreme loads

For the normal operating conditions in the DLC1.2, a reduced set of simulations has been considered with respect to the dataset generated in WP2, in order to reduce the needed computational time. The ranges of variation of the environmental characteristics considered in the analyses are indicated in the following table. The chosen combinations of the environmental parameters cover the 80% of the overall expected environmental conditions.

Table 10. Ranges of variation of the environmental parameters for DLC 1.2 in WP5 simulations.

Environmental parameters	Range of variation
Wind speed	5 – 23 m/s
Significant wave height	1 – 7 m
Peak wave period	4 – 16 s
Wind wave misalignment	-150° - 150°

Other details on the simulated datasets can be found in [20]. The wind climate considered for the analysis is described in more details in section 7.1.

Moreover, for the estimation of the expected extreme loads, also the parked condition DLCs (DLC 6.1, 6.2, 6.3) have been taken into account using the results of the simulations performed in FLOATECH WP2 (reported in a publicly available database [20]), based on the fact that the control is not active in the parked state and, thus, no effect due to the control is expected in these DLCs.

The environmental conditions are defined using the met-ocean data for a specific site located close to the Scottish isle of Barra, designated as “West of Barra”. This site has already been used in the FLOATECH WP2 study [20], and in other similar projects [21], and is characterized by severe environmental conditions.

6.3 POWER CURVES FOR THE BASELINE AND THE FEED-FORWARD CONTROLLED CASES

The results of the simulations can be used to estimate the FOWT power curve, which represents the energy production characteristics of the turbine and is of primary importance for LCOE estimation. Based on the simulated power output results, an estimate of the power curve of the isolated FOWT (assuming no wake interactions with other turbines) can be obtained using a classic binning approach, complying with typical standard procedures (as indicated in [22]).

Using the results of the simulations gathered during FLOATECH WP2, publicly available on a Zenodo repository [20] [23], a set of simulated power production data were already available. These results have been used to get a first reference estimate of the power curve. This result will be compared with the outcomes from the new datasets for both the cases with and without control.

In the process of power curve estimation, the simulation results are binned with respect to the wind speed, considering binning intervals of 2 m/s, spanning the operating conditions range from 5 m/s (close to cut-in wind speed) to 25 m/s (close to cut-off wind speed). In each bin, the wind speed and power output are averaged; the results of the procedure are reported in the following tables for different configurations:

- for the WP2 simulation data (reported as a reference case, indicated as “WP2 Reference”);
- for the case with the newly implemented control system but with the feed-forward strategy not active (indicated as “AWC Baseline”);
- for the case with the AWC control (indicated as “FF control”).

As already mentioned, the last two datasets, generated during WP5 activities, comprise a reduced range of operating conditions compared to the WP2 analysis, according to the preliminary character of the current study. The simulations for the AWC baseline, already present in WP2 database, have been replicated in the new dataset in order to consider the possible effects of changing the controller implementation. The control system has been, in fact, slightly modified in order to implement the new feed-forward strategy.

The estimated power curve results are presented in the following tables.

Table 11. Power curve from simulated normal operating conditions (DLC 1.2). Reference curve from WP2 analyses. “WP2 Reference”.

Wind speed WS (m/s)	Mean Power P_{avg} (kW)	Power std dev (kW)
5.1	1003.7	43.8
7.2	2735.2	69.7
9.2	5601.2	131.1
11.2	9437.8	151.8
13.3	10033.0	21.0
15.3	10012.7	6.9
17.3	10002.1	7.4
19.3	9997.4	7.1
21.4	9979.2	5.8
23.4	9973.5	12.9
25.5	9984.6	5.7

Table 12. Power curve from simulated normal operating conditions (DLC 1.2). AWC baseline case: feed-forward controller inactive. “AWC Baseline”.

Wind speed WS (m/s)	Mean Power P_{avg} (kW)	Power std dev (kW)
5.2	799.6	70.7
7.2	2818.8	102.2
9.2	5774.1	130.3
11.2	9093.6	182.4
13.3	9949.7	43.9
15.3	9996.4	13.7
17.4	9999.2	6.2
19.4	10004.1	6.6
21.4	9998.3	2.9
23.6	9994.3	5.2

Table 13. Power curve from simulated normal operating conditions (DLC 1.2). AWC baseline case: feed-forward controller activated. "FF control"

Wind speed WS (m/s)	Mean Power P_{avg} (kW)	Power std dev (kW)
5.2	798.7	70.1
7.2	2818.5	101.7
9.2	5773.2	130.7
11.2	9093.5	182.4
13.3	9949.7	43.9
15.3	9996.4	13.7
17.4	9999.2	6.2
19.4	10004.1	6.6
21.4	9998.3	2.8
23.6	9994.3	5.2

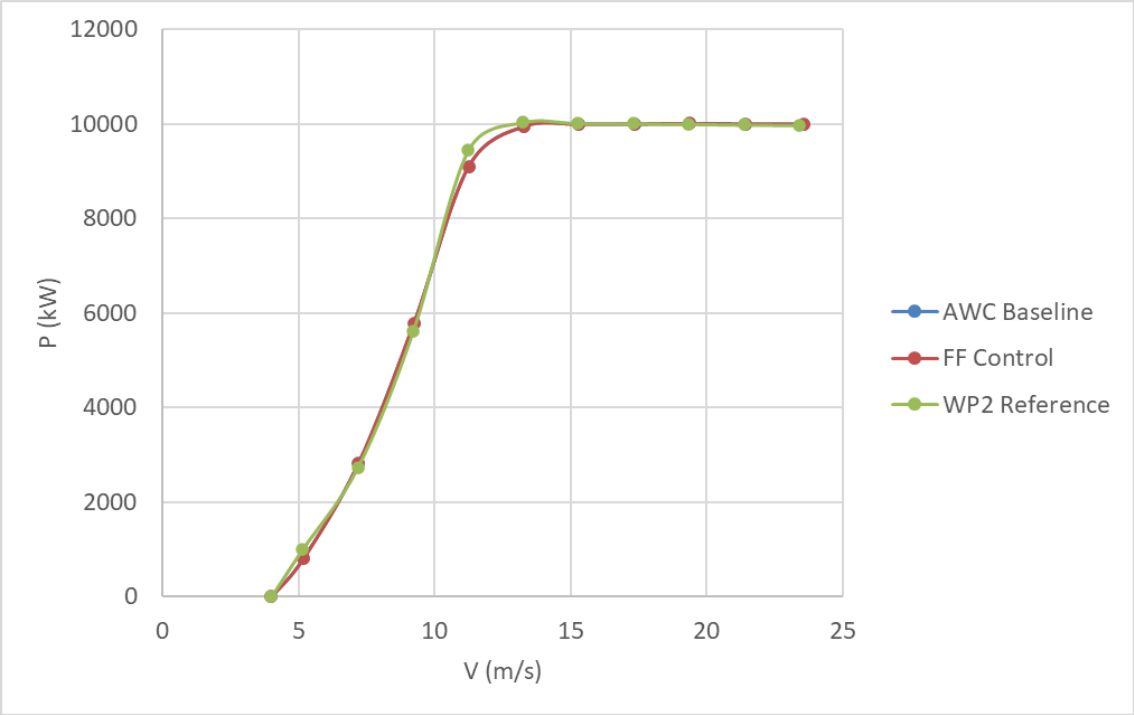

Figure 40. Power curve from simulated normal operating conditions (DLC 1.2). Reference curve from WP2 analyses.

It can be seen that in terms of average output power, the effect of the variation of the control system is substantially negligible; the average output power is almost equal with and without the control. The power standard deviation around the mean value, indicated in the tables for each wind speed bin, is also very similar between the two cases with the new control implementation. The results of the new control are also in good agreement with the original control model used in the WP2 analysis, although some slight differences can be observed, particularly closer to the cut-in wind speed and around the knee close to the rated wind speed.

The cut-in and cut-out wind speeds have been assumed equal to 4 m/s and 26 m/s, respectively, according to [24], in the subsequent energy production estimates.

It can be noted that the results for both the Baseline (AWC inactive) and with FF control show a quite similar trend. Anyway, a difference with respect to the WP2 results can be observed, which can be ascribed to the different implementation of the control system used for WP5 simulation for the implementation of the FF control.

6.4 THRUST COEFFICIENT

From the DLC 1.2 simulations, the variation of the thrust coefficient with wind speed can also be determined. This result is necessary for the definition of the wake losses used in the estimation of the overall energy production of a farm. The following figure represents the trend of the thrust coefficient as a function of wind speed, as obtained from the simulation data (using the same naming scheme defined in the previous section).

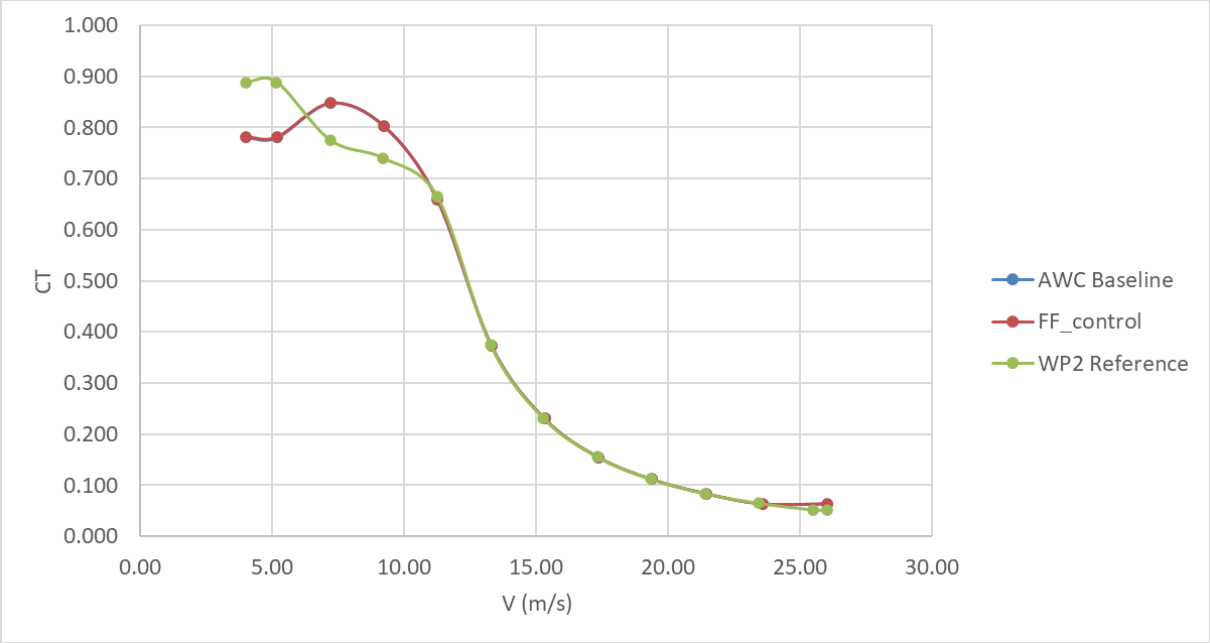

Figure 41. Thrust coefficient as a function of wind speed as obtained from DLC1.2 simulation data.

As already observed for the power curve, the thrust coefficient shows a quite similar trend for the baseline and the FF control cases, but some differences may be observed in comparison to the results from the WP2 analyses, probably due to the difference in the control implementation, as also previously stated.

6.5 DAMAGE EQUIVALENT LOADS COMPARISON

Based on the results obtained for the normal operation condition DLC1.2, the Damage Equivalent Loads for the main considered components have been estimated. The simulation data have been processed using MLife, a tool developed at NREL [25] [26], for the estimation of the fatigue loadings of wind turbines. The tool has been used for estimating the 1Hz DEL loads for the following loadings over an assumed 20 years long project life:

- tower base loadings;
- blade root loadings;

- mooring lines loadings.

The tool requires the definition of a statistical distribution of the environmental characteristics to estimate a probability for each of the simulated time history. In this work, consistently with the approach followed in WP2 [20] [23], a joint statistic distribution of wind speed, wave height, wave period and wind-wave misalignment has been considered, based on long term publicly available data (ERA5), for the above indicated West of Barra site.

Based on simulation results and on the assumed local climatic conditions, the results for the DEL estimations are indicated in Table 15. An explanation of the symbols used in the comparison is reported in Table 14.

Table 14. Description of load components for the considered loads.

	idx	Label	Description	Note
Blade	**RootMxb[i]**	B**[i]** Root Mx	Blade root out of plane bending moment for the i-th blade	In the blade reference system
	RootMyb[i]	B**[i]** Root My	Blade root in plane bending moment for the i-th blade	
	RootMzb[i]	B**[i]** Root Mz	Blade root pitch moment for the i-th blade	
Tower	**TwrBsFxt** **TwrBsFyt** **TwrBsFzt** **TwrBsMxt** **TwrBsMyt** **TwrBsMzt**	TB Fx TB Fy TB Fz TB Mx TB My TB Mz	Tower base forces and bending moments	
Mooring	**FAIRTEN[i]**	FAIRTEN[i]	Mooring line tension	Measured at the bridles' delta connection point

Table 15. Comparison of DEL loads with (FF control) and without (Baseline) the feed-forward controller.

idx	Label	Units	Softwind Baseline	Softwind FF control	FF control - Baseline diff. (%)
RootMxb1	B1 Root Mx	[kN-m]	18494.0	18494.0	0.000%
RootMyb1	B1 Root My	[kN-m]	18335.0	18324.0	-0.060%
RootMzb1	B1 Root Mz	[kN-m]	290.6	290.5	-0.052%
RootMxb2	B2 Root Mx	[kN-m]	18499.0	18499.0	0.000%
RootMyb2	B2 Root My	[kN-m]	18327.0	18320.0	-0.038%
RootMzb2	B2 Root Mz	[kN-m]	291.3	291.1	-0.062%
RootMxb3	B3 Root Mx	[kN-m]	18502.0	18503.0	0.005%
RootMyb3	B3 Root My	[kN-m]	18324.0	18314.0	-0.055%
RootMzb3	B3 Root Mz	[kN-m]	291.1	290.9	-0.058%
TwrBsFxt	TB Fx	[kN]	756.8	757.1	0.037%
TwrBsFyt	TB Fy	[kN]	933.4	933.4	0.002%
TwrBsFzt	TB Fz	[kN]	170.1	170.9	0.453%

TwrBsMxt	TB Mx	[kN-m]	68652.0	68654.0	0.003%
TwrBsMyt	TB My	[kN-m]	62130.0	62176.0	0.074%
TwrBsMzt	TB Mz	[kN-m]	7248.5	7247.2	-0.018%
FAIRTEN1	FAIRTEN1	[N]	158520.0	158480.0	-0.025%
FAIRTEN2	FAIRTEN2	[N]	195800.0	195830.0	0.015%
FAIRTEN3	FAIRTEN3	[N]	198090.0	198100.0	0.005%

It can be observed that only very slight differences in the DELs are generated by the change in the control system. The largest variation in DEL loads (excluding the vertical force on tower base, which has a relatively small value) can be observed on the tower base fore-aft bending moment (TB My), with an almost negligible value of about 0.074%.

6.6 EXTREME LOADS COMPARISON

The results from the simulation of the DLCs 1.3, 1.4, 1.6 have been used to investigate possible variations in extreme loads due to the effect of changing the control strategy.
A comparison of the maximum loads for the cases with and without the feed-forward control is reported in the following table (the meaning of symbols is reported in Table 14). For each load, the maximum and minimum vales are reported. It has to be noted, as already pointed out, that in the estimation of the overall extreme loads the parking conditions has also been taken into account, considering the results from WP2 simulations, based on the fact that such results are not influenced by the control.

Table 16. Comparison of the extreme load estimations with (FF control) and without (Baseline) the feed-forward control.

idx	Type	Label	Units	DLC Name Baseline	Baseline value	DLC Name FF Control	FF value	Baseline-FF control diff. (%)
RootMxb1	**Minimum**	B1 Root Mx	[kNm]	DLC6.2	-47259.98	DLC6.2	-47259.98	0.00%
	Maximum	B1 Root Mx	[kNm]	DLC6.2	50763.19	DLC6.2	50763.19	0.00%
RootMyb1	**Minimum**	B1 Root My	[kNm]	DLC1.4	-42987.27	DLC1.4	-42998.65	0.03%
	Maximum	B1 Root My	[kNm]	DLC1.6	52584.92	DLC1.6	50784.14	-3.42%
RootMxb2	**Minimum**	B2 Root Mx	[kNm]	DLC6.2	-35156.88	DLC6.2	-35156.88	0.00%
	Maximum	B2 Root Mx	[kNm]	DLC6.2	39416.30	DLC6.2	39416.30	0.00%
RootMyb2	**Minimum**	B2 Root My	[kNm]	DLC1.4	-41792.32	DLC1.4	-41678.04	-0.27%
	Maximum	B2 Root My	[kNm]	DLC1.6	55061.71	DLC1.6	48552.02	-11.82%
RootMxb3	**Minimum**	B3 Root Mx	[kNm]	DLC6.2	-48049.89	DLC6.2	-48049.89	0.00%
	Maximum	B3 Root Mx	[kNm]	DLC6.2	49656.50	DLC6.2	49656.50	0.00%
RootMyb3	**Minimum**	B3 Root My	[kNm]	DLC1.4	-36188.22	DLC1.4	-36596.00	1.13%
	Maximum	B3 Root My	[kNm]	DLC1.6	54308.94	DLC1.3	49093.69	-9.60%
RootMxc1	**Minimum**	B1 Root Mx	[kNm]	DLC6.1	-30646.29	DLC6.1	-30646.29	0.00%
	Maximum	B1 Root Mx	[kNm]	DLC6.2	34112.41	DLC6.2	34112.41	0.00%
RootMyc1	**Minimum**	B1 Root My	[kNm]	DLC6.2	-50746.78	DLC6.2	-50746.78	0.00%
	Maximum	B1 Root My	[kNm]	DLC1.6	52552.75	DLC1.6	51062.47	-2.84%
RootMxc2	**Minimum**	B2 Root Mx	[kNm]	DLC6.2	-31435.25	DLC6.2	-31435.25	0.00%
	Maximum	B2 Root Mx	[kNm]	DLC6.2	33441.59	DLC6.2	33441.59	0.00%
RootMyc2	**Minimum**	B2 Root My	[kNm]	DLC1.4	-48363.92	DLC1.4	-48091.12	-0.56%
	Maximum	B2 Root My	[kNm]	DLC1.6	55025.70	DLC1.6	48788.54	-11.34%
RootMxc3	**Minimum**	B3 Root Mx	[kNm]	DLC6.2	-29283.04	DLC6.2	-29283.04	0.00%
	Maximum	B3 Root Mx	[kNm]	DLC6.2	36544.82	DLC6.2	36544.82	0.00%
RootMyc3	**Minimum**	B3 Root My	[kNm]	DLC6.2	-49652.06	DLC6.2	-49652.06	0.00%

	Maximum	B3 Root My	[kNm]	DLC1.6	54287.08	DLC1.3	48999.48	-9.74%
TwrBsFxt	**Minimum**	TB Fx	[kN]	DLC6.1	-9741.97	DLC6.1	-9741.97	0.00%
	Maximum	TB Fx	[kN]	DLC6.1	12104.16	DLC6.1	12104.16	0.00%
TwrBsFyt	**Minimum**	TB Fy	[kN]	DLC6.2	-8811.22	DLC6.2	-8811.22	0.00%
	Maximum	TB Fy	[kN]	DLC6.2	9074.25	DLC6.2	9074.25	0.00%
TwrBsMxt	**Minimum**	TB Mx	[kNm]	DLC6.2	-647279.50	DLC6.2	-647279.50	0.00%
	Maximum	TB Mx	[kNm]	DLC6.2	648285.06	DLC6.2	648285.06	0.00%
TwrBsMyt	**Minimum**	TB My	[kNm]	DLC6.1	-702085.50	DLC6.1	-702085.50	0.00%
	Maximum	TB My	[kNm]	DLC6.1	836544.88	DLC6.1	836544.88	0.00%
FAIRTEN1	**Minimum**	FAIRTEN1	[N]	DLC6.1	247.92	DLC6.1	247.92	0.00%
	Maximum	FAIRTEN1	[N]	DLC1.6	3710769.25	DLC1.6	3836652.50	3.39%
FAIRTEN2	**Minimum**	FAIRTEN2	[N]	DLC6.1	754.43	DLC6.1	754.43	0.00%
	Maximum	FAIRTEN2	[N]	DLC1.6	3991756.75	DLC1.6	4027924.00	0.91%
FAIRTEN3	**Minimum**	FAIRTEN3	[N]	DLC6.1	776.13	DLC6.1	776.13	0.00%
	Maximum	FAIRTEN3	[N]	DLC1.6	4296803.50	DLC1.6	4202696.00	-2.19%

Regarding the prediction of extreme loads, more significant variations can be noted, particularly in the case of the blade root bending moment, with a reduction in the maximum load of about 12%. The most significant effect appears in the DLC1.6. With respect to the mooring loads, different trend can be seen on different lines with an asymmetric behaviour; however, extreme mooring load variations seem to be lower, with a maximum absolute value approximately in the 2÷3% range. Clearly the extreme loads related to parking conditions (DLC6.x) remains unaltered, being unaffected by the control.

6.7 LOAD VARIATIONS CONSIDERED FOR ESTIMATING THE EFFECTS ON COMPONENT COST

Based on the comparisons of the DELs and maximum loads between the baseline and modified cases, the load variations considered for the estimation of the control effect on component costs are indicated in the following tables.

Table 17. DEL variations used for the estimation of component cost change.

Blade root	***Baseline***	***FF***	***Diff***
	(kNm)	(kNm)	(%)
Root Mx	18502.0	18503.0	0.005%
Root My	18335.0	18324.0	-0.060%
Root Mxy	26048.0	26040.9	-0.027%
Tower top	***Baseline***	***FF***	***variation***
	(kN)	(kN)	(%)
TT Fx	473.4	473.7	0.076%
TT Fy	435.5	435.5	0.002%
TT Fxy	643.18	643.45	0.042%
Tower base	***Baseline***	***FF***	***variation***
	(kNm)	(kNm)	(%)
TB Mx	68652.00	68654.00	0.003%
TB My	62130.00	62176.00	0.074%
TB Mxy	92591.76	92624.12	0.035%
Mooring	***Baseline***	***FF***	***variation***
	(kN)	(kN)	(%)
FAIRTEN	198.09	198.10	0.005%

The blades DEL variations are estimated as an average between the three blades results. The resulting M_{xy} components have been used for the estimation of the cost variations.

Table 18. Maximum load variations used for the estimation of component cost change.

Blade root	***Baseline***	***FF***	***Diff.***
	(kNm)	(kNm)	(%)
B Root Mx max	50763.2	50763.2	0.00%
B Root My max	55061.7	50784.1	-7.77%
B root Mxy	74891.2	71804.8	-4.12%
Tower top	***Baseline***	***FF***	***variation***
	(kN)	***(kN)***	***(%)***
TT Fx	4921.6	4921.6	0.00%
TT Fy	4283.8	4283.8	0.00%
TT Fxy	6524.8	6524.8	0.00%
Tower base	***Baseline***	***FF***	***Diff.***
	(kNm)	(kNm)	(%)
TB Mx	648285.1	648285.1	0.00%
TB My	836544.9	836544.9	0.00%
TB Mxy	1058338.7	1058338.7	0.00%
Mooring	***Baseline***	***FF***	***Diff.***
	(kN)	(kN)	(%)
FAIRTEN MAX	4296.8	4202.7	-0.022

The blade maximum load variations are estimated as the maximum value between the results for the three blades.
It can be noted that the maximum loads at the tower base were observed for a parking load condition and thus are not altered by the control variation.

6.8 ADDITIONAL ANALYSES FOR THE ESTIMATION OF LOAD VARIATION

In order to get an estimate of the potential effects of the AWC control technique, a higher value of the control gain has been also considered: in particular, a set of simulations with gain set equal to 1 has been carried out. Moreover, in these additional simulations a set of conditions has been examined with environmental conditions closer to the ones for which the control has been developed. The DLC1.3 from the IEC standard with no misalignment between wind and waves has been, in fact, considered. This DLC is generally used for extreme load analyses, but, in this study, it has been used for Damage Equivalent Load evaluation, in order to explore the behaviour of the control in more severe conditions, where the control could in principle provide a larger improvement. Anyway, also in this case only relatively small variations of loads can be observed, as reported in the following table.

Table 19. Comparison of DELs estimated using results of the DLC 1.3 (notwithstanding the standard requirements) between the baseline and AWC controlled case.

Load component label	Units	Softwind Baseline	Softwind FF control	FF control - Baseline diff. (%)
B1 Root Mx	[kNm]	19562.0	19539.0	-0.118%
B1 Root My	[kNm]	24456.0	24541.0	0.348%
B1 Root Mz	[kNm]	359.4	358.8	-0.167%
B2 Root Mx	[kNm]	19565.0	19542.0	-0.118%
B2 Root My	[kNm]	24371.0	24597.0	0.927%
B2 Root Mz	[kNm]	360.8	359.9	-0.238%
B3 Root Mx	[kNm]	19557.0	19529.0	-0.143%
B3 Root My	[kNm]	24433.0	24477.0	0.180%
B3 Root Mz	[kNm]	359.8	359.6	-0.081%
B1 Root Mx fix	[kNm]	20288.0	20282.0	-0.030%
B1 Root My fix	[kNm]	23736.0	23894.0	0.666%
B1 Root Mz fix	[kNm]	359.4	358.8	-0.167%
B2 Root Mx fix	[kNm]	20286.0	20283.0	-0.015%
B2 Root My fix	[kNm]	23714.0	23924.0	0.886%
B2 Root Mz fix	[kNm]	360.8	359.9	-0.238%
B3 Root Mx fix	[kNm]	20286.0	20279.0	-0.035%
B3 Root My fix	[kNm]	23894.0	23901.0	0.029%
B3 Root Mz fix	[kNm]	359.8	359.6	-0.081%
TB Fx	[kN]	1554.4	1559.5	0.328%
TB Fy	[kN]	324.4	324.5	0.049%
TB Fz	[kN]	221.6	215.0	-2.969%
TB Mx	[kNm]	28833.0	28862.0	0.101%
TB My	[kNm]	121510.0	122000.0	0.403%
TB Mz	[kNm]	10721.0	10709.0	-0.112%
FAIRTEN1	[N]	212430.0	212520.0	0.042%
FAIRTEN2	[N]	222950.0	222830.0	-0.054%
FAIRTEN3	[N]	219660.0	219390.0	-0.123%

As previously mentioned, the action of the control has been mainly oriented during the development of the project to the reduction of the output power oscillations. A comparison of the standard deviations, here assumed as a concise measure of the output power quality, with and without the AWC control is reported in the following table, for the DLC 1.3 condition.

Table 20. Standard deviation (intended as a simplified measure of output power quality) comparison between the cases with and without the AWC control.

Baseline				FF control			
Vel (m/s)	P_{avg} (kW)	P_{std} (kW)		Vel (m/s)	P_{avg} (kW)	P_{std} (kW)	diff (FF - Baseline)
5	1008.6	635.9		5	1004.6	634.3	-0.26%
7	2726.0	1457.0		7	2735.6	1463.5	0.45%
9	5945.6	2192.0		9	5928.3	2189.9	-0.09%
11	8691.0	2178.3		11	8687.7	2177.7	-0.03%
13	9850.6	1652.8		13	9849.8	1652.3	-0.04%
15	9990.1	1342.8		15	9990.0	1341.6	-0.09%
17	10003.4	1117.3		17	10003.4	1113.1	-0.38%
19	9995.7	1004.8		19	9995.7	997.7	-0.71%
21	9999.1	853.3		21	9999.1	843.2	-1.18%
23	10000.0	821.8		23	10000.0	808.4	-1.64%

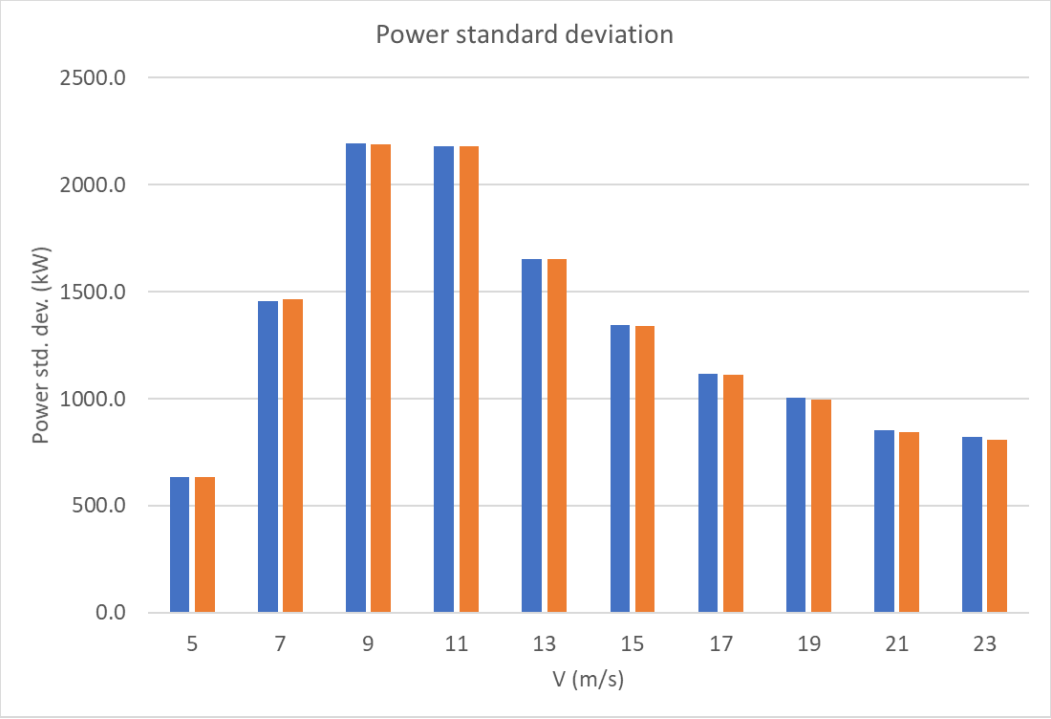

Figure 42. Comparison of the standard deviations (assumed as a simplified measure of output power quality) with and without AWC in DLC 1.3.

A slight reductions of power oscillations (measured by the standard deviation) can be observed for almost all the examined wind speed (except for lower wind speed), while it can be seen that a larger reduction of power oscillations is expected close to cut-off wind speed conditions, generally associated to more severe sea states.

Anyway, this variation cannot be included in the estimation of the LCOE variation, with the developed evaluation model, not being directly related to the component costs.

7 ANNUAL ENERGY PRODUCTION

7.1 SITE CHARACTERISTS

In order to estimate the Annual Energy production, some assumptions on the wind speed distribution have been be made. The wind distribution at the West of Barra site has been considered. Data related to the met-ocean conditions of this site can be found in [21] [27]. The distribution of wind speeds and directions is reported in graphical form in Figure 43 and Figure 44, which represent the wind speed magnitude and direction statistical distributions. The data used for estimating such distributions have been obtained by processing long term statistics retrieved from the ERA5 public database [28].

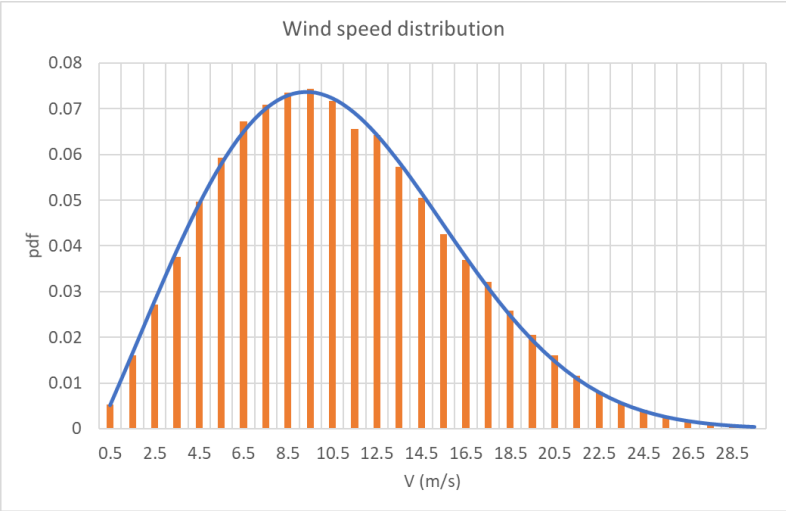

Figure 43. Wind speed statistical distribution (West of Barra site).

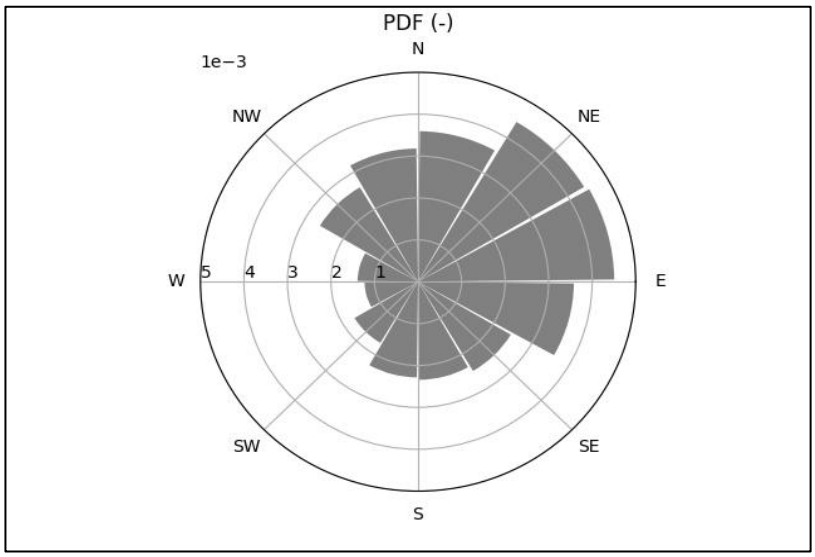

Figure 44. Wind direction statistical distribution (West of Barra site).
(Note: the above reported direction data are expressed using the mathematical convention, thus indicating the direction towards which the wind flows, as opposed to the meteorological convention).

An analytical distribution is fitted to the wind speed magnitude data, using the following expression for the cumulative probability distribution

$$f(U) = \left(1 - e^{-\left(\frac{U}{\alpha}\right)^{\beta}}\right)^{\delta} \quad (4)$$

The estimated values of such distribution parameters are reported in the following table at the hub height (119 m) as indicative of the overall wind climate in the considered site. Anyway, for the purpose of this study, a joint distribution of wind speed magnitude and direction will be considered.

Table 21. Weibull distribution parameters fitted to the wind speed distribution at hub height.

Hub height	**119 m a.s.l.**
Wind speed statistical distribution parameters	$\alpha = 12.8$ m/s
	$\beta = 2.345$
	$\delta = 0.88$
Average wind speed	$V_m = 10.7$ m/s

In this study, in order to estimate the effect of the wake interaction in a farm, it is important to take into account the combined variability of wind speed and direction. The following figure shows the assumed joint statistical distribution of wind speed and direction for the considered site, as determined from the ERA5 database. The figure shows the joint occurrence probability of each considered bin of magnitude and direction: magnitude is discretized in the range from 2 m/s to 38 m/s with a 2 m/s step, while the directions are spanned over the range from -180° to 180° with a 8° step.

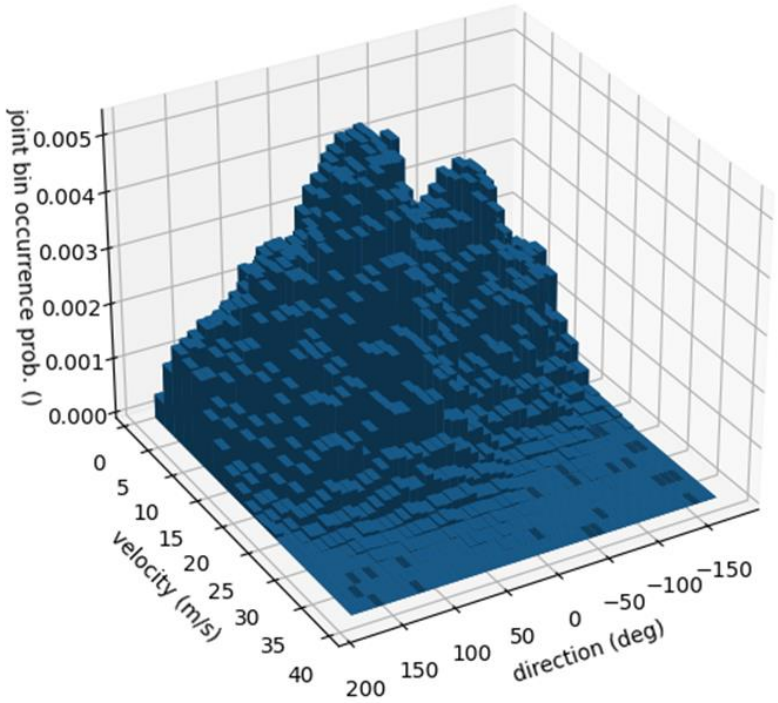

Figure 45. Joint distribution of wind speed and direction (West of Barra site).
(The reported directions represent the directions towards which the wind is oriented)

Beside the wind statistical distribution, the actual energy production of a real wind farm is strongly dependent also on the layout of the farm. In this study, mainly oriented to the investigation of the control system effect rather than to the optimization of the energy output, a simplified layout will be considered, consisting in a square arrangement of FOWT units with one side aligned to the prevailing wind direction. The power curve determined from simulations for the baseline and modified cases will be used for the evaluation of energy production.

Once the layout has been assumed and the wind climate has been described through an occurrence probability matrix for the combination of wind speed magnitude and direction, the effect of wake interaction between each pair of turbines in the farm can be estimated for each incoming wind direction. To evaluate the wake interaction between turbines, the wake velocity deficit has to be described as a function of the wind speed and of the relative distance of the FOWTs. Wake deficit can be estimated using engineering models, as assumed in this study. In this way, the overall energy production for the simplified layout under investigation can be estimated, allowing the LCOE evaluation in the two compared scenarios (with/without AWC).

7.2 FARM LAYOUT AND WAKE MODELLING ASSUMPTIONS

The effect of the AWC control is relatively independent of the wind farm layout and of the number of installed FOWTs, which affect mainly the overall wake interactions. In order to study the control strategy impact on the farm LCOE, some assumptions on the farm geometrical arrangement have to be accepted. Future studies will explore the impact of the control methodology in the case of more complex wind farm designs. As previously indicated, in this study a square distribution of the turbines is considered, as illustrated in Figure 46.

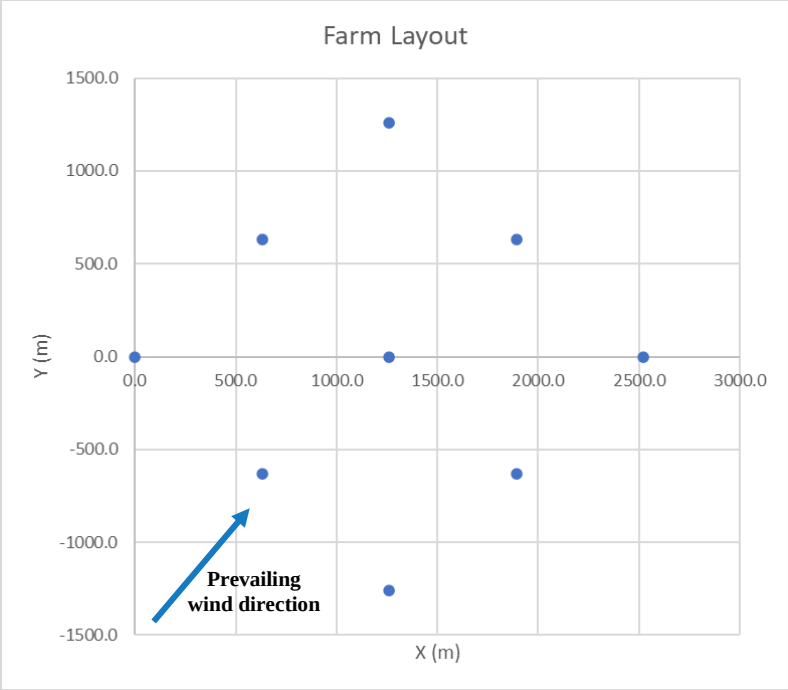

Figure 46. Assumed farm layout (the number of turbines is varied in a parametric study).

The distance between the turbines is also fixed, in both the directions (lines and rows), to a value equal to a given multiple of the rotor diameter, D. Throughout the study, the nondimensional turbine distance, Λ, has been assumed equal to

$$\Lambda = 8D \tag{5}$$

For the calculation of annual energy production, a simplified algorithm has been applied. The steps involved in the calculation are here briefly reported:

- for each wind direction and for each couple of turbines in the assumed layout, the distance between the turbines along the considered direction is calculated;
- the diameter of the wake at the inter-turbine distance is estimated using a simplified linear expression [29] (equal to the rotor diameter directly behind the upwind turbine)

$$D_w = D_{in}\left(1 + \frac{2k_w x}{D_{in}}\right) \tag{6}$$

where D_{in} is the initial wake diameter, here assumed equal to the rotor diameter, k_w is the wake expansion rate, assumed equal to 0.05 according to [30]; if the downwind turbine is comprised within the calculated wake diameter at the estimated distance along the considered wind direction, then the turbine pair is considered interacting (as illustrated in Figure 47);

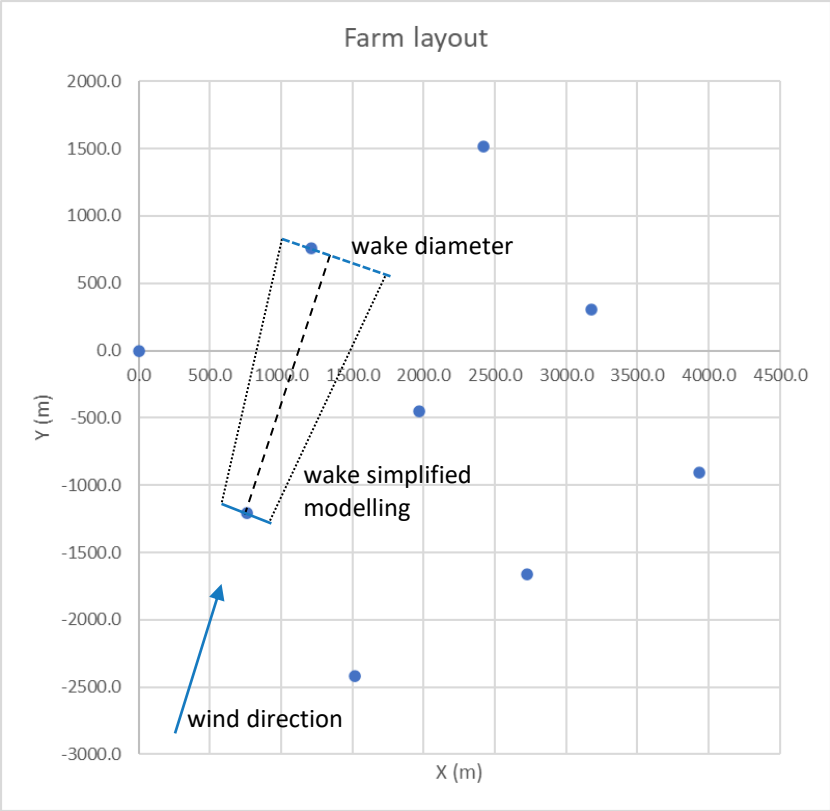

Figure 47. Simplified wake interaction modelling.

- the wake velocity deficit at the calculated inter-turbine distance has been assumed equal to the maximum wake velocity deficit at the wake centre line for the gaussian wake model, as reported in [31], which is described in more detail further in this section; the wake deficit depends also on the thrust coefficient and, consequently, on the wind speed;
- once the wake deficit is known, the power generated by the trailing turbine is estimated considering the power curve output at the reduced wind speed in the wake;
- the process of wake deficit estimation is cycled over all the pairs of turbines and for all wind speeds and directions in the assumed discretization; the contributions of each wind speed and direction bin, accounting for the reduction due to the wake losses, are summed up to estimate the overall energy production.

In this case, where no direct effects of the control are expected on the wake behaviour, the wake modelling has been treated using an engineering model, i.e., the gaussian model described in [31] and briefly recalled also here, although using a simplified approach. The main approximation in the assumed implementation of the wake modelling is related to the absence of a model for the possible partial wake superpositions (the simplified check only considers if the turbine placement falls within the wake of an upwind turbine, neglecting the possibility that the wake may only partially interact with the trailing turbine).
In the case of larger farms, the wake effects from different turbines may superimpose on the trailing units for a given wind direction. In such cases, a superposition formulation has to be assumed in order to estimate the combined effect; in this study, an approach based on the squared sum combination method is applied, as widely used in classical engineering models for wake interaction [32]; it is assumed that, when more than one upwind turbine wake affect a trailing turbine, the overall wake reduction can be expressed as follows:

$$\delta_i^2 = \sum_{j=1}^{n} \delta_{ij}^2 \tag{7}$$

where δ_i represents the overall wake velocity deficit on the i-th turbine in the farm, due to the superposition of the wake deficits, δ_{ij}, caused by the j-th interacting turbine on the i-th turbine. The wake deficit δ_{ij} can be expressed as a function of the wind speed and of the distance behind the upwind turbine; in this study, we assume that the wake deficit behind the turbine, estimated using the gaussian model, can be represented in a matrix form as reported in the following table.

Table 22. Assumed wake deficit as a function of wind speed and distance for the Baseline case (assumed equal with and without farm control).

	distance (Diam)							
Vm	**3**	**5**	**7**	**9**	**11**	**13**	**15**	**50**
1.0	0.000	0.000	0.000	0.000	0.000	0.000	0.000	0.000
3.0	0.000	0.000	0.000	0.000	0.000	0.000	0.000	0.000
5.0	0.376	0.220	0.147	0.106	0.080	0.063	0.050	0.003
7.0	0.378	0.225	0.151	0.110	0.083	0.065	0.053	0.003
9.0	0.379	0.223	0.149	0.108	0.082	0.064	0.052	0.003
11.0	0.347	0.201	0.133	0.095	0.072	0.056	0.045	0.003
13.0	0.219	0.129	0.085	0.061	0.046	0.035	0.028	0.002
15.0	0.133	0.079	0.052	0.037	0.028	0.022	0.018	0.001
17.0	0.088	0.052	0.035	0.025	0.019	0.015	0.012	0.001
19.0	0.062	0.037	0.025	0.018	0.013	0.010	0.008	0.000
21.0	0.047	0.028	0.019	0.013	0.010	0.008	0.006	0.000
23.5	0.033	0.020	0.013	0.010	0.007	0.006	0.005	0.000
27.5	0.000	0.000	0.000	0.000	0.000	0.000	0.000	0.000
35.0	0.000	0.000	0.000	0.000	0.000	0.000	0.000	0.000
45.0	0.000	0.000	0.000	0.000	0.000	0.000	0.000	0.000

As previously stated, in this analysis a simplified assumption is made for the evaluation of wake losses. The effect of the control system is, in fact, assumed to be not related to the wake behaviour (contrary to other control strategies specifically designed to enhance wake recovery, such as the AWM control technique). The values here indicated for wake losses are currently based on an assumption, waiting for more accurate results from wake recovery simulations. Wake deficit in Table 22 are based on the maximum wake deficit for a gaussian wake model, as described in [31] [30]. The wake deficit at the wake centre line is estimated using the following expression [30]:

$$\delta_{w\,\max} = 1 - \sqrt{1 + \frac{C_T}{8\left(k_* \frac{x}{D} + \epsilon\right)^2}} \tag{8}$$

where k_* is a function of the atmospheric turbulence intensity, I_{turb}, defined by the following regression formula

$$k_* = 0.3837\, I_{\text{turb}} + 0.003678 \tag{9}$$

while ϵ is expressed using the following relation

$$\epsilon = 0.2\sqrt{\beta} \tag{10}$$

$$\beta = \frac{1}{2}\frac{\left(1 + \sqrt{1 - C_T}\right)}{\sqrt{1 - C_T}} \tag{11}$$

where C_T is the wind turbine thrust coefficient. The thrust coefficient has been determined considering the results of the simulations in normal condition (DLC1.2); such results are shown in Figure 41 as a function of wind speed.

A turbulence intensity of $I_{\mathrm{turb}} = 12\%$ has been considered, according to the assumption reported in [21] related to a similar site in a project context similar to the study performed in the current work.

8 ESTIMATION OF LCOE VARIATION

8.1 LCOE VARIATION WITH FEEDFORWARD CONTROL STRATEGY. EFFECT OF FARM SIZE

Based on the results of the simulations, the variation of the LCOE value can be estimated, accounting for the variation in component cost, based on structural mass variation, and on the variation in annual energy production, between the baseline configuration (without AWC control) and the modified configuration (with AWC control).
Assuming the layout described in 7.2, a set of LCOE values can be estimated for different numbers of wind turbines with the same spatial distributions. The following table and figure gather the results estimated for the assumed layout with a variable number of installed units.

Table 23. Effect on LCOE of the farm size. Percent reduction of LCOE with/without control.

n. rows	n. lines	n turbines	AEP w/o AWC	AEP w AWC	LCOE w/o AWC	LCOE w AWC	LCOE variation
			(MWh/year)	(MWh/year)	(€/MWh)	(€/MWh)	(%)
1	1	1	54262	54259	177.0 €	177.0 €	0.0%
2	2	4	212865	212854	167.9 €	167.9 €	0.0%
3	3	9	473384	473360	167.5 €	167.5 €	0.0%
4	4	16	833836	833795	168.2 €	168.2 €	0.0%
5	5	25	1293449	1293384	169.1 €	169.1 €	0.0%
6	6	36	1851906	1851813	169.8 €	169.8 €	0.0%
7	7	49	2508995	2508869	170.5 €	170.5 €	0.0%

Relatively large values of the LCOE can be observed. This is due mainly to two issues. On the one side, the considered material costs are based on the inflation rate observed in 2022, which negatively affects the overall costs. On the other side, a simplified layout has been assumed with the purpose of comparing the effects of control variation in standardized conditions; it may be argued that a layout optimization, outside the scope of this study, could in principle improve the annual energy production, thus reducing the LCOE levels. The last observation may be also related to the non-monotonic trend of the LCOE, shown in Figure 48; the increased wake interactions between a larger number of turbines, in a suboptimal layout, can partly explain the slight increase of LCOE for increasing number of units beyond the minimum point observed in the figure.
It has to be noted that the difference in LCOE between the cases with the two different types of control is negligible, contrary to what initially expected. This result is related to the fact that only slight changes in loads and power curves have been observed. In fact, during project development, the control

optimization has been reoriented towards a different objective, related to the improvement of the output power quality, which is not accounted for in the cost model.

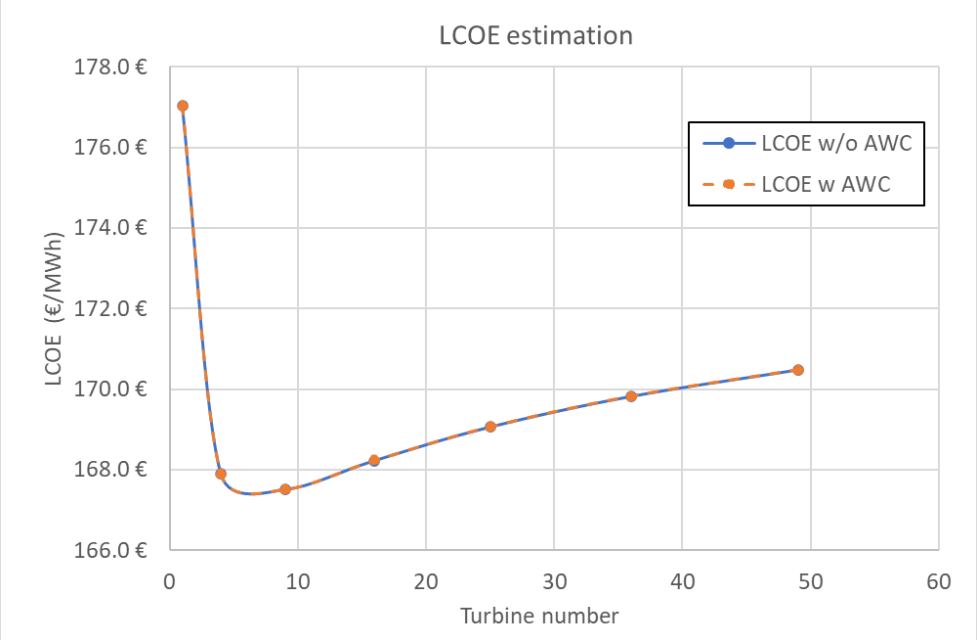

Figure 48. Variation of LCOE estimation as a function of the number of FOWT units in the farm, with and without the AWC control strategy.

It can be seen from Figure 48 that the estimated value of LCOE without the AWC control strategy, shows a range of variation between about 168 €/MWh and 177 €/MWh, variable with the farm size. Similar results are observed for the case with the AWC control active.

8.2 EFFECT OF MET-OCEAN CONDITIONS

The particular wind climate may also have an impact on the LCOE estimation. In principle, met-ocean conditions may also influence the effectiveness of the considered control strategy, but in this specific case the wake behaviour is not directly influenced by the control.

As an example of the possible effect on LCOE, in order to consider an extreme case, in this study we can consider a fictitious wind regime, based on the West of Barra case, with the same wind speed distribution but with a constant directional distribution, with the wind always oriented as the prevailing wind direction in Figure 46. This condition is, of course, purely theoretical, but it is reported here for comparison purposes for a given farm size (3x3 farm layout), as a limiting case for estimating the theoretical economic performance of the control technology in different local weather conditions:

Table 24. LCOE variation for 3x3 farm layout. Fictitious extreme case with constant wind direction.

	Baseline	*Modified*	
LCOE (3x3 farm layout)	177.3 €	177.3 €	€/MWh

A larger LCOE value can be observed (about 177 €/MWh compared to about 168 €/MWh, with an increase of about 5.9%). This increase may be related to the larger influence of the wake effects in the considered fictitious extreme climate.

It can be seen, that also in this limiting case the LCOE reduction is almost similar to the results for a more realistic wind direction distribution, confirming the negligible effect of the control on the estimated value of the LCOE.

9 CONCLUSIONS ON LCOE ESTIMATION

The study described in this document was intended as a preliminary estimation of the LCOE of a floating wind turbine, accounting for the possible effects of a novel control strategy. A simulation-based approach has been used to estimate the loads and power curves for the two cases with and without control. The results of the simulations showed a negligible difference between the two cases, consequently giving negligible effect of the control on estimated values of the LCOE.

The most significant effect is related to the observed reduction of LCOE with the size of a wind farm. A sensitivity study parametrized on the number of turbines, for a given farm layout, showed a rapid decrease of the LCOE with the number of installed units, with the expected LCOE values reaching a minimum level of about $168\ €/\mathrm{MWh}$ between 4 and 9 installed units, followed by a slight increase for larger farm sizes, up to a value of about $171\ €/\mathrm{MWh}$ for the maximum considered farm size (with 49 units).

The relatively large values of the estimated LCOE can be explained considering two issues:

- the non-optimal square grid layout of the farm assumed in the study;
- the high inflation rate assumed (related to year 2022) which affects the material costs.

The results on LCOE have been estimated also in a limiting fictitious case with a single wind direction corresponding to the prevailing direction at the considered site. Larger LCOE values can+ be seen in this fictitious limiting case, but similar values of the LCOE have been obtained for the two alternative control strategies confirming the results previously reported.

As already noted, the analyses of the results showed no significant variation in LCOE, due to a very small variation in the overall loading conditions on the components, as observed in this study after the comparison of the simulation results with and without the AWC control. These results, although initially unexpected, indicates a possibility for further improvements, also considering other performance parameters which cannot be directly accounted in a cost model, such as, for example, an improvement of the output power quality.

Another important observation on the results of this study concerns the choice of the specific type of floating foundation considered for the analyses, which was made for maximizing the uniformity of the analyses throughout the FLOATECH project. The spar buoy platform type is known to have, generally, a

lower response to wave actions, compared to other configurations, such as for example the semisubmersible; this type of behaviour can reduce the efficacy of the considered control, which is specifically oriented to the reduction of wave induced perturbations on platform motion or on other affected performance parameters, such as power quality. This situation is partly highlighted by the results, which have shown that in severe sea states the control has a higher capability to positively alter the target output variables. This observation supports the possibility of extending the application of the feed-forward control strategy to other platform types through further dedicated optimization studies.

REFERENCES

[1] Wind-Europe, "Wind energy in Europe," 2023.

[2] K. Yilmazlar, S. Cacciola, M. Xiolesmy, A. Rodriguez and A. Croce, "Development of engineering cost models for integrated design optimization of onshore and offshore wind farms," in *The Science of Making Torque from Wind (TORQUE 2022)*, Delft, Netherlands, 2022.

[3] Delft University of Technology, Technical university of Berlin, "An advanced open source wind turbine controller for power generation and load mitigation using real-time feedforward wave information," Floatech research project, 2022.

[4] S. Santhakumar, G. Smart, M. Noonan, H. Meerman and A. Faaij, "Technological progress observed for fixed-bottom offshore wind in the EU and UK," *Technological Forecasting & Social Change,* vol. 182, no. 121856, 2022.

[5] W. Kuckshinrichs, «LCOE: A Useful and Valid Indicator—Replica to James Loewen and Adam Szymanski,» *Energies,* vol. 14, n. 406, 2021.

[6] J. Aldersey-Williams and T. Rubert, "Levelised cost of energy – A theoretical justification and critical assessmen," *Energy Policy,* no. 124, pp. 169-179, 2019.

[7] C. Kost, S. Shammugam, V. Fluri, D. Peper, A. D. Memar and T. Schlegl, "LEVELIZED COST OF ELECTRICITY RENEWABLE ENERGY TECHNOLOGIES," Fraunhofer ISE, Freiburg, 2021.

[8] B. Steffen, «Estimating the cost of capital for renewable energy projects,» *Energy Economics,* vol. 88, n. https://doi.org/10.1016/j.eneco.2020.104783, 2020.

[9] V. Arnal, «Experimental Modelling of a floating wind turbine using a "software-in-the-loop" approach.,» ECN, Nantes, 2020.

[10] R. B. D. L. Sebastian Perez-Becker, «D2.1. Aero-Hydro-Elastic Model Definition in QBlade Ocean,» Floatech Project, 2022.

[11] A. Hegazy, P. Naayen and J.-W. v. Wingerden, "D3.1 An advanced open source wind turbine controller for power generation and load mitigation using real-time feedforward wave information," Floatech, 2023.

[12] M. Maness, B. Maples and A. Smith, "NREL Offshore Balance-ofSystem Model," NREL, DENVER (CO), USA, 2017.

[13] J. N. Sørensen and G. C. Larsen, "A Minimalistic Prediction Model to Determine Energy Production and Costs of Offshore Wind Farms," *Energies, MDPI,* vol. 14, no. 448, 2012.

[14] L. Fingersh, M. Hand and A. Laxson, "Wind Turbine Design Cost and Scaling Model," NREL, 2006.

[15] P. Beiter, W. Musial, A. Smith, L. Kilcher, R. Damiani, M. Maness, S. Sirnivas, T. Stehly, V. Gevorgian, M. Mooney and G. Scott, "A Spatial-Economic CostReduction Pathway Analysis Reduction Pathway Analysis for U.S. Offshore Wind Energy Development from 2015–2030," NREL, 2016.

[16] DNV, “Offshore Mooring Chain DNV-OS-E302,” DNV, 2013.

[17] M. Ikhennicheu, M. Lynch, S. Doole, F. Borisade, D. Matha, J. L. Dominguez, R. D. Vicente, T. Habekost, L. Ramirez, S. Potestio, C. Molins and P. Trubat, “Review of the state of the art of mooring and anchoring designs, technical COREWIND D2.1,” COREWIND project, 2020.

[18] SOTRA ANCHOR & CHAIN AS, “Anchor and Chain Handbook,” Norway, 2021.

[19] DNV, “Position Mooring DNV-OS-E301,” DNV, 2008.

[20] F. Papi, R. Behrens de Luna, J. Saverin, D. Marten, C. Combreau, G. Troise, G. Mirra and A. Bianchini, “Deliverable 2.3 Design Load Case Database for Code to Code Comparison,” Floatech, 31 10 2022. [Online]. Available: https://zenodo.org/record/7817708.

[21] P. Gómez, G. Sánchez, A. Llana and G. Gonzalez, “Lifes50+ Deliverable D1.1 Oceanographic and meteorological conditions for the design,” Lifes50+, 2015.

[22] IEC, «IEC 61400-12-1 Wind energy generation systems - Part 12-1: Power performance measurements of electricity producing wind turbines,» IEC, 2022.

[23] F. Papi, A. Bianchini, G. Troise, G. Mirra, D. Marten, J. Saverin, R. Behrens de Luna, M.-L. Ducasse and J. Honnet, “Deliverable 2.4 Full report on the estimated reduction of uncertainty in comparison to the state-of-the-art codes OpenFAST and DeepLines Wind,” Floatech, 2022.

[24] S. Wang, T. J. Larsen and H. Bredmose, “Ultimate load analysis of a 10 MW offshore monopile wind turbine,” DTU Library, 2021.

[25] G. J. Hayman and J. M. Buhl, “MLife User’s Guide for Version 1.00,” 2012.

[26] G. J. Hayman, “MLife Theory Manual for Version 1.00,” 2012.

[27] F. Vigara, L. Cerdán, R. Durán, S. Muñoz, M. Lynch, S. Doole, C. Molins, P. Trubat and R. Guanche, “Corewind project deliverable D1.2 Design Basis,” 2020.

[28] F. Papi, Y. Perignon and A. Bianchini, “Derivation of Met-Ocean Conditions for the Simulation of Floating Wind Turbines: a European case study,,” in *Journal of Physics: Conference Series*, 2022.

[29] T. Göçmen, P. v. d. Laan, P.-E. Réthoré, A. P. Diaz, G. C. Larsen and S. Ott, “Wind turbine wake models developed at the technical university of Denmark: A review,” *Renewable and Sustainable Energy Reviews,* no. 60, p. 752–769, 2016.

[30] M. Krutova, M. B. Paskyabi, F. G. Nielsen and J. Reuder, “Evaluation of Gaussian wake models under different atmospheric stability conditions: Comparison with large eddy simulation results,” *Journal of Physics: Conference Series,* vol. 1669, p. 012016, 2020.

[31] M. Bastankhah and F. Porté-Agel, “A new analytical model for wind-turbine wakes,” *Renewable Energy,* no. 70, pp. 116-123, 2014.

[32] A. Peña, P.-E. Réthoré and M. P. v. d. Laan, “On the application of the Jensen wake model using a turbulence-dependent wake decay coefficient: the Sexbierum case,” *WIND ENERGY,* 2015.

[33] P. Bortolotti, D. Berry, R. Murray, E. Gaertner, D. Jenne, R. Damian, G. B. and K. Dykes, “A Detailed Wind Turbine Blade Cost Model,” NREL, 2019.

[34] A. d. Carvalho, “STEEL MARKET DEVELOPMENTS Q4 2015,” OECD, Paris, Fr, 2016.

[35] A. Ghigo, L. Cottura, R. Caradonna, G. Bracco and G. Mattiazzo, “Platform Optimization and Cost Analysis in a Floating Offshore Wind Farm,” *Journal of Marine Science and Engineering,* vol. 8, no. 835, 2020.

[36] A. Myhr, C. Bjerkseter, A. Ågotnes and T. A. Nygaard, “Levelised cost of energy for offshore floating wind turbines in a life cycle perspective,” *Renewable Energy,* vol. 66, pp. 714-728, 2014.

[37] H. Ahn, Y.-J. Ha and K.-H. Kim, “Load Evaluation for Tower Design of Large Floating Offshore Load Evaluation for Tower Design of Large Floating Offshore,” *Energies,* vol. 16, no. 1862, 2023.

[38] S. Allegretto, Performance analysis and cost modelling for offshore floating wind turbines, Master thesis, 2021.

[39] OECD, “"Prices: Producer prices"Main Economic Indicators (database),,” 2023. [Online]. Available: https://doi.org/10.1787/data-00535-en. [Accessed 2023 March 30].

[40] A. Martinez and G. Iglesias, “Mapping of the levelised cost of energy for floating offshore wind in the European Atlantic,” *Renewable and Sustainable Energy Reviews,* vol. 154, 2022.

[41] J. A. Frederik, B. M. Doekemeijer, S. P. Mulders and J.-W. v. Wingerden, “The helix approach: Using dynamic individual pitch control to enhance wake mixing in wind farms,” *Wind Energy,* no. 23, p. 1739–1751, 2020.

[42] S. Heidari, Economic modelling of floating offshore wind power. Calculation of levelized cost of energy, Sweden: School of business, society and engineering: Master thesis., 2017.

[43] P. Chaviaropoulos, I. Karga, C. Harkness and B. Hendriks, “PIPI-based Assessment of Innovative Concepts (Methodological Issues),” INNWIND Deliverable 1.2.3, 2014.